Development and Implementation of *Ab Initio* Quantum Chemistry Techniques for Application to Large Molecules

Thesis by
Richard P. Muller
in partial fulfillment of the requirements
of the Degree of Doctor of Philosophy,

California Institute of Technology,
Pasadena, California.
Submitted May 4, 1994.

©1994
Richard P. Muller

Second Revision
©1997 All Rights Reserved.

January 29, 2002

Contents

1 Introduction **4**

2 Overview of *Ab Initio* Electronic Structure Theory **8**
2.1 Introduction 8
2.2 The Electronic Hamiltonian and Hartree-Fock Wave Functions 9
2.3 Open Shell Hartree-Fock Wave Functions 16
2.4 Interpretation of Hartree-Fock Theory Results 18
2.5 Shortcomings of Hartree-Fock Theory 19
2.6 Generalized Valence Bond Theory 20
2.7 Summary of Equations for General HF/GVB Wave Functions 23
2.8 Configuration Interaction 25
2.9 Multi-Configurational Self-Consistent Field Wave Functions 26
2.10 Conclusion 27

3 Pseudospectral - Generalized Valence Bond (PS-GVB) Theory **28**
3.1 Introduction 28
3.2 The Scaling of Hartree-Fock and GVB Calculations 29
3.3 The Pseudospectral Method 29
3.4 Naive Grid-based Calculation of Coulomb and Exchange Matrices . . 30
3.5 Pseudospectral Coulomb and Exchange Operators 33
3.6 Grids, Dealiasing Functions, and Atomic Corrections 34
3.7 The Structure of the PS-GVB Program 36
3.8 PS-GVB Applications 38
3.8.1 Methylene 38
3.8.2 Silylene 41
3.8.3 Ethylene 41
3.9 Conclusion 43

4 Pseudospectral Parameters for Calculations on Nickel Clusters **46**
4.1 Introduction 46
4.2 Nickel Cluster and Metal Bonding 47
4.3 Grid Parameters 48
4.4 Dealiasing Function Parameters 50
4.5 Optimization Procedure 53

4.6 Application to Ni_4 Clusters 55
4.7 Conclusions 56

5 Direct Inversion in the Iterative Subspace Convergence for Generalized Valence Bond Wave Functions 59
5.1 Introduction 59
5.2 Closed-Shell HF-DIIS 61
5.3 General Fock Operators 63
5.3.1 Simplest Approach: Combine Separate Fock Operators 63
5.3.2 The Pulay Multi-shell Fock Operator 64
5.3.3 The Page and McIver Fock Operator 64
5.3.4 The GVB-DIIS Multi-shell Fock Operator 65
5.4 Choice of the Error Vector 65
5.5 Related Convergence Issues 67
5.6 Results 68
5.6.1 One pair GVB wave functions 69
5.6.2 Multiple GVB pair wave functions 71
5.7 Conclusions 77

6 *Ab Initio* Calculation of Porphyrin Excited States 78
6.1 Introduction 78
6.2 The Four-Orbital Model and Four-Orbital Excited States 80
6.3 The Multi-Configurational Nature of FOES 82
6.4 The Frozen Core Four Orbital Excited State Method 83
6.5 Results of FC-FOES Porphine Calculations 85
6.6 Self-Consistent Orbital Optimization in FOES 87
6.6.1 Core-Active Mixing 89
6.6.2 Active-Active Mixing 89
6.6.3 Occupied-Virtual Mixing 90
6.7 PS-GVB Calculation of Multi-Configurational Operators for SC-FOES 91
6.8 Convergence Acceleration in SC-FOES 91
6.9 SC-FOES Results for Porphine 92
6.9.1 Orbital Energies 92
6.9.2 SC-FOES Porphine Calculations 93
6.10 Frozen Core Corrections to SC-FOES: SC-FOES-CI 95
6.11 Reduced Porphyrins 96
6.12 Conclusion 100

A A Technique for Evaluating Hamiltonian Matrix Elements 101
A.1 Introduction 101
A.2 The Method 101
A.2.1 Break Into Individual Determinants 101
A.2.2 Transform to Spin Orbitals 102
A.2.3 Order and Classify Determinants 102
A.2.4 Evaluate Matrix Elements between Operators 103
A.2.5 Transform Back to Spatial Orbitals 103

A.2.6 Example: One Pair GVB Energy 104
A.3 Conclusion 104

B The Self-Consistent Optimization of Restricted Configuration Interaction Wave Functions: Two-Pair, Closed-Shell Special Case 106
B.1 Introduction 106
B.2 The GVB-RCI Wave Function 107
B.3 RCI Spin Coupling 108
B.4 Determinants in the GVB-RCI Wave Function 109
B.5 Matrix Elements Between Determinants in the GVB-RCI Wave Function 110
B.6 The GVB-RCI Energy Expression 112
B.7 Energy Coefficients and the Yaffe-Goddard Form 114
B.8 GVB-RCI Orbital Optimization 116
B.8.1 Active-Core Mixing 117
B.8.2 Active-Active Mixing 118
B.8.3 Occupied-Virtual Mixing 118
B.9 Operators Required For GVB-RCI 119
B.10 Conclusions 119

Bibliography 119

Chapter 1

Introduction

This thesis describes new methods for extending *ab initio* electronic structure theory calculations to larger molecules. *Ab initio* methods are important for investigation of the chemical properties of large molecules because they remain the most accurate method of computing the electronic structure of a molecule. For the purposes of this thesis, the term large molecules refers to those molecules that require more than 200 basis functions (*vide infra*). Molecules of this size are difficult to describe with standard methods in *ab initio* electronic structure theory because they require large amounts of CPU time, disk storage space, and physical memory. Subsequent chapters will describe *ab initio* calculations in greater detail, but to summarize briefly, the principal expense of *ab initio* methods arises from the basis function techniques used to evaluate the two-electron integrals. Basis function methods, also known as spectral methods, expand the one- and two-electron integrals as a sum of integrals that can be evaluated analytically. *Ab initio* calculations use basis function methods because these methods provide a high degree of accuracy, especially for the one-electron terms where the fact that basis functions are analytically differentiable yields highly accurate integration. These methods become expensive as the size of the molecule increases. In particular, evaluation of the two-electron integrals using N_{bf} basis functions scales as $\mathcal{O}(N_{bf}^4)$, which becomes prohibitively expensive as N_{bf} increases. Evaluation of the one-electron integrals using N_{bf} basis functions is much less expensive, scaling only as $\mathcal{O}(N_{bf}^2)$.

The notation $\mathcal{O}(N_{bf}^4)$ denotes that when N_{bf} is doubled, the computation requires $2^4 = 16$ times as much CPU time to complete; similarly, the notation $\mathcal{O}(N_{bf}^2)$ means that when N_{bf} is doubled the computation requires 4 times as much CPU time to complete. When N_{bf} is large—the assumption made throughout the rest of this thesis for scaling comparisons—the higher-order scalings dominate the smaller order ones, so that a calculation that depends upon different elements scaling as $\mathcal{O}(N_{bf}^4)$ and $\mathcal{O}(N_{bf}^2)$ scales overall as $\mathcal{O}(N_{bf}^4)$. Clearly, one of the requirements in making *ab initio* electronic structure calculations possible on larger molecules is to determine methods that scale with molecular size better than $\mathcal{O}(N_{bf}^4)$.

Numerical methods provide a less expensive alternative to integral evaluations. Numerical techniques evaluate one- and two-electron integrals over a grid of points in

three-dimensional space. Numerical methods scale roughly as $\mathcal{O}(N^3)$, where N is related to the number of grid points (*vide infra*). Traditionally, numerical methods have not been used for electronic structure theory because the accuracy required by electronic structure theory can be achieved using numerical methods only with an impractically large number of grid points. The one-electron integrals are particularly difficult to integrate using numerical methods.

For electronic structure theory calculations there has traditionally been a tradeoff between the accuracy of basis function methods and the speed of numerical methods. Because *ab initio* calculations on small molecules are not as computationally intensive as those on larger molecules, basis function methods have predominated. As the size of the molecule—and thus N_{bf}—increases, the $\mathcal{O}(N_{bf}^4)$ scaling of basis function methods makes these methods impossible. Thus, to solve the *ab initio* electronic structure of large molecules new methods must be developed.

The solution to the problem of applying *ab initio* electronic structure theory to large molecules is to use a hybrid approach, the pseudospectral method. The pseudospectral method utilizes the speed of numerical techniques to evaluate the two-electron integrals; and it utilizes the accuracy of basis function techniques to evaluate the one-electron integrals. Evaluation of the two electron integrals using the pseudospectral method with N_{grid} grid points and N_{bf} basis functions scales as $\mathcal{O}(N_{grid}N_{bf}^2)$—approximately $\mathcal{O}(N_{bf}^3)$. At the same time the accuracy achieved by basis function techniques for one electron integrals is preserved with the pseudospectral method. The improvement in scaling from $\mathcal{O}(N_{bf}^4)$ to $\mathcal{O}(N_{bf}^3)$ reduces the expense of calculations on larger molecules, and promises to make *ab initio* electronic theory calculations possible on larger molecules that are impossible with pure basis function techniques.

The work presented in this thesis develops programs that use pseudospectral operator construction to calculate the electronic structure of real chemical systems. Chapter 2 presents an overview of *ab initio* electronic structure theory, describing not only the manner in which basis function techniques are used to evaluate the requisite one- and two-electron operators in electronic structure theory, but also how these operators are used to obtain converged wave functions. Chapter 3 describes the formation of *ab initio* one- and two-electron operators using the pseudospectral method; and it outlines the procedure for using these operators to calculate the electronic structure of molecules with a wide variety of compositions, geometries, orbital occupancies, and wave functions. The orbital optimization techniques used in standard basis function methods are used with the pseudospectral method; this combination results in a program that has the flexibility of the basis function methods and the speed of the pseudospectral operator construction. The accuracy of the pseudospectral method is demonstrated using examples of calculations on methylene, silylene, and ethylene, with a variety of geometries, spin states, and wave functions. Chapter 3 demonstrates that the speed and accuracy pseudospectral methods displayed with closed-shell Hartree-Fock wave functions can be extended to: (i) general wave functions with arbitrary numbers of doubly-occupied core orbitals, singly-occupied open-shell orbitals, and variably occupied GVB natural orbitals; (ii) the calculation of physical properties of molecules rather than total electronic energies; (iii) a variety of quality basis sets, including ones with diffuse functions; (iv) elements not in the first row of the periodic table, in partic-

ular Silicon; (v) molecules that use effective core potentials. This work demonstrates that the pseudospectral method can be applied to any of the molecules containing main group elements that the standard basis function methods can describe.

Chapter 4 extends the methods of Chapter 3 to metallic elements, which present particular problems for the pseudospectral method. The nature of the chemical bonding is qualitatively different between metallic elements than between non-metallic main group elements. Metallic systems have a wider range of bond angles, bond lengths and coordinations than do non-metallic molecules. Moreover, the electrons in metallic systems localize between atoms in metallic systems, whereas the electrons in molecules composed of main-group elements localize on the atoms themselves. Chapter 4 demonstrates that the pseudospectral method can be used to form the *ab initio* one- and two-electron operators for Nickel clusters without loss of accuracy. Chapter 4 also describes the adjustments to the parameters used by the pseudospectral method that are needed to describe these systems. These parameters are optimized using Ni_3 clusters with several different geometries. The generality of the optimized parameters is demonstrated by using them to determine a chemical property of another Ni system. Chapter 4 demonstrates that on the scale of chemical properties the error that the pseudospectral method makes relative to the standard basis function method is negligible. This work demonstrates that with the appropriate modifications to the pseudospectral parameters to reflect the different nature of the metallic bonding, the pseudospectral method may be used to describe metallic systems with virtually no loss of accuracy.

Chapters 3 and 4 present methods to speed the construction of the operators required in *ab initio* electronic structure theory. Operator construction is the most computationally intensive part of an *ab initio* calculation, and fast operator construction is essential for performing this level of calculation on large molecules. Even with fast operator construction *ab initio* calculations can be difficult on large molecules because of slow convergence of the wave function that describes the electronic structure. The electronic wave function is obtained in an iterative fashion. A large number of iterations does not pose a serious difficulty for small molecules because little work is required for each iteration; as the molecular size increases the work required for each iteration becomes significant, and an efficient method for converging the electronic wave function is essential. Chapter 5 introduces the Direct Inversion in the Iterative Subspace method, developed by Pulay for converging Hartree-Fock wave functions, and extends it to general wave functions with arbitrary numbers of doubly-occupied core orbitals, singly-occupied open-shell orbitals, and variably occupied GVB natural orbitals. These general wave functions are necessary to describe physical properties of real chemical systems. The convergence method described in Chapter 5 rapidly converges these wave functions, often in a fraction of the time required by standard convergence methods.

The combination of the fast operator construction described in Chapters 3 and 4 and the rapid convergence algorithm described in Chapter 5 provides a method of accurately computing the electronic structure of large molecules. Chapter 6 describes an application of these methods to porphyrin molecules. Porphyrin molecules are tetrapyrrole rings that appear in a variety of biological applications including the photosynthetic reaction center and the heme group, as well as many applications in chemical catalysis. Because much of the chemistry of porphyrin rings proceeds through the excited states, and because porphyrins are primarily characterized through their

optical absorption spectra, the porphyrin excited states have long been an area of intense experimental and theoretical investigations. Approximate methods of electronic structure calculations have suggested that the porphyrin excited states are composed of coupled single excitations from the ground state. The combination of the large size of the porphyrin rings and the multi-configurational nature of the excited states have prevented *ab initio* calculations on the porphyrin excited states. Chapter 6 presents two different approaches to solve this difficulty, both of which use the pseudospectral method of operator construction. The first method takes advantage of the planar geometry of many porphyrin rings to separate the s and p orbitals of the molecules. A potential to replace the s electrons is calculated using the pseudospectral method. This potential is incorporated into standard basis function methods for calculating the multi-configurational excited states in the p space only. The second method calculates explicitly the multi-configurational excited state energies and optimum orbitals. All of the operators required for the energy expression and orbital optimization equations are computed using the pseudospectral method. Both methods yield excellent agreement with experimental results.

This thesis also includes two appendices. The first appendix describes an effective method to evaluate Hamiltonian matrix elements between electronic wave functions. Such evaluations are necessary in deriving energy expressions for Hartree-Fock, Generalized Valence Bond, and other types of wave functions. They also can be useful in computing coupling terms between ground and excited determinants in Configuration Interaction and properties calculations. The second appendix describes the energy expression and orbital optimization equations for the Restricted Configuration Interaction wave function, a more accurate way to include electron correlation in a wave function that does not require a full transformation of the two-electron integrals. These appendices are included because they may be of help to other researchers in this field.

The work presented in this thesis develops new methods for calculating and converging electronic wave functions. These methods allow ab initio electronic structure theory calculations on molecules much larger than those that can be addressed by standard basis function methods. The use of larger molecules, in turn, allows theoretical chemists to use more accurate models to investigate chemical interactions. This thesis also presents an application of these methods to the study of porphyrin excited states. The calculations on the porphyrins are significant not only because they demonstrate the types of molecules that can be studied with the pseudospectral method, but also because these calculations show good agreement with experimental results for an important class of molecules.

Chapter 2

Overview of *Ab Initio* Electronic Structure Theory

2.1 Introduction

Chapter 2 presents an overview of *ab initio* electronic structure theory and it reviews the standard methods that relate to topics later in this thesis. Section 2.2 describes the nature of electronic wave functions in general, and the closed-shell Hartree-Fock (HF) wave functions in particular. Closed-shell Hartree-Fock wave functions are important because they are the simplest wave functions used in electronic structure theory. Much of the work described in this thesis involves extending methods developed for closed-shell Hartree-Fock wave functions to the more general wave functions described in Section 2.7. Section 2.3 describes open-shell Hartree-Fock wave functions, an extension of closed-shell Hartree-Fock theory to wave functions where some orbitals are singly-occupied. These wave functions are significant because they are the simplest wave functions where orbital optimization between occupied orbitals is necessary.

Hartree-Fock calculations generate a great deal of information about the electronic energy and density of the molecules they describe; Section 2.4 describes how this information is interpreted to yield chemically important insights. Although Hartree-Fock calculations can provide a great deal of important chemical information, there are many types of systems for which these wave functions are impractical or inappropriate, for example distorted or dissociated bonds or excited states. Section 2.5 describes these shortcomings, and Section 2.6 describes a convenient solution to many of them, namely the generalized valence bond wave (GVB) function. Generalized valence bond wave functions introduce degrees of functional freedom to the electronic wave function and allow it to adjust more accurately to its particular environment. In addition, the equations for optimizing this type of wave function are presented in this section.

Section 2.7 summarizes Sections 2.2–2.6 by presenting the form of the general wave function having an arbitrary number of doubly-occupied core orbitals, singly-occupied open-shell orbitals, and variably occupied GVB natural orbitals. The energy expression and orbital optimization equations for this wave function are also presented

in this section. These equations are significant because, as stated earlier, much of the work in this thesis involves expanding methods developed for closed-shell Hartree-Fock calculations to general wave functions of the type described in this section. In particular, Chapter 3 describes expanding the pseudospectral method from one that describes only Hartree-Fock wave functions to one that can describe this type of general wave function. Chapter 5 describes expanding the direct inversion in the iterative subspace method from one that could describe only Hartree-Fock and single-pair generalized valence bond wave functions to one that can describe the type of general wave function described in this section. Moreover, the concepts of orbital optimization described here are also crucial in Chapter 6, where the porphyrin excited state wave functions are optimized.

The final two sections of this chapter describe two other related methods from *ab initio* electronic structure theory. Section 2.8 describes configuration interaction, where the ground state wave function is allowed to mix with excited wave functions. Configuration interaction can more accurately correct the flaws of Hartree-Fock theory than can generalized valence bond theory, but at greater computational cost. Multi-configurational self-consistent field theory, described in Section 2.9, is a method of iteratively optimizing the orbitals of a wave function that consists of more than one electronic configuration. Configuration interaction and multi-configurational self-consistent field theory are significant to the work described in this thesis not only because they present an important contrast to the way that generalized valence bond wave functions describe accurate chemical bonding, but also because these two methods are the methods normally used to describe the porphyrin excited states in Chapter 6, and the methods described in that section are a less expensive method of performing the same calculations.

The next section, Section 2.2, describes the nature of wave function used in *ab initio* electronic structure theory, and it presents the simplest case of these wave functions, the closed-shell Hartree-Fock wave function.

2.2 The Electronic Hamiltonian and Hartree-Fock Wave Functions

Electronic structure theory seeks to find approximate solutions to the non-relativistic time-independent Schrodinger equation [1]

$$H\Psi = E\Psi \tag{2.1}$$

where H is the Hamiltonian operator for the nuclei and electrons in a molecule. H is given by

$$\begin{aligned} H &= -\sum_{i=1}^{N_{el}} \frac{\nabla_i^2}{2} - \sum_{A=1}^{N_{at}} \frac{\nabla_A^2}{2M_A} - \sum_{i=1}^{N_{el}} \sum_{A=1}^{N_{at}} \frac{Z_A}{r_{iA}} \\ &\quad + \sum_{i>j}^{N_{el}} \frac{1}{r_{ij}} + \sum_{A=1}^{N_{at}} \sum_{B=1}^{N_{at}} \frac{Z_A Z_B}{R_{AB}} \end{aligned} \tag{2.2}$$

for a system with N_{el} electrons and N_{at} nuclei, where the quantities in H are expressed in atomic units, M_A is the nuclear mass of atom A in units of electron mass, Z_A is the charge on nucleus A, r_{iA} is the distance of electron i from nucleus A, r_{ij} is the distance between electrons i and j, and R_{AB} is the distance between nuclei A and B.

The Hamiltonian is commonly simplified using the Born-Oppenheimer approximation, which derives from the observation that nuclei are much heavier than electrons, and consequently move much more slowly than do electrons. To a good approximation one can fix the nuclear coordinates and consider only the electronic part of the Hamiltonian. The consequence of this approximation is that the Hamiltonian H now becomes H_{el}, the electronic Hamiltonian, and is given by [1]

$$H_{el} = -\sum_{i=1}^{N_{el}} \frac{\nabla_i^2}{2} - \sum_{i=1}^{N_{el}} \sum_{A=1}^{N_{at}} \frac{Z_A}{r_{iA}} + \sum_{i>j}^{N_{el}} \frac{1}{r_{ij}} \tag{2.3}$$

For simplicity, the terms in H_{el} involving only one electron are grouped into a single term h,

$$h = -\sum_{i=1}^{N_{el}} \left(\frac{\nabla_i^2}{2} + \sum_{i=1}^{N_{el}} \sum_{A=1}^{N_{at}} \frac{Z_A}{r_{iA}} \right) \tag{2.4}$$

and H_{el} is given by

$$H_{el} = h + \sum_{i>j}^{N_{el}} \frac{1}{r_{ij}} \tag{2.5}$$

The nuclear repulsion energy

$$E_{nr} = \sum_{A>B}^{N_{at}} \frac{Z_A Z_B}{R_{AB}} \tag{2.6}$$

is constant for a fixed geometry and can be evaluated separately. H will hereafter refer to only the electronic Hamiltonian H_{el}.

The solutions to H are in the form of a product of molecular orbitals [1]

$$\Psi = \prod_{i}^{N_{el}} \psi_i \tag{2.7}$$

The molecular spin orbitals ψ_i are composed of a spatial function ϕ_i and a spin function θ_i. The spatial orbital ϕ_i is a function of the position r_i of electron i. ϕ_i describes the spatial distribution of electron i such that $|\phi_i(r)|^2 dr$ is the probability of finding the electron in the volume element dr. This probability for each orbital integrated over all space must be one, giving the normalization condition [2]

$$\int \phi_i^*(r)\phi_i(r)dr = 1 \tag{2.8}$$

Spatial molecular orbitals can be taken to form an orthonormal set [1]

$$\int \phi_i^*(r)\phi_j(r)dr = \delta_{ij} \tag{2.9}$$

Orbital ϕ_i also has a spin component θ_i [1]. The spin of an electron in orbital ϕ_i is described by one of the orthogonal pair of functions α—*spin up*—and β—*spin down*. Each spatial orbital can accommodate one electron with α-spin, and one electron with β-spin. Thus, the simple product wave function has the form

$$\phi_1\alpha\phi_1\beta\phi_2\alpha\phi_2\beta\cdots\phi_{N_{occ}}\alpha\phi_{N_{occ}}\beta \tag{2.10}$$

where $N_{occ} = N_{el}/2$. The wave function for an electron that describes both the spatial and spin components is the spin orbital ψ

$$\begin{aligned} \psi_1 &= \phi_1\alpha, \\ \psi_2 &= \phi_1\beta, \\ &\vdots \\ \psi_{2N_{occ}-1} &= \phi_{N_{occ}}\alpha, \\ \psi_{2N_{occ}} &= \phi_{N_{occ}}\beta. \end{aligned} \tag{2.11}$$

Spin orbitals are convenient for evaluating many of the energy expressions in electronic structure theory; Appendix I describes techniques for evaluating matrix elements using spin orbitals.

Because each of the individual orbitals is normalized, the total probability [2] of finding an electron anywhere in the wave function is equal to N_{el}.

$$|\Psi|^2 = \int \Psi^*(1\cdots N_{el})\Psi(1\cdots N_{el})dr_1\ldots dr_{N_{el}} \tag{2.12}$$

The Pauli exclusion principle [1] states that a wave function must change sign when the spatial and spin components of any two electrons are exchanged.

$$\Psi(1,2,\cdots,i,\cdots,j,\cdots,N_{el}) = -\Psi(1,2,\cdots,j,\cdots,i,\cdots,N_{el}) \tag{2.13}$$

The Pauli principle derives from the fact that electrons are indistinguishable particles, so that observable properties of the wave function cannot change upon exchange of electrons. Because these observables depend on $|\Psi|^2$, the wave function must either be symmetric (having the same sign) or anti-symmetric (having opposite sign) when electrons are exchanged. In practice only anti-symmetric wave functions are observed.

Because the wave functions must be anti-symmetric, the simple product wave function form 2.10 will not work. A convenient method of making a simple product wave function anti-symmetric is to write use a Slater determinant. For the two electron simple product wave function $\phi_1(1)\alpha(1)\phi_1(2)\beta(2)$, the anti-symmetric wave function is given by evaluating

$$\Psi(1,2) = 2^{-1/2}\begin{vmatrix} \phi_1(1)\alpha(1) & \phi_1(1)\beta(1) \\ \phi_1(2)\alpha(2) & \phi_1(2)\beta(2) \end{vmatrix} \tag{2.14}$$

$$= 2^{-1/2}\phi_1(1)\phi_1(2)(\alpha(1)\beta(2) - \beta(1)\alpha(2)) \tag{2.15}$$

The generalization of the Slater determinant to an arbitrary number of particles (and using spin orbitals to signify an arbitrary spin coupling) is [2]

$$\Psi(1,2,\ldots,N) = (N!)^{-1/2} \begin{vmatrix} \psi_1(1) & \psi_2(1) & \cdots & \psi_N(1) \\ \psi_1(2) & \psi_2(2) & \cdots & \psi_N(2) \\ \vdots & \vdots & & \vdots \\ \psi_1(N) & \psi_2(N) & \cdots & \psi_N(N) \end{vmatrix} \tag{2.16}$$

The $(N!)^{-1/2}$ is the normalization condition. For convenience, two shorthand notations are often used for 2.16. The first

$$\Psi(1,\ldots,N) = (N!)^{1/2}\mathcal{A}\left[\psi_1(1)\psi_2(2)\cdots\psi_N(N)\right] \tag{2.17}$$

uses the anti-symmetry operator $\mathcal{A}$ to represent the determinant and explicitly normalizes the wave function. The second notation uses Dirac bracket notation

$$\Psi(1,\ldots,N) = |\psi_1(1)\psi_2(2)\cdots\psi_N(N)\rangle \tag{2.18}$$

to represent both the Slater determinant and the normalization constant $(N!)^{-1/2}$. Both notations use only the diagonal of the Slater determinant to represent the wave function.

Because Slater determinants are so commonly used to antisymmetrize wave functions, individual configurations (as shown above) of a wave function are often referred to as determinants.

Even with the restrictions already made, it is not in general possible to solve 2.3 for many electron wave functions. Therefore, rather than solve the exact electronic Hamiltonian given by 2.3 the Hartree-Fock [1] (HF) approximation is made, which solves an electron's wave function in the average field of all the other electrons. This reduces the electronic Hamiltonian to [1]

$$H_{HF} = h + v_{HF} \tag{2.19}$$

where v_{HF} is a two-electron operator representing the Hartree-Fock field. Given a wave function with N doubly-occupied orbitals

$$\Psi = |\phi_1(1)\alpha(1)\phi_1(2)\beta(2)\cdots\phi_N(2N-1)\alpha(2N-1)\phi_N(2N)\beta(2N)\rangle \tag{2.20}$$

we can simplify the notation by writing

$$\Psi = |\phi_1\bar{\phi_1}\cdots\phi_N\bar{\phi_N}\rangle \tag{2.21}$$

$$= |1\bar{1}\cdots N\bar{N}\rangle \tag{2.22}$$

where a bar over an orbital signifies spin down, and no bar signifies spin up, and the order of the orbitals implies electron index. The energy of Ψ is thus given by

$$E = \frac{\langle\Psi|H|\Psi\rangle}{\langle\Psi|\Psi\rangle} \tag{2.23}$$

$$= \frac{\langle 1\bar{1}\cdots N\bar{N}|h + v^{HF}|1\bar{1}\cdots N\bar{N}\rangle}{\langle 1\bar{1}\cdots N\bar{N}|1\bar{1}\cdots N\bar{N}\rangle} \tag{2.24}$$

The denominator will be unity if the wave function is properly orthonormalized. The numerator can be broken into one-electron and two-electron terms, where the one-electron terms are given by

$$\langle 1\bar{1}\cdots N\bar{N}|h|1\bar{1}\cdots N\bar{N}\rangle = \sum_{i=1}^{N} 2h_{ii} \tag{2.25}$$

and the two-electron terms are given by

$$\langle 1\bar{1}\cdots N\bar{N}|v^{HF}|1\bar{1}\cdots N\bar{N}\rangle = \sum_{i,j=1}^{N} (2J_{ij} - K_{ij}) \tag{2.26}$$

The electronic energy is given by

$$E_{el} = \sum_{i}^{N} 2h_{ii} + \sum_{ij}^{N} (2J_{ij} - K_{ij}) \tag{2.27}$$

The J_{ij} terms are matrix elements of the Coulomb operator [2], which is the quantum mechanical operator corresponding to the macroscopic Coulombic repulsion between electrons i and j. The one-particle Coulomb operator $J^i(1)$ is given by

$$J^i(1) = \int \frac{\phi_i^*(2)\phi_i(2)}{r_{12}} dr_2 \tag{2.28}$$

where r_{12} is the distance between electrons 1 and 2. The matrix element J_{ij} is given by

$$J_{ij} = \int \phi_j^*(1) J^i(1) \phi_j(1) dr_1 = \int \phi_i^*(1) J^j(1) \phi_i(1) dr_1 \tag{2.29}$$

This element is commonly written $(ii|jj)$, where the first half of the symbol corresponds to electron 1 and the second part of the symbol corresponds to electron 2.

The K_{ij} terms are elements of the exchange operator [2], which is purely a manifestation of the anti-symmetry of the wave function and has no macroscopic correspondence. The one-particle exchange operator $K^i(1)$ is most easily defined in terms of its action on another orbital ϕ_j:

$$K^i(1)\phi_j(1) = \left(\int \frac{\phi_i^*(2)\phi_j(2)}{r_{12}} dr_2 \right) \phi_i(1). \tag{2.30}$$

The K_{ij} matrix element is given by

$$K_{ij} = \int \phi_j^*(1) K^i(1) \phi_j(1) dr_1 = \int \phi_i^*(1) K^j(1) \phi_i(1) dr_1 \tag{2.31}$$

This matrix element is often written as $(ij|ij)$.

The variational principle states that the energy evaluated via 2.27 of any approximate wave function is an upper bound to the exact energy. Therefore, the optimal

orbitals ϕ_i are those that give the lowest energy of the total wave function. As orbital ϕ_i changes to $(\phi_i + \delta\phi_i) = (\phi_i + \delta)$, the electronic energy from 2.27 changes to [2, 3]

$$E(i+\delta) = E(i) + 4\sum_{i}^{N} \langle \delta | F^i | i \rangle + \mathcal{O}(\delta^2) \tag{2.32}$$

where F^i is the *Fock operator* given by

$$F^i = h + J^i + \sum_{j \neq i} (2J^i - K^i) \tag{2.33}$$

The Fock operator corresponds to the first derivative of the electronic energy with respect to variations in the orbitals. Because $J_{ii} = K_{ii}$,

$$J_{ii} = 2J_{ii} - K_{ii} \tag{2.34}$$

and we can add and subtract self-terms to obtain the closed-shell Fock operator [3]

$$F^c = h + \sum_{j} (2J^j - K^j) \tag{2.35}$$

$$F^c_{ij} = \langle i | F^c | j \rangle \tag{2.36}$$

which is the same for all orbitals in our doubly-occupied core. It is easy to show that variations between occupied orbitals do not change the electronic energy for the closed-shell wave function being considered, and consequently the orbital variations $\delta\phi_i$ must be orthogonal to all occupied orbitals.

In practice, the orbital optimization is achieved by expanding the orbitals in a set of Gaussian basis functions [2] χ_μ

$$\phi_i = \sum_{\mu}^{N_{bf}} c_{\mu i} \chi_\mu \tag{2.37}$$

for a basis set with N_{bf} basis functions. Using Gaussian basis functions both one-electron and two-electron integrals are easily evaluated.

$$h_{ij} = \sum_{\mu\nu}^{N_{bf}} c_{\mu i} c_{\nu j} h_{\mu\nu} \tag{2.38}$$

is the expression for the h_{ij} matrix element, where $h_{\mu\nu}$ is the one electron operator element between basis functions χ_μ and χ_ν, and

$$\begin{aligned} J^k_{ij} &= \langle i | J^k | j \rangle && (2.39) \\ &= (kk|ij) && (2.40) \\ &= \sum_{\mu\nu}^{N_{bf}} c_{\mu i} c_{\nu j} (kk|\mu\nu) && (2.41) \\ &= \sum_{\mu\nu}^{N_{bf}} c_{\mu i} c_{\nu j} \sum_{\sigma\eta}^{N_{bf}} D^k_{\sigma\eta} (\sigma\eta|\mu\nu) && (2.42) \end{aligned}$$

is the expression for the ij-th element of the J^k Coulomb operator and

$$\begin{aligned} K^k_{ij} &= \langle i|K^k|j\rangle && (2.43)\\ &= (ki|kj) && (2.44)\\ &= \sum_{\mu\nu}^{N_{bf}} c_{\mu i}c_{\nu j}(k\mu|k\nu) && (2.45)\\ &= \sum_{\mu\nu}^{N_{bf}} c_{\mu i}c_{\nu j}\sum_{\sigma\eta}^{N_{bf}} D^k_{\sigma\eta}(\sigma\mu|\eta\nu) && (2.46)\end{aligned}$$

is the expression for the ij-th element of the K^k exchange operator. The terms

$$(\sigma\eta|\mu\nu) = \int \frac{\chi^*_\sigma(1)\chi_\eta(1)\chi^*_\mu(2)\chi_\nu(2)}{r_{12}} dr_1 dr_2 \tag{2.47}$$

are the two-electron integrals over basis functions, and

$$D^k_{\sigma\eta} = c_{\sigma k}c_{\eta k} \tag{2.48}$$

is the corresponding density matrix element for orbital ϕ_k. The set of orbitals are varied by varying the coefficients $c_\mu i$ of the basis functions.

A wave function of the form of 2.20 that contains only doubly occupied orbitals is called a closed-shell wave function [3]. Because all of the orbitals can be described by a single Fock operator F^c the wave function is said to have only one shell or Hamiltonian [3].

For closed-shell wave functions, the orbitals are optimized by first forming the closed-shell Fock operator Fc, given by 2.33 [3]. F^c is obtained by first forming the core density matrix D_c

$$D^c_{\sigma\eta} = \sum_i^{occ} c_{\sigma i}c_{\eta i} \tag{2.49}$$

where the summation occurs only over doubly-occupied orbitals. F^c is given by

$$F^c_{\mu\nu} = h_{\mu\nu} + \sum_{\sigma\eta}^{N_{bf}} D^c_{\sigma\eta}\left(2(\mu\nu|\sigma\eta) - (\mu\sigma|\nu\eta)\right) \tag{2.50}$$

in basis-function space, and

$$F^c_{ij} = \sum_{\mu\nu}^{N_{bf}} c_{\mu i}c_{\nu j}F^c_{\mu\nu} \tag{2.51}$$

over molecular orbitals, where i and j now range over both occupied and virtual (unoccupied) orbitals. The Fock matrix in molecular orbital space is diagonalized

$$U^\dagger F U = \epsilon \tag{2.52}$$

and the eigenvectors U_i give the linear combination of occupied and virtual orbitals that give the improved set of orbitals ϕ_i, and the eigenvalues ϵ_i give the orbital energies for these orbitals. This procedure is repeated iteratively until either the orbitals or the energy stops changing; at this point the optimal set of orbitals has been obtained and the wave function is said to be converged.

The next section extends HF wave functions to systems where some orbitals are singly-occupied.

2.3 Open Shell Hartree-Fock Wave Functions

Section 2.2 outlines the equations for closed-shell HF wave functions, which describe molecules where each orbital is doubly-occupied. Many molecules cannot be restricted to this type of wave function, either because of an odd number of electron or because of a spin coupling that forces multiple orbitals to be high-spin coupled. This section describes an extension of the closed-shell HF wave function for such molecules: the open-shell HF wave function. For a molecule that consists of N_c doubly-occupied core orbitals and N_o singly-occupied, high-spin coupled open-shell orbitals, the wave function is given by [3]

$$\Psi = |\phi_1 \bar{\phi_1} \cdots \phi_{N_c} \bar{\phi_{N_c}} \phi_{N_c+1} \cdots \phi_{N_c+N_o}\rangle \tag{2.53}$$

The energy of this wave function is given by [3]

$$E_{el} = \sum_{i}^{N_c+N_o} 2 f_i h_{ii} + \sum_{ij}^{N_c+N_o} (a_{ij} J_{ij} + b_{ij} K_{ij}) \tag{2.54}$$

where f_i is the occupation for orbital i [3]

$$f_i = \quad 1 \quad \phi_i \text{ is doubly-occupied} \tag{2.55}$$

$$f_i = \quad 1/2 \quad \phi_i \text{ is singly-occupied} \tag{2.56}$$

and

$$a_{ij} = 2 f_i f_j \tag{2.57}$$

$$b_{ij} = -f_i f_j \tag{2.58}$$

with the added condition that $b_{ij} = -1/2$ if i and j are both open-shell orbitals. Note that 2.54 reduces to 2.27 when all orbitals are doubly occupied.

Because an open-shell wave function of the form of 2.53 requires two sets of f_i coefficients ($f_i = 1$ and $f_i = 1/2$), the wave function is said to have two shells. Because $(N_o + 1)$ Fock operators are required (see next paragraph), the wave function is said to have $(N_o + 1)$ Hamiltonians.

The procedure for optimizing the orbitals [3, 4] is slightly more complicated with the open-shell wave function in 2.53 than it was for the closed shell wave function in 2.20. For optimizing the occupied orbitals with the unoccupied orbitals $(N_o + 1)$ Fock operators are now required. For the core orbitals, F^c, given by

$$F^c_{\mu\nu} = f_c h + \sum_{k}^{N_{ham}} (a_{ck} J^k_{\mu\nu} + b_{ck} K^k_{\mu\nu}) \tag{2.59}$$

is formed, and for each open-shell orbital

$$F^i_{\mu\nu} = f_i h + \sum_k^{N_{ham}} (a_{ik} J^k_{\mu\nu} + b_{ik} K^k_{\mu\nu}) \tag{2.60}$$

is formed. Note that the summation here is over N_{ham}, the number of Hamiltonians, equal to $N_o + 1$. One density matrix, D_c, is formed for all the core orbitals, and density matrices D_i are formed for each of the open-shell orbitals. The Coulomb and exchange operators associated with each of these density matrices are given by

$$J^k_{\mu\nu} = \sum_{\sigma\eta}^{N_{bf}} D^k_{\sigma\eta} (\mu\nu|\sigma\eta) \tag{2.61}$$

and

$$K^k_{\mu\nu} = \sum_{\sigma\eta}^{N_{bf}} D^k_{\sigma\eta} (\mu\sigma|\nu\eta) \tag{2.62}$$

Forming the matrices in this fashion saves considerable effort because only one Coulomb and one exchange matrix are needed for all of the N_c core orbitals [5].

Once the N_{ham} Fock operators are formed in the basis function space, they are again transformed into molecular orbital space by multiplying by the appropriate transformation coefficients [3, 4, 5]

$$F^k_{ij} = \sum_{\mu\nu}^{N_{bf}} c_{\mu i} c_{\nu j} F^k_{\mu\nu} \tag{2.63}$$

For the core Fock operator F^c, i and j range over all core orbitals and all unoccupied orbitals; for the open shell Fock operator F^k, i and j range over open-shell orbital k and all unoccupied orbitals. Once each Fock operator is transformed to the molecular orbital basis it is diagonalized; the eigenvectors yield the linear combination of orbitals required for the next more optimized set of orbitals, and the eigenvalues yield the orbital energies.

Unlike the closed-shell example given earlier, mixing occupied orbitals that have different f, a, and b coefficients can change the energy. Starting from the energy expression 2.54 and taking the pairwise mixing [3, 4] of orbitals ϕ_i and ϕ_j

$$\phi'_i = \frac{\phi_i + \delta_{ij}\phi_j}{\sqrt{1 + \delta^2_{ij}}} \tag{2.64}$$

and

$$\phi'_j = \frac{\phi_j + \delta_{ij}\phi_i}{\sqrt{1 + \delta^2_{ij}}} \tag{2.65}$$

to preserve orthonormality, and expanding through second order in δ_{ij} gives the equation for the change in energy

$$\Delta E_{ij}(1 + \delta^2_{ij}) = 2\delta_{ij} A_{ij} + \delta^2_{ij} B_{ij} \tag{2.66}$$

where [4]

$$A_{ij} = \langle i|F^j - F^i|j\rangle \tag{2.67}$$

$$B_{ij} = \langle i|F^j - F^i|i\rangle - \langle j|F^j - F^i|j\rangle + \gamma_{ij} \tag{2.68}$$

$$\gamma_{ij} = 2(a_{ii} + a_{jj} - 2a_{ij})K_{ij} + (b_{ii} + b_{jj} - 2b_{ij})(J_{ij} + K_{ij}) \tag{2.69}$$

Requiring the energy change be stationary [3] with respect to δ_{ij} gives

$$\delta_{ij} = -\frac{A_{ij}}{B_{ij}} \tag{2.70}$$

To preserve orbital orthonormality [3], $\delta_{ji} = -\delta_{ij}$. One way of making these variations simultaneously is to form the rotation matrix Δ, the anti-symmetric matrix with zero diagonal defined by [3]

$$\Delta = \begin{bmatrix} 0 & \frac{A_{ij}}{B_{ij}} \\ -\frac{A_{ij}}{B_{ij}} & 0 \end{bmatrix} \tag{2.71}$$

The new set of orbitals $\{\phi^{New}\}$ are obtained from the old set of orbitals $\{\phi^{Old}\}$ via the transformation [5, 6]

$$[\phi^{New}] = \exp(\Delta)[\phi^{Old}] \tag{2.72}$$

This method computes the optimal mixing of the occupied orbitals with respect to each other while preserving orbital orthonormality.

It should be noted that if two orbitals have the same f, a, and b coefficients, as defined by 2.56 and refeq:abdef, $A_{ij} = 0$, and, consequently, no mixing is done between those orbitals [3, 5]. Thus, when the wave function only consists of closed-shell orbitals no occupied-occupied mixing is done, and only occupied-unoccupied mixing is performed via diagonalization of the Fock operator F^c. The occupied-occupied mixing would have no effect because the numerator of the rotation matrix D would be zero, and the orbitals would not change.

In a given iteration [5], first the optimal occupied-occupied mixing is computed via equation 2.72, and the occupied-virtual mixing is computed by forming and diagonalizing the Fock operators for each Hamiltonian, via equations 2.59–2.63. The iterations continue until the orbitals stop changing, at which point the wave function is said to be *converged*.

This section described methods of obtaining converged orbitals and electronic energies for Hartree-Fock wave functions. The next section describes how this data is interpreted to yield chemically significant information about the molecule.

2.4 Interpretation of Hartree-Fock Theory Results

A converged wave function and energy can yield a number of chemically important bits of information. The energy can be used to determine the relative energy of the particular geometry with respect to other conformations or other molecules [1]. Moreover, the square norm of the converged wave function gives the electron density of the wave function [1]. This interpretation of the wave function can be extended to the individual

orbitals, so the electron density in each orbital is easily obtained. The electron density may be used to calculate a set of atomic charges and multipole moments for the molecule [7]. Finally, the individual orbital energies, via Koopman's theorem[1], are often good approximations to the ionization potential of an electron in that orbital.

Although HF wave functions describe important properties of many different types of molecules, there are some types of molecules or states for which HF wave functions are inappropriate. HF wave functions are appropriate for molecules near their equilibrium geometries, but become increasingly problematic as the molecules are distorted. The next section details these and other shortcomings of HF theory.

2.5 Shortcomings of Hartree-Fock Theory

Hartree-Fock theory is appropriate for many different applications in electronic structure theory, especially for the ground states of molecules near their equilibrium geometries. It does have two major shortcomings: it ignores much of the electron correlation, and excited states are difficult to calculate.

The first shortcoming of HF theory is that electron correlation is ignored [1], except in an averaged sense. Electron correlation is the interactions between the motions of the individual electrons, and HF theory, because it calculates an electron's motion in the average field produced by the other electrons rather than the exact positions of the other electrons, leaves much of the electron correlation out.

One manifestation of the incorrect treatment of electron correlation in HF theory is the well-known fact that HF wave functions of the type of equations 2.20 or 2.53 do not dissociate properly. Consider the H2 molecule described by two basis functions, χ_r and χ_l. The ground state HF wave function will be given by

$$\Psi_{HF} = |(\chi_r + \chi_l)(\chi_r + \chi_l)\alpha\beta\rangle \tag{2.73}$$

$$= \frac{1}{\sqrt{2}}[\chi_r\chi_r + \chi_r\chi_l + \chi_l\chi_r + \chi_l\chi_l](\alpha\beta - \beta\alpha) \tag{2.74}$$

which is an accurate description of the bonding when the molecule is near equilibrium bond length. As the molecule dissociates the terms $\chi_l\chi_l$ and $\chi_r\chi_r$ in the wave function become increasingly unstable because they correspond to heterolytic bond cleavage. The wave function should dissociate only to the terms corresponding to homolytic cleavage, $\chi_l\chi_r$ and $\chi_r\chi_l$. The valence bond (VB) wave function starts from the correct dissociation fragments $\chi_l\chi_r$ and $\chi_r\chi_l$. Consequently, the VB wave function is given by

$$\Psi_{VB} = |\chi_l\chi_r\alpha\beta + \chi_r\chi_l\alpha\beta\rangle \tag{2.75}$$

$$= \frac{2}{\sqrt{2}}[\chi_l\chi_r + \chi_r\chi_l](\alpha\beta - \beta\alpha) \tag{2.76}$$

which dissociates to the correct limit because it does not contain the heterolytic cleavage terms $\chi_l\chi_l$ and $\chi_r\chi_r$. A generalization of the VB wave function, the generalized valence bond (GVB) wave function, described at length in the next section, always

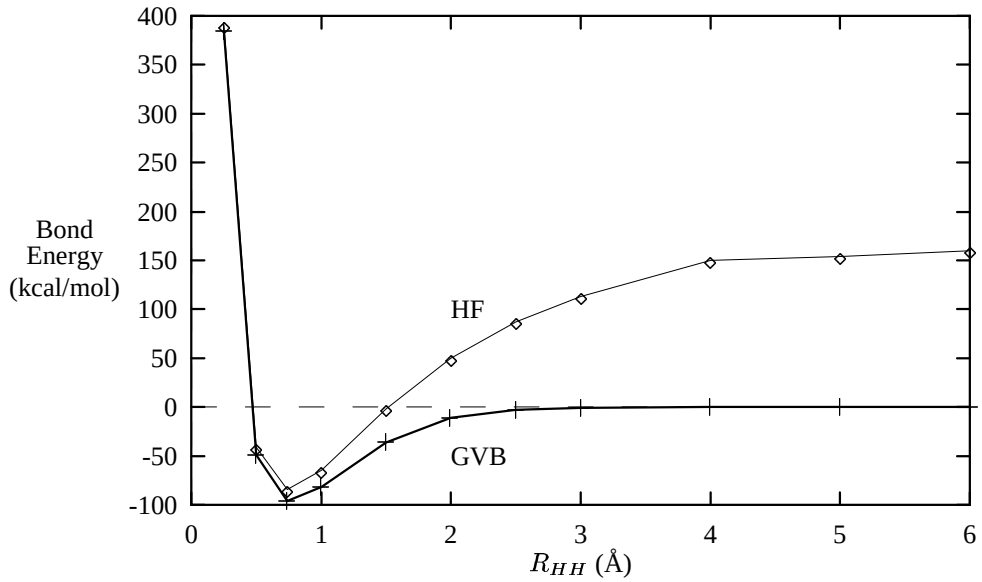

Figure 2.1: Dissociation of diatomics using HF and GVB wave functions.

yields a lower energy than the HF wave functions, but the difference in energies is negligible for small bond distances.

Figure 2.1 shows an example of the incorrect dissociation of HF wave functions. Shown is the dissociation of H_2 using a HF wave function, with respect to the fragment energy of the individual H atoms. On the same plot is the GVB wave function that will be discussed in the next section. As is evident from figure 2.1, the HF wave function dissociates to an incorrect limit, one higher in energy than the individual H fragments. The GVB wave function, on the other hand, dissociates to the correct energy.

Another shortcoming of HF theory is that it is often difficult to converge excited states of wave functions [8]. Unless the excited state has a different overall symmetry than the ground state, it generally collapses to the ground state upon orbital optimization. This prevents HF theory from providing chemically useful information about excitation energies and charge densities of excited states.

The next section presents a simple correction to some of the HF shortcomings, the aforementioned GVB wave function, which generalizes the two electron wave function from equation 2.76 for many electron wave functions.

2.6 Generalized Valence Bond Theory

One simple correction to HF theory that overcomes many of HF's shortcomings is Generalized Valence Bond (GVB) theory [3, 4, 5, 6]. GVB theory replaces the closed-

shell HF wave function

$$\Psi_{HF} = \left| \prod_{i}^{occ} \phi_i^2 \alpha\beta \right\rangle \tag{2.77}$$

with the GVB wave function [3]

$$\Psi_{GVB} = \left| \left[\prod_{i}^{occ} (\phi_{i1}\phi_{i2} + \phi_{i2}\phi_{i1}) \right] \Theta(1, 2, \ldots, N_{occ}) \right\rangle \tag{2.78}$$

where $\Theta(1, 2, \ldots, Nocc)$ is a general spin wave function for the N_{occ} electrons and the GVB orbitals ϕ_{i1} and ϕ_{i2} are not orthogonal. It is generally convenient to replace the general spin coupling Θ in equation 2.78 with the GVB-Perfect Pairing (GVB-PP) wave function where the two electrons in each GVB pair are paired only with each other. This reduces equation 2.78 to [3]

$$\Psi_{GVB} = \left| \prod_{i}^{occ} (\phi_{i1}\phi_{i2} + \phi_{i2}\phi_{i1})\alpha\beta \right\rangle, \tag{2.79}$$

or

$$\Psi_{GVB} = \left| \prod_{i}^{occ} \phi_{i1}\phi_{i2}(\alpha\beta - \beta\alpha) \right\rangle. \tag{2.80}$$

Equation 2.80 may be regarded as a generalization of equation 2.77, where each orbital ϕ_i in equation 2.77 is replaced by a GVB pair consisting of two non-orthogonal orbitals $\phi_{i1}\phi_{i2}$

$$\phi_i\phi_i\alpha\beta \rightarrow \phi_{i1}\phi_{i2}(\alpha\beta - \beta\alpha) = (\phi_{i1}\phi_{i2} + \phi_{i2}\phi_{i1})\alpha\beta. \tag{2.81}$$

For computational purposes, it is convenient to replace the GVB pair

$$(\phi_{i1}\phi_{i2} + \phi_{i2}\phi_{i1})\,\alpha\beta \tag{2.82}$$

with the natural orbital representation [3]

$$(c_{ig}\phi_{ig}\phi_{ig} + c_{iu}\phi_{iu}\phi_{iu})\,\alpha\beta \tag{2.83}$$

where ϕ_{ig} and ϕ_{iu} are now orthogonal and given by

$$\phi_{i1} = \frac{c_{ig}^{1/2}\phi_{ig} + c_{iu}^{1/2}\phi_{iu}}{\sqrt{c_{ig} + c_{iu}}} \tag{2.84}$$

$$\phi_{i2} = \frac{c_{ig}^{1/2}\phi_{ig} - c_{iu}^{1/2}\phi_{iu}}{\sqrt{c_{ig} + c_{iu}}}. \tag{2.85}$$

With the strong orthogonality constraint, which assumes that GVB orbitals of different pairs are orthogonal, the energy may once again be written in the familiar form

$$E_{el} = \sum_{i}^{N_{occ}} 2f_i h_{ii} + \sum_{ij}^{N_{occ}} (a_{ij}J_{ij} + b_{ij}K_{ij}) \tag{2.86}$$

except now f_i is given by [3]

$$f_i = 1 \quad \phi_i \text{ is doubly-occupied} \tag{2.87}$$

$$f_i = 1/2 \quad \phi_i \text{ is singly-occupied} \tag{2.88}$$

$$f_i = c_i^2 \quad \phi_i \text{ is a pair orbital with GVB CI coefficient } c_i. \tag{2.89}$$

Similarly,

$$a_{ij} = 2 f_i f_j \tag{2.90}$$

$$b_{ij} = -f_i f_j \tag{2.91}$$

except that $b_{ij} = -1/2$ if ϕ_i and ϕ_j are both singly-occupied.

Furthermore, if ϕ_i is a pair orbital

$$a_{ii} = f_i \tag{2.92}$$

$$b_{ii} = 0 \tag{2.93}$$

and if ϕ_i and ϕ_j are in the same pair,

$$a_{ij} = 0 \tag{2.94}$$

$$b_{ij} = -c_i c_j \tag{2.95}$$

Because equations 2.66–2.69 in Section 2.3 are derived based on the general energy expression in equation 2.54, the orbital optimization equations are still appropriate for our modified definitions of f_i, a_{ij}, and b_{ij}. Thus, the same equations that were used to optimize open-shell HF wave functions can be used to optimize GVB-PP wave functions.

For a GVB wave function of the form of equation 2.80 with N_p pairs and $2N_p$ natural orbitals (often referred to as a "GVB $N_p/2N_p$" wave function), $2N_p$ different values of f_i are obtained, and hence the wave function is said to have $2N_p$ shells. $2N_p$ Fock operators must also be formed, and hence the wave function is said to also have $2N_p$ Hamiltonians.

The coefficients c_{ig} and c_{iu} for the GVB orbital are optimized each iteration [3, 5] by solving a two-by-two configuration interaction (*vide infra*) for each GVB pair to minimize the overall energy with respect to the c_{ig} and c_{iu} coefficients. This amounts to solving [3]

$$Y^i c_i = c_i E_i \tag{2.96}$$

where

$$Y^i = \begin{bmatrix} Y^i_{gg} & Y^i_{gu} \\ Y^i_{gu} & Y^i_{uu} \end{bmatrix} \tag{2.97}$$

$$Y^i_{gu} = K_{ig,iu} \tag{2.98}$$

$$Y^i_{gg} = \frac{F^{ig}}{f_{ig}} \tag{2.99}$$

$$Y^i_{uu} = \frac{F^{iu}}{f_{iu}} \tag{2.100}$$

The added functional freedom associated with having a pair of orbitals describe the electron pair allows the GVB-PP wave function to incorporate the appropriate amount of ionic and covalent character for any particular internuclear separation. Such a modification to the wave function for the electron pair is tantamount to including electron correlation between the two electrons in the GVB pair. One important result is that GVB-PP wave functions dissociate to the correct limits, yielding accurate physical data for chemical systems. Moreover, by selecting a higher root to equation 2.96 excited states can be selected [8].

Generally, molecular wave functions have a combination of orbitals described by HF and GVB wave functions. The next section summarizes equations from Sections 2.2–2.6 for these wave functions.

2.7 Summary of Equations for General HF/GVB Wave Functions

The orbital optimization equations given in Sections 2.2–2.6 will be referred to often later in this thesis. Consequently, the equations are summarized in this section. The general wave function composed of N_c doubly-occupied core orbitals, N_o singly-occupied open-shell orbitals, and N_p pairs of variably-occupied GVB natural orbitals is given by

$$\Psi = |\Psi_{Core}\Psi_{Open}\Psi_{Pair}\rangle \tag{2.101}$$

where

$$\Psi_{Core} = \prod_{i=1}^{N_c} \phi_i\phi_i\alpha\beta \tag{2.102}$$

$$\Psi_{Open} = \prod_{i=1}^{N_o} \phi_i\alpha \tag{2.103}$$

$$\Psi_{Pair} = \prod_{i=1}^{N_p} (c_{ig}\phi^2_{ig} + c_{iu}\phi^2_{iu})(\alpha\beta - \beta\alpha) \tag{2.104}$$

and c_{ig} and c_{iu} are optimized each iteration via equation 2.96.

The electronic energy of this general wave function is given by

$$E = \sum_{i=1}^{N_{occ}} 2f_ih_{ii} + \sum_{i,j=1}^{N_{occ}} (a_{ij}J_{ij} + b_{ij}K_{ij}). \tag{2.105}$$

Here

$$N_{occ} = N_c + N_o + 2N_p, \tag{2.106}$$

h, J, and K, are the standard one- and two-electron operators given by equations 2.38, 2.42, and 2.46.

Once again, f_i is given by [3]

$$f_i = 1 \quad \phi_i \text{ is doubly-occupied} \tag{2.107}$$

$$f_i = 1/2 \quad \phi_i \text{ is singly-occupied} \tag{2.108}$$

$$f_i = c_i^2 \quad \phi_i \text{ is a pair orbital with GVB CI coefficient } c_i. \tag{2.109}$$

$$a_{ij} = 2f_i f_j, \tag{2.110}$$

$$b_{ij} = -f_i f_j, \tag{2.111}$$

except that $b_{ij} = -1/2$ if ϕ_i and ϕ_j are both singly-occupied.

Furthermore, if ϕ_i is a pair orbital

$$a_{ii} = f_i \tag{2.112}$$

$$b_{ii} = 0 \tag{2.113}$$

and if ϕ_i and ϕ_j are in the same pair,

$$a_{ij} = 0 \tag{2.114}$$

$$b_{ij} = -c_i c_j \tag{2.115}$$

Because the general wave function in equation 2.101 requires $(2 + 2N_p)$ different values of f_i, this wave function is said to have $(2 + 2N_p)$ shells. Furthermore, because the general wave function requires $(1+N_o+2N_p)$ different Fock operators, the general wave function is said to have $(1 + N_o + 2N_p)$ Hamiltonians. These numbers assume that there are both core and open-shell orbitals. If there are no open-shell orbitals but there are core orbitals, the number of shells and Hamiltonians is $(1 + 2N_p)$; similar changes are made when there are no core orbitals.

To optimize the orbitals of this general wave function, first the optimal mixing of the occupied orbitals with the other occupied orbitals is calculated. The optimal mixing is determined by first calculating the Δ matrix,

$$\Delta = \begin{bmatrix} 0 & \frac{A_{ij}}{B_{ij}} \\ -\frac{A_{ij}}{B_{ij}} & 0 \end{bmatrix} \tag{2.116}$$

where

$$A_{ij} = \langle i|F^j - F^i|j\rangle, \tag{2.117}$$

$$B_{ij} = \langle i|F^j - F^i|i\rangle - \langle j|F^j - F^i|j\rangle + \gamma_{ij}, \tag{2.118}$$

$$\gamma_{ij} = 2(a_{ii} + a_{jj} - 2a_{ij})K_{ij} + (b_{ii} + b_{jj} - 2b_{ij})(J_{ij} + K_{ij}) \tag{2.119}$$

The new set of orbitals $\{\phi^{New}\}$ are obtained from the old set of orbitals $\{\phi^{Old}\}$ via the transformation

$$[\phi^{New}] = \exp(\Delta)[\phi^{Old}] \tag{2.120}$$

The next step in the wave function optimization is the calculation of the optimal mixing of the occupied orbitals with the virtual orbitals. This optimization is done by forming the Fock operator

$$F^i_{\mu\nu} = f_i h_{\mu\nu} + \sum_{k=1}^{N_{ham}} (a_{ik} J^k_{\mu\nu} + b_{ik} K^k_{\mu\nu}) \tag{2.121}$$

One Fock operator is required for all of the core orbitals, and another is required for each open-shell and GVB pair orbital. The Fock operator is transformed into molecular orbitals via equation 2.63, and diagonalized. The eigenvectors yield the optimal linear combination of occupied and virtual orbitals to form the new set of occupied orbitals. The optimization process is repeated until the orbitals stop changing.

Much of the work in later sections of this thesis involves extending closed-shell HF methods to the general HF/GVB wave function described in Section 2.6. Chapter 3 combines the standard orbital optimization equations 2.116–2.119 with pseudospectral operator construction to produce a method with the speed of the pseudospectral method and the flexibility of the general HF/GVB wave functions. Likewise, Chapter 5 combines these wave functions with the rapid direct inversion in the iterative subspace convergence method. This method replaces the standard orbital optimization equations with a single Fock matrix diagonalization. Chapter 5 describes a method of incorporating the general HF/GVB wave functions and the standard orbital mixings in the Fock matrix diagonalization. Finally, Chapter 6 uses the pairwise orbital mixings from equations 2.116–2.119 to derive the orbital optimization equations from an energy expression more complex than that in equation 2.105. Although the resulting orbital optimization equations are more complex than those in Section 2.7, the same method of obtaining the improved orbitals by forming and exponentiating the rotation matrix Δ is used with the more complex wave functions there.

The final two sections in this chapter describe more rigorous methods of correcting the shortcomings of HF theory, configuration interaction and multi-configurational self-consistent field theory. These methods can be more accurate than the general wave functions described in this section, but at much greater computational expense.

2.8 Configuration Interaction

Another method of correcting for the shortcomings of HF theory is Configuration Interaction [1] (CI). CI considers the interaction of excited wave functions with the ground state wave function. As with GVB wave functions, the excited wave functions give additional functional freedom for the total CI wave function to use to adjust to find an optimal energy. For a wave function consisting of N spin orbitals

$$\Psi = |12 \cdots i \cdots j \cdots N\rangle \tag{2.122}$$

with unoccupied spin orbitals $\psi_r, \psi_s, \ldots$ the wave function

$$\Psi^r_i = |12 \cdots i \cdots Nr\rangle \tag{2.123}$$

is a singly excited wave function obtained from taking an electron out of occupied orbital ψ_i and putting it into orbital ψ_r. Similarly, the wave function

$$\Psi_{ij}^{rs} = |12 \cdots Nrs\rangle \tag{2.124}$$

is a doubly excited wave function obtained by taking an electron out of each of the occupied orbitals ψ_i and ψ_j and putting them into unoccupied orbitals ψ_r and ψ_s. In a similar fashion triply, quadruply, and so on, excited wave functions may be formed.

CI wave functions can add electron correlation by including a linear combination of excited wave functions with the ground state wave function [1]

$$\Psi_{CI} = \Psi + \sum_{i}^{occ} \sum_{r}^{Virt} C_i^r \Psi_i^r + \sum_{ij}^{occ} \sum_{rs}^{Virt} C_{ij}^{rs} \Psi_{ij}^{rs} + \cdots \tag{2.125}$$

The CI coefficients C are obtained by forming the CI matrix A_{IJ}, whose elements are given by

$$A_{IJ} = \langle \Psi_I | H | \Psi_J \rangle \tag{2.126}$$

where Ψ_I and Ψ_J are any of the ground state or multiply excited wave functions. Diagonalizing A_{IJ} yields the coefficients C as the eigenvectors, and the correlated energy as the lowest eigenvalue. The singly-excited wave functions interact weakly with the ground state, and consequently the doubly-excited determinants are the most important for the correlated energy [1].

The CI wave function can also be used to calculate excited states [8]. When I and J range over the singly-excited determinants the eigenvectors of A_{IJ} yield the linear combination of excited wave functions in the various excited states, and the eigenvalues yield the energies of the excited states.

Although the CI wave function does correct the shortcomings of HF theory, one major drawback is that the elements in A_{IJ} require a full transformation of the two-electron integrals $(\mu\nu|\sigma\eta)$. This transformation scales as $\mathcal{O}(N_{bf}^5)$ where N_{bf} is the number of basis functions. HF and GVB calculations scale only as $\mathcal{O}(N_{bf}^4)$, which means that a CI calculation is significantly more expensive than a HF or GVB calculation for large molecules. For CI calculations diagonalization of the A_{IJ} matrix is often a much more computationally intensive process than the $\mathcal{O}(N_{bf}^5)$ integral transformation, depending on what levels of excitations are included, and so the work required to transform the integrals is negligible. Nonetheless, because the CI calculations scale as at least $\mathcal{O}(N_{bf}^5)$ they are generally too expensive for large molecules, and methods that do not require a full integral transformation, such as the general HF/GVB wave functions described in Section 2.7 become more attractive.

2.9 Multi-Configurational Self-Consistent Field Wave Functions

Another method of correcting the shortcomings of HF theory is the Multi-Configurational Self-Consistent Field (MCSCF) method [1, 6]. Whereas a CI wave

function merely diagonalizes the Hamiltonian matrix between various excited configurations, the MCSCF solve self-consistently for the optimal orbitals among the excited configurations. Again, the additional functional degrees of freedom afforded by the excited wave functions give the total MCSCF wave function the ability to more accurately adjust to the constraints of the molecule, which allows MCSCF wave functions to describe correlated wave functions and excited states. Each iteration the coefficients of the various component wave functions in the MCSCF wave function are recalculated, and the orbitals are optimized using these coefficients. The GVB wave functions described in Section 2.6 are a special case of MCSCF wave function [3]. The GVB wave function does not require an integral transformation to compute its energy and optimize its wave functions, but in general, the MCSCF energy and orbital optimization equations do require a transformation of the two-electron integrals. Like the CI wave function, the integral transformation makes MCSCF calculations prohibitively expensive for large molecules.

CI and MCSCF calculations are the way that calculations on states with more than one significant electron configuration, such as those in Chapter 6 on porphyrin excited states, are normally performed. In Chapter 6 the size of the porphyrin molecule prohibits a full transformation of the two-electron integrals, and consequently the methods presented there are necessary. Although CI and MCSCF wave functions do provide more computational rigor, often general HF/GVB wave functions of the form of equation 2.101 can describe the same interactions with considerably less expense.

2.10 Conclusion

The remainder of this thesis describes improved methods of *ab initio* electronic structure theory. This chapter outlines the foundation upon which the improved methods are built by describing in detail the methods that standard electronic structure theory uses to obtain converged wave functions and electronic energies. In particular, Section 2.7 summarizes the most important equations for converging a general HF/GVB wave function. The methods described in the remainder of this thesis develop faster methods of calculating the operators required in Section 2.7 (Chapters 3 and 4), develop faster convergence methods than equations 2.116–2.119 (Chapter 5), and apply these improved methods to study an important class of large molecules (Chapter 6).

Chapter 3

Pseudospectral - Generalized Valence Bond (PS-GVB) Theory

3.1 Introduction

Chapter 2 outlined the basic methods behind *ab initio* electronic structure theory calculations, particularly for general HF/GVB wave functions. This chapter describes how pseudospectral methods may improve the efficiency of forming the operators required for those calculations. Faster operator construction allows electronic structure calculations on larger molecules. The work presented in this chapter extends the basic pseudospectral program—a numerical method of calculating the Coulomb and exchange operators for HF wave functions—to the general HF/GVB wave functions described in Section 2.7. The resulting program, pseudospectral-generalized valence bond (PS-GVB), maintains the speed advantages of the pseudospectral method and introduces the flexibility of general wave functions, different basis sets, effective core potentials, and new elements.

In this chapter, Section 3.2 discusses scaling considerations between numerical and spectral methods for electronic structure theory calculations. Section 3.3 introduces the pseudospectral method, a hybrid method that uses a numerical integration scheme for the two-electron operators and basis function methods for the one-electron operators. Section 3.4 presents a simple method of constructing Coulomb and exchange operators using a numerical integration scheme rather than the standard basis function methods. Although the simple method presented in Section 3.4 is not accurate enough for the purposes of electronic structure theory calculations, it does demonstrate why numerical integration schemes can be faster than standard basis function methods. Section 3.5 describes how using a least-square's fitting procedure can improve the numerical integration scheme. Section 3.6 describes (i) the grids over which the pseudospectral method performs the numerical integration; (ii) the dealiasing functions that remove noise in the numerical integration caused by finite grids; and (iii) atomic corrections, with which the pseudospectral integration performs part of the integration analytically—over basis functions—and the rest numerically, over grid points. Section

3.7 describes how all of the elements described in Sections 3.2–3.6 are combined to form the Coulomb and exchange operators required to calculate the electronic structure of a general HF/GVB wave function such as the one described in Section 2.7. Finally, Section 3.8 describes applications of the PS-GVB program to a series of molecules that demonstrate the flexibility and accuracy of the method.

3.2 The Scaling of Hartree-Fock and GVB Calculations

The largest impediment to applying HF or GVB theory to large molecules—those requiring more than 200 basis functions—arises from the way these calculations scale with the size of the molecule. For a molecule with Nbf basis functions the amount of time required for a HF or GVB calculation scales as $\mathcal{O}(N_{bf}^4)$, meaning that if N_{bf} is doubled the calculation will require $2^4 = 16$ times as much CPU time to complete. The $\mathcal{O}(N_{bf}^4)$ scaling of HF or GVB calculations is still a significant improvement over the $\mathcal{O}(N_{bf}^5)$ scaling required for a full transformation of the two-electron integrals required for CI and general MCSCF calculations, but even $\mathcal{O}(N_{bf}^4)$ becomes prohibitively expensive for large molecules.

The most computationally intensive step in a HF or GVB calculation is the formation of the Coulomb and exchange matrices. Recalling equations 2.42–2.46, these matrices for Hamiltonian k—where k can represent either a closed shell or an open shell Hamiltonian—are formed from the corresponding density matrix $\mathbf{D}^k$ and the two-electron integrals $(\mu\nu|\sigma\eta)$ via [2]

$$J_{\mu\nu}^k = \sum_{\sigma\eta}^{N_{bf}} D_{\sigma\eta}^k (\mu\nu|\sigma\eta) \tag{3.1}$$

and

$$K_{\mu\nu}^k = \sum_{\sigma\eta}^{N_{bf}} D_{\sigma\eta}^k (\mu\sigma|\nu\eta). \tag{3.2}$$

Because each element of the J or K operators requires a summation over N_{bf}^2 elements, and because there are N_{bf}^2 elements in each operator, forming an entire J^k or K^k matrix requires an $\mathcal{O}(N_{bf}^4)$ process. Such a process becomes too expensive for large molecules.

3.3 The Pseudospectral Method

The basis function techniques, also known as spectral techniques, used to compute the one-electron, Coulomb, and exchange matrices via equations 2.38–2.46 yield excellent accuracy, particularly for the one-electron terms, where basis functions provide an accurate method of calculating derivatives because they are themselves analytically differentiable. Unfortunately, as the previous section shows, the scaling of basis function techniques with the size of the basis set is poor.

Numerical techniques, also known as grid-based techniques or physical space techniques, can be much faster for the types of calculations needed to form the Coulomb and exchange matrices. These techniques evaluate the requisite integrals over a grid of points in three-dimensional space. Although such a method of evaluating integrals is fast, the integrals are not as accurate as those from basis function techniques, particularly the one-electron terms.

The solution [9, 10, 11, 12, 13, 14, 15, 16] is to use a combination of basis function and numerical techniques. Numerical techniques are used to form the Coulomb and exchange matrices, which are subsequently transformed back to basis function space, and added to the one-electron matrix calculated over basis functions. The result is a reduction of the formal scaling of the electronic structure calculation from $\mathcal{O}(N_{bf}^4)$ to $\mathcal{O}(N_g N_{bf}^2)$ (where N_g is the number of gridpoints used in the numerical part), which is roughly equal to $\mathcal{O}(N_{bf}^3)$. This method is called pseudospectral [9] because rather than only using spectral (basis function) methods, it uses a combination of grid-based and spectral methods. The factor of Nbf saved in the scaling makes pseudospectral techniques much better suited to large molecules.

3.4 Naive Grid-based Calculation of Coulomb and Exchange Matrices

The derivation of the pseudospectral formulas for the Coulomb and exchange operators begins in this section with a simplified numerical formulation of these operators. This naive formulation is not accurate enough for electronic structure theory, but provides a convenient bridge between the spectral formalism presented in Chapter 2, and the pseudospectral formalism presented in this chapter. Section 3.5 shows that the final forms of the pseudospectral Coulomb and exchange operators is very similar to the naive numerical forms presented in this section.

Rewriting the Coulomb operator in equation 2.42 in the more appropriate form

$$J_{\mu\nu}^k = \langle \chi_\mu | J^k | \chi_\nu \rangle \tag{3.3}$$

$$= \int \chi_\mu^*(1) J^k(1) \chi_\nu(1) dr_1 \tag{3.4}$$

where

$$J^k(1) = \sum_{\sigma\eta} D_{\sigma\eta}^k \int \frac{\chi_\sigma^*(2)\chi_\eta(2)}{r_{12}} dr_2 \tag{3.5}$$

and r_{12} is the distance between electrons 1 and 2. The Coulomb operator may be formed numerically by first forming the matrix [9]

$$A_{\sigma\eta}(r_g) = \int \frac{\chi_\sigma^*(2)\chi_\eta(2)}{|r_2 - r_g|} dr_2 \tag{3.6}$$

over a set of gridpoints at coordinates $r_g = (x_g, y_g, z_g)$. The numerical analog to the spectral $J^k(1)$ operator in equation 2.28 is formed via

$$J^k(r_g) = \sum_{\sigma\eta} D_{\sigma\eta}^k A_{\sigma\eta}(r_g). \tag{3.7}$$

The collocation matrix [9] $R(r_g, n)$ is defined as the basis function χ_η evaluated at grid point r_g

$$R(r_g, \eta) = \chi_\eta(r_g). \tag{3.8}$$

Using the collocation matrix, a naive definition of the Coulomb operator is [10]

$$J^k_{\mu\nu} = \sum_g^{N_g} R(r_g, \mu) J^k(r_g) R(r_g, \nu) \tag{3.9}$$

or

$$J^k_{\mu\nu} = \sum_g^{N_g} R(r_g, \mu) \left[\sum_{\sigma\eta} D^k_{\sigma\eta} A_{\sigma\eta}(r_g) \right] R(r_g, \nu). \tag{3.10}$$

The integration over the coordinates of electron 2 (the formation of $A_{\sigma\eta}(r_g)$ in equation 3.6) is still done using basis functions, whereas the integration over the coordinates of electron 1 (the final formation of $J^k_{\mu\nu}$ in equation 2.61) is done numerically using the set of grid points.

By similar reasoning, the numerical exchange operator may be formed. Writing the exchange operator in the more appropriate form

$$K^k_{\mu\nu} = \langle \chi_\mu | K^k | \chi_\nu \rangle \tag{3.11}$$

$$= \int \chi^*_\mu(1) K^k(1) \chi_\nu(1) dr_1 \tag{3.12}$$

where

$$K^k(1)\chi_\nu(1) = \sum_{\sigma\eta} D^k_{\sigma\eta} \left(\int \frac{\chi^*_\sigma(2)\chi_\nu(2)}{r_{12}} dr_2 \right) \chi_\nu(1). \tag{3.13}$$

The exchange operator may be formed numerically by again first forming the matrix

$$A_{\sigma\nu}(r_g) = \int \frac{\chi^*_\sigma(2)\chi_\nu(2)}{|r_2 - r_g|} dr_2. \tag{3.14}$$

The numerical analog to the spectral space product $K^k(1)\chi_\nu(1)$ in equation 2.30 is [9]

$$K^k(r_g) R(r_g, \nu) = \sum_{\sigma\eta} D^k_{\sigma\eta} A_{\sigma\nu}(r_g) R(r_g, \eta) \tag{3.15}$$

and a naive definition of the numerical exchange operator is thus given by [10]

$$K^k_{\mu\nu} = \sum_g^{N_g} R(r_g, \mu) \sum_{\sigma\eta} D^k_{\sigma\eta} A_{\sigma\nu}(r_g) R(r_g, \eta) \tag{3.16}$$

The naive numerical Coulomb and exchange matrices in equations 3.10 and 3.16 are unfortunately not accurate enough to be useful in electronic structure theory. These definitions are important because their conceptual simplicity makes their derivation from the standard Coulomb and exchange matrices, equations 2.61 and refeq:kkop,

straightforward. Moreover, as the next section shows, the final pseudospectral form of the Coulomb and exchange matrices is quite similar to the naive numerical forms here.

The simple form of the numerical operators presented in this section also makes scaling comparisons easy. Forming the spectral Coulomb operator given in equation 2.61 requires the following operations in a Fortran program [5]:

```
do k = 1, nham
     do ij = 1, nbf*nbf
          j(k,ij)=0.
          do kl = 1, nbf*nbf
               j(k,ij) = j(k,ij) + den(k,kl)*int(ij,kl)
          enddo
     enddo
enddo
```

where the matrix element `j(k,ij)` in the program corresponds to the Coulomb operator element $J^k_{\mu\nu}$ in equation 2.61, `den(k,kl)` corresponds to density matrix element $D^k_{\sigma\eta}$ in equation 2.48, and `int(ij,kl)` corresponds to the two-electron integral $(\mu\nu|\sigma\eta)$ in equation. It is evident that forming all of the Coulomb matrix elements requires $N_{ham}N^4_{bf}$ operations, or $\mathcal{O}(N^4_{bf})$, assuming that N_{ham} is much smaller than and independent of N_{bf}.

In contrast to the $\mathcal{O}(N^4_{bf})$ scaling of the spectral Coulomb operator, the first step in forming the naive numerical Coulomb operator in equation 3.10 is the formation of the $D^k_{\sigma\eta}A_{\sigma\eta}(r_g)$ product, requiring operations of the form [16]

```
do k = 1, nham
     do rg = 1, ngrid
          j(k,rg) = 0.
          do kl = 1, nbf*nbf
               j(k,rg) = j(k,rg) + den(k,kl)*A(kl,rg)
          enddo
     enddo
enddo
```

which requires a total of $N_{ham}N_{grid}N^2_{bf}$ operations. The next step is the final summation, which requires operations of the form [16]

```
do k = 1, nham
     do i = 1, nbf
          do j = 1, nbf
               do rg = 1, ngrid
                    j(k,ij) = j(k,rg)*R(rg,i)*R(rg,j)
               enddo
          enddo
     enddo
enddo
```

requiring another $N_{ham}N_{grid}N^2_{bf}$ operations. Thus, the naive numerical algorithm is faster than the spectral formulation because it requires $\mathcal{O}(N_{grid}N^2_{bf})$ operations instead

of $\mathcal{O}(N_{bf}^4)$ operations. In practice, although N_{grid} is larger than N_{bf}, it is smaller than N_{bf}^2, and increases proportionally to the size of the molecule, and thus proportionally to N_{bf}.

The actual programs [16] that form the spectral and numerical Coulomb operators use routines to construct the matrices that are more efficient than those in equations 3.10 and 3.16, but the inherent scaling of each routine is dictated by the form expressed in those equations.

The next sections detail methods of making the numerical Coulomb and exchange operator formation accurate enough for use in *ab initio* electronic structure calculations.

3.5 Pseudospectral Coulomb and Exchange Operators

The numerical integration in equations 3.10 and 3.16 is not accurate enough to make the pseudospectral method useful for electronic structure theory. To make the integration more accurate, the product

$$J^k(r_g)R(r_g,\nu) = \left[\sum_{\sigma\eta} D^k_{\sigma\eta} A_{\sigma\eta}(r_g)\right] R(r_g,\nu) \tag{3.17}$$

is fit onto a set of basis functions via a least squares fitting procedure [10], and is then multiplied by the collocation matrix $R(r_g,\mu)$. Thus,

$$\begin{aligned} J^k(r_g)R(r_g,\nu) &= \left[\sum_{\sigma\eta} D^k_{\sigma\eta} A_{\sigma\eta}(r_g)\right] R(r_g,\nu) && (3.18)\\ &= \sum_{\sigma} c_\sigma R(r_g,\sigma) && (3.19) \end{aligned}$$

In matrix form,

$$(\mathbf{D}^k\mathbf{A})\mathbf{R} = \mathbf{R}\mathbf{c}, \tag{3.20}$$

where the matrices $\mathbf{D}^k$, $\mathbf{A}$, and $\mathbf{R}$ in equation 3.20 replace the individual elements in equation 3.19.

Multiplying both sides of equation 3.20 by the transpose of the collocation matrix, $\mathbf{R}^\dagger$,

$$\mathbf{R}^\dagger(\mathbf{D}^k\mathbf{A})\mathbf{R} = \mathbf{R}^\dagger\mathbf{R}\mathbf{c}, \tag{3.21}$$

and solving for $\mathbf{c}$ yields

$$\mathbf{c} = [\mathbf{R}^\dagger\mathbf{R}]^{-1}\mathbf{R}^\dagger(\mathbf{D}^k\mathbf{A})\mathbf{R}. \tag{3.22}$$

In practice [10] this procedure can be made more accurate by using a quadrature scheme where each gridpoint has a different weight, w_g. Using such a scheme modifies equation 3.22 to

$$\mathbf{c} = [\mathbf{R}^\dagger\mathbf{w}\mathbf{R}]^{-1}\mathbf{R}^\dagger(\mathbf{w}\mathbf{D}^k\mathbf{A})\mathbf{R}. \tag{3.23}$$

Inserting equation 3.23 into 3.19 , and multiplying by the other collocation matrix to form the Coulomb matrix, yields [11]

$$\mathbf{J}^k = \mathbf{S}[\mathbf{R}^\dagger\mathbf{w}\mathbf{R}]^{-1}\mathbf{R}^\dagger(\mathbf{w}\mathbf{D}^k\mathbf{A})\mathbf{R}, \tag{3.24}$$

where $\mathbf{S}$ is the usual overlap matrix between the basis functions, produced by the product of $\mathbf{R}^\dagger \mathbf{w} \mathbf{R}$. Thus, the final result of the least-squares fitting procedure is to replace equation 3.10 with

$$J^k_{\mu\nu} = \sum_g^{N_g} Q(r_g, \mu) \left[\sum_{\sigma\eta} D^k_{\sigma\eta} A_{\sigma\eta}(r_g) \right] R(r_g, \nu) \tag{3.25}$$

where the matrix $\mathbf{Q}$ is given by [11]

$$\mathbf{Q} = \mathbf{S}[\mathbf{R}^\dagger \mathbf{w} \mathbf{R}]^{-1} \mathbf{R}^\dagger \mathbf{w}. \tag{3.26}$$

One of the reasons so much emphasis was placed on the naive equations for the two-electron operators in the Section 3.4 is that, as equation 3.25 shows, they have very similar form to the final equations, the only difference being that $R(r_g, \mu)$ in equation 3.10 is replaced by $Q(r_g, \mu)$ in equation 3.25.

In a similar fashion, fitting the product

$$K^k(r_g) R(r_g, \nu) = \left[\sum_{\sigma\eta} D^k_{\sigma\eta} A_{\sigma\eta}(r_g) \right] R(r_g, \eta) \tag{3.27}$$

onto a set of basis functions via a least squares fitting procedure and multiplying the result by the collocation matrix $R(r_g, \mu)$ has the effect of replacing (3.5.14) with [11]

$$K^k_{\mu\nu} = \sum_g^{N_g} Q(r_g, \mu) \left[\sum_{\sigma\eta} D^k_{\sigma\nu} A_{\sigma\eta}(r_g) \right] R(r_g, \eta) \tag{3.28}$$

where $\mathbf{Q}$ is once again given by equation 3.26.

The least squares fitting procedure for the Coulomb matrix in equation 3.25 and for the exchange matrix in equation 3.28 provides greater accuracy than do the naive numerical Coulomb and exchange formulae in equations 3.10 and 3.16. The least squares procedure is necessary to achieve the high degree of accuracy required by electronic structure theory calculations without using an impossibly large number of grid points in the numerical integration procedure.

3.6 Grids, Dealiasing Functions, and Atomic Corrections

This section describes three components of the pseudospectral method: quality grids, dealiasing functions, and atomic corrections. These components significantly increase the accuracy of the numerical integration scheme in the pseudospectral method.

The pseudospectral method requires accurate molecular grids over which to perform the numerical integration [12, 13, 14]. These molecular grids are obtained by patching together atomic grids. The atomic grids are a set of concentric spherical grids of different radii from the nucleus. The spherical grids are based on the Lebedev grids

[12, 17, 18] which integrate the spherical harmonics exactly and have either octahedral or icosahedral symmetry. The symmetry of the grids is important to insure that the PS-GVB results are independent of orientation, and that small changes in molecular geometry do not cause large changes in the PS-GVB accuracy. These grids are placed at selected radii to achieve a higher density of gridpoints near the nucleus than away from it. The atomic grids are patched together by removing gridpoints beyond the Voronai surface [11] between adjacent atoms; often additional points beyond the surface are retained with diminished grid weights to allow the grids to dissociate smoothly [12]. The atomic grids are specific to each element, and parameters must be determined for every new element the pseudospectral method can describe.

Dealiasing functions are an additional set of N_{daf} basis functions that are added to the basis set to make the least squares fit more accurate [10, 11]. These functions are necessary because the action of the Coulomb or exchange operator on a basis function

$$J^k(r_g)R(r_g,\nu) = \left[\sum_{\sigma\eta} D^k_{\sigma\eta} A_{\sigma\eta}(r_g)\right] R(r_g,\nu) \tag{3.29}$$

contains an *alias*—noise that is outside of the basis set due to finite grid size. By least squares fitting onto a set of $(N_{bf} + N_{daf})$ functions the alias can be discarded so that it does not contaminate the genuine part of the integration product in equation 3.29. Because the alias is generated by finite grid size, the nature of the dealiasing functions is closely tied to the particular characteristics of the grid. Consequently, different dealiasing sets are chosen for each atomic grid, and each dealiasing set must be modified whenever the grid changes.

The dealiasing functions do not severely affect the overall scaling of the pseudospectral calculation because they are used only for the least-squares fitting procedure and then are discarded. The dealiasing functions are discarded by replacing overlap matrix S in the Q matrix definition in equation 3.26 with the overlap of the basis set with the dealiasing set, which projects out any character on the dealiasing functions.

As Section 3.5 describes, for two-electron operator construction basis set methods offer high accuracy at high computational expense, whereas numerical methods offer lesser computational expense with slightly lesser accuracy. It is possible to evaluate a few of the dominant integrals using basis functions, and evaluate the remaining part of the integration using the numerical grid. Integrals of the type $(\mu\nu|\sigma\eta)$, with all four basis functions on the same atom, can be included at virtually no extra cost because there are only $\mathcal{O}(N_{at})$ (where N_{at} is the number of atoms in the molecule and is much less than N_{bf}) such terms, negligible compared to the $\mathcal{O}(N_g N_{bf}^2)$ scaling of the pseudospectral integration scheme. These integrals can be evaluated more accurately using basis functions, which leads to greater overall accuracy in the integration scheme.

These corrections are called *atomic corrections* [11]. When all integrals that have all four basis functions on the same atom are included analytically, the program is said to use one center corrections (1C). When all integrals that have all four basis functions on two atoms are included analytically the program is said to use two center corrections (2C) [12]. Faster methods of evaluating two electron integrals allow higher levels of atomic corrections to be included. Atomic corrections improve the accuracy of the program because highly localized integrals, e.g., those with all four basis functions on

the same atom, are the most difficult to integrate numerically. By integrating these functions analytically, higher accuracy may be achieved. Moreover, fewer gridpoints are required for the remaining integrations, and hence the program can run faster to achieve the same level of accuracy.

3.7 The Structure of the PS-GVB Program

The Pseudospectral-Generalized Valence Bond (PS-GVB)[15, 16] program uses pseudospectral operator construction to solve HF and GVB wave functions whose energy expression is of the form in equation 2.105. PS-GVB combines the speed of PS with the flexibility of the GVB wave function optimization as described in Section 2.7.

Because PS-GVB is targeted toward large molecules, disk storage and physical memory must be carefully monitored so that their size does not increase unmanageably as the size of the molecule is increased. Specifically, no matrices larger than Nbf2 may be stored, and only two Nbf matrices may be kept in memory at any given time. Although these constraints somewhat limit the way the PS-GVB program may be arranged, they allow very large molecules to be computed.

As a preprocessing step the least squares fitting matrix Q and the trial wave function are computed. In the main SCF program these matrices are input and the iterative sequence begins. At the beginning of each iteration the density matrix for each of the required Hamiltonians is computed. The corresponding Coulomb and exchange matrices are formed from the density matrix via equations 3.25 and 3.28. These matrices are stored on disk, and then the next Hamiltonian's density matrix, Coulomb, and exchange operators are computed and stored [16]. This sequential method is slower than the method the GVB programs such as GVB2P5 use. In GVB2P5 [5], a large buffer of memory is allocated for the integrals. This buffer is filled with as many $\mu\nu$ pairs of the $(\mu\nu|\sigma\eta)$ integrals as it can hold; these integrals are read off of disk storage and held in physical memory in the buffer space. The $\sigma\eta$ components are multiplied by the $\sigma\eta$ components of all of the density matrices at once, forming the first $\mu\nu$ elements of all of the Coulomb (or exchange) matrices. Pictorially, the transformation is shown in Figure 3.1. Here the last matrix ("Ints") can have any number of columns, corresponding to the buffer space of physical memory. Formation of two-electron integrals in this fashion is particularly fast because the transformation shown in Figure 3.1 can be performed using matrix multiply routines, which are very efficient on computers with vector processors.

Although such a procedure is fast, it uses too much memory to be practical for large molecules. The Coulomb and density matrices are each $(N_{ham}N_{bf}^2)$ long, and the buffer space that holds the integrals is $(N_{buff}N_{bf}^2)$ long. This yields a total memory size of $(3N_{ham} + N_{buff})N_{bf}^2$—a number that rapidly approaches $N_b f^4$. The goal of the PS-GVB program is to keep memory and disk space requirements to $\mathcal{O}(N_{bf}^2)$, and hence memory use in the PS-GVB program is limited to two N_{bf}^2 matrices. Consequently, PS-GVB uses a sequential procedure to compute the two-electron operator. In this procedure, as each shell's density matrix $\mathbf{D}^k$ is formed the corresponding Coulomb and exchange matrices $\mathbf{J}^k$ and $\mathbf{K}^k$ are computed and stored on disk. Then the next

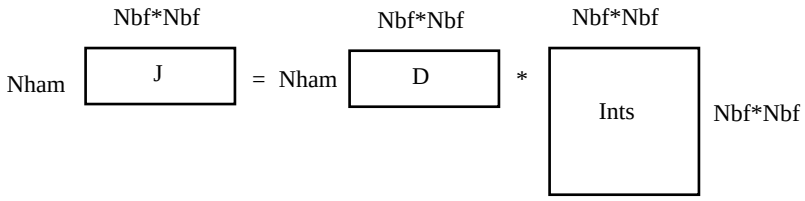

Figure 3.1: GVB2P5 formation of multiple Coulomb operators.

density matrix is formed, and so on. Although this procedure cannot take advantage of matrix multiply routines to form all of the Coulomb and exchange matrices at once, with the use of out-of-core math routines memory use is kept to $2N_{bf}^2$. Because of such care to keep memory use down, PS-GVB is capable of calculating the electronic structure of molecules with many more basis functions than the GVB2P5 limit of 180 without the memory increasing unmanageably.

Once the Coulomb and exchange matrices for all of the shells have been formed and stored on disk, the orbital optimization procedure begins. First the optimal mixing of the occupied orbitals is computed, following the procedure outlined in equations 2.116–2.119. Then Fock operators for the core, open shell, and GVB pairs are formed and diagonalized, via the procedure outlined in equation 2.121. The procedure is essentially the same as that in GVB2P5, except, as with orbital construction, memory use is kept to $2N_{bf}^2$. In forming the necessary matrices for orbital optimization, only one (N_{bf}^2) matrix $(\mathbf{h}, \mathbf{J}^c, \mathbf{K}^c, \ldots)$ is input at a given time, and from this matrix all of the orbital optimization terms that depend upon it are computed before the next matrix is input. This keeps disk access to a minimum, which significantly speeds up the PS-GVB program because every time a disk is accessed the rest of the program must wait for the access to complete before it can continue.

PS-GVB combines the flexibility of general wave functions having arbitrary numbers of core, open shell, and GVB orbitals with the speed of pseudospectral operator construction. The result is a program capable of much larger molecules than had previously been calculated. The GVB2P5 program had a limit of 180 basis functions. This limit is caused primarily by an indexing procedure GVB2P5 uses to store the sorted two-electron integrals, but even without that limit it would be extremely difficult to compute molecules much larger than that because of the high memory use and the slow two-electron operator construction. The limit of 180 basis functions means that GVB2P5 is limited to molecules with roughly 7 heavy atoms and the associated H's, and even molecules of that size run extremely slowly. In contrast, PS-GVB is routinely capable of calculating molecules with 500 basis functions (20-30 heavy atoms), and has on occasion run molecules with as many as 1500 basis functions.

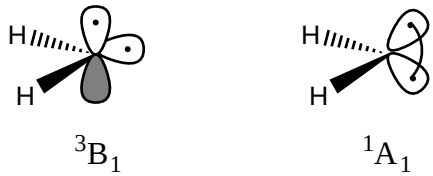

Figure 3.2: Ground ($^3B_1$) and first excited ($^1A_1$) states of methylene.

3.8 PS-GVB Applications

This section describes results for three test systems that demonstrate the accuracy with which PS-GVB reproduces the results of a program (GVB2P5) that uses standard methods to compute the molecular integrals [15]. The systems described here are methylene (CH_2), silylene (SiH_2), and ethylene (C_2H_4). While these are not large molecules by any definition, this work confirms many important aspects of the PS-GVB program necessary before application to larger systems. This research demonstrates four crucial aspects of PS-GVB: (i) that PS-GVB is capable of using general GVB wave functions of the type described in Section 2.7; (ii) that PS-GVB is capable of working on elements that are not in the first row of the periodic table; (iii) that PS-GVB is capable of working with effective core potential to replace the core electrons; and (iv) that PS-GVB is capable of reproducing bond energies and other physical quantities to a high degree of accuracy.

In contrast to earlier work with the pseudospectral algorithm [12], each example given here computes physical quantities—energy differences, excitation energies, or dissociation energies—rather than merely the total energies. For methylene and silylene the quantities considered here are the differences in energy between the singlet and the triplet states. In addition, an effective core potential is tested for Si to demonstrate that PS-GVB is compatible with core potentials. For ethylene the quantities computed are the π–π^* excitation energy, the rotational barrier about the C-C bond, and the energy required to double the C-C bond length.

3.8.1 Methylene

The first system studied in this section is methylene, CH_2. The ground state of methylene is a triplet state with $^3B_1$ symmetry and σ and π nonbonding orbitals, and the first excited state is a singlet with $^1A_1$ symmetry with the two nonbonding electrons spin paired [19], as shown in Figure 3.2.

Because of the difference in the nonbonding orbitals the geometries of the two states are quite different. Using the GVB-CI configuration interaction program, Harding and Goddard [19] determined R_{CH} = 1.084 Å, θ_{HCH} = 133.2° for the triplet state, and R_{CH} = 1.113 Å, θ_{HCH} = 101.8° for the singlet state. The same calculations determined that the triplet-singlet gap is 9.09 kcal/mol.

In studying methylene, the goals are to test (i) the accuracy of PS-GVB with a variety of high quality basis sets, and (ii) the accuracy of PS-GVB with wave functions

more accurate than simple HF, i.e., those with GVB pairs correlating the bonds.

Tables 3.1 and 3.2 show the results of calculations on methylene with a variety of basis sets and wave functions. Three different basis sets are used [20, 21]:

VDZ uses the Dunning-Huzinaga valence double-zeta basis set (based on (9s/5p)) with one set of d polarization functions (a = 0.64) on C, and the Dunning-Huzinaga basis (based on four s functions contracted to two, with the exponents scaled by z=1.2) and one set of p functions (a = 1.0) on H.

VDZ2 replaces the 4s H scaled basis with a 6s H unscaled basis, contracted to 3s triple zeta. The d and p polarization functions in this basis are replaced by pair of functions scaled by the factors $(2.3)^{1/2}$ and $(2.3)^{-1/2}$ from the above values.

VDZ+ adds to the second basis a diffuse set of s and p functions (as = 0.45, ap = 0.34) on the C atom, optimized for the negative ion of C.

In describing the basis sets, the symbol ζ denotes an effective Slater exponent, whereas α denotes a Gaussian exponent. Thus, for H, ζ = 1.2 implies that the standard exponents for the Gaussian expansion have all exponents scaled by 1.44.

For the triplet state, the two C-H bonds are correlated with GVB pairs, leading to two pairs overall, and for the singlet state the two C-H bonds and the doubly-occupied lone pair are correlated with GVB pairs, leading to three pairs overall. These wave functions have the same total number of orbitals, yielding to a consistent level of description for the two states.

Table 3.1 compares total energies for the various calculations on methylene. The GVB2P5 results are expressed in hartrees, and the PS-GVB results are expressed as the difference in kcal/mol from the GVB2P5 results. Results for PS-GVB program are reported using both one center atomic corrections (PS-GVB 1C) and two center atomic corrections (PS-GVB 2C).

For the singlet state, using one-center corrections, the errors in the total energy range from 0.015 to 0.032 kcal/mol; when two-center corrections are employed this error drops to a maximum of 0.005 kcal/mol. In the triplet state the errors are a factor of 3 to 5 larger, ranging from 0.054 to 0.117 kcal/mol for one center corrections, and up to 0.013 kcal/mol for two center corrections.

Table 3.2 shows the singlet-triplet gap obtained for both HF and GVB-PP wave functions. In both cases the error is smaller than 0.09 kcal/mol using one center corrections, and smaller than 0.02 kcal/mol for two center corrections.

An important feature demonstrated by Tables 3.1 and 3.2 is that the errors do not increase as the size or complexity of the basis set increases. This shows that PS-GVB does not have any intrinsic problems in manipulating the diffuse functions present in larger basis sets. These two tables show that the errors in the PS-GVB integration scheme compared to standard methods are negligible compared to the magnitude of the quantities involved; in a 10 kcal/mol quantity an error of 0.02 kcal/mol is hardly significant. Moreover, even the best *ab initio* electronic structure calculations often differ from experimental results by as much as 1 kcal/mol, and so the PS-GVB error is negligible compared to the magnitude of errors in all electronic structure calculations.

Table 3.1: Total energy for CH_2 using GVB-PP wave functions. A GVB (3/6) wave functions is used for the ${}^1A_1$ state, and a GVB (2/4) wave functions used for the ${}^3B_1$ state. GVB2P5 results are present in hartrees, and the PS-GVB error is presented in kcal/mol. PS-GVB results are given using both one center (1C) and two center (2C) atomic corrections.

		Basis Sets		
Method	State	VDZ	VDZ2	VDZ+
		Total Energy (h)		
GVB2P5	${}^1A_1$	-38.938766	-38.942557	-38.943274
GVB2P5	${}^3B_1$	-38.953285	-38.955554	-38.955771
		PS-GVB Error (kcal/mol)		
PS-GVB 1C	${}^1A_1$	0.015	0.032	0.024
PS-GVB 2C	${}^1A_1$	-0.005	0.005	0.004
PS-GVB 1C	${}^3B_1$	-0.054	0.117	0.112
PS-GVB 2C	${}^3B_1$	0.001	0.013	0.013

Table 3.2: The singlet-triplet gap (ΔE_{ST}) for CH_2, in kcal/mol. Experimental results are 9.09 kcal/mol. All other details are similar to Table 3.1.

		Basis Sets		
Method	Wave Function	VDZ	VDZ2	VDZ+
GVB2P5	HF	26.11	25.48	25.13
PS-GVB 1C	HF	26.18	25.41	25.06
PS-GVB 2C	HF	26.11	25.48	25.12
GVB2P5	GVB-PP	9.11	8.16	7.84
PS-GVB 1C	GVB-PP	9.18	8.07	7.75
PS-GVB 2C	GVB-PP	9.11	8.15	7.83

3.8.2 Silylene

The next molecule studied is silylene, SiH_2, which is the Silicon analog of methylene. Table 3.3 reports results for silylene calculations. For silylene the two low-lying states are of the same form as those in Figure 3.2; however, the singlet state is the ground state of silylene, where the triplet state was the ground state of methylene. The PS-GVB studies on silylene tested two important features, (i) the ability of PS-GVB to describe a second-row element, and (ii) the ability of PS-GVB to use an effective core potential (ECP). Two sets of calculations were carried out, one with all core electrons described with basis functions, and the other using the shape and Hamiltonian consistent (SHC) effective core potential to replace them.

For the $^1A_1$ state a geometry with R_{SiH} = 1.508 Å, θ_{HSiH} = 92.4° was used, and for the $^3B_1$ state a geometry with R_{SiH} = 1.471 Å, θ_{HSiH} = 118.2° was used; these geometry were based on geometry optimizations using MP2 and unrestricted MP2 with a 6-31G** basis set. With no ECP present, a Huzinaga valence double-zeta basis set (11s8p/4s3p) was used for Si, and a Huzinaga unscaled double-zeta basis set (4s/2s) was used for hydrogen. A set of d polarization functions (a = 0.42) was used with the Si basis, and a set of p polarization functions (a = 0.6) was used with the H basis. The SHC ECP [22, 23] was used to eliminate the Si core electrons. The corresponding VDZ basis set (3s3p/2s2p) was augmented with the same d polarization functions as before, and the same basis set was used for H.

Table 3.3 compares total energy calculations and singlet-triplet gaps (ΔE_{ST}) between GVB2P5 and PS-GVB for silylene. The errors are of the same order of magnitude as those for methylene. The maximum error is 0.079 kcal/mol when one center corrections are included, and 0.014 kcal/mol when two center corrections are used. As Table 3.3 shows, the magnitude of the errors is consistent whether HF or GVB wave functions are used.

The presence of an ECP introduces no new error into the PS-GVB method. The errors remain of the same magnitude as those from calculations where all core electrons are included.

3.8.3 Ethylene

The final system considered here is ethylene. With this system the focus is shifted away from electronic criteria—basis sets, wave functions, and effective core potentials—and centers on the effect of larger geometric changes on the accuracy of the PS-GVB program. Four geometries are used here:

Experimental the ground state geometry with a torsional angle ϕ = 0°, R_{CC} = 1.338 Å, R_{CH} = 1.085 Å, and θ_{HCH} = 117.8°.

Twisted the experimental geometry with ϕ set to 90° and all other quantities unchanged.

Stretched the experimental geometry with R_{CC} = 2.676 Åand all other quantities unchanged.

Table 3.3: Energy comparison for SiH_2. Experimental geometry (see text) with VDZ basis set. The GVB2P5 results report total energies in hartrees, the PS-GVB results report error in kcal/mol. A GVB (2/4) wave function is used for the $^3B_1$ state, a GVB (3/6) wave function is used for the $^1A_1$ state. Both one center (1C) and two center (2C) atomic corrections are reported.

Calculation	State	GVB2P5 Total Energy (hartrees)	PS-GVB 1C Error (kcal/mol)	PS-GVB 2C Error (kcal/mol)
		All-Electron		
HF	$^3B_1$	-289.920507	0.065	0.007
HF	$^1A_1$	-289.929006	0.08	0.025
ΔE_{ST}		0.008499	-0.015	-0.019
GVB	$^3B_1$	-289.940694	-0.062	0.008
GVB	$^1A_1$	-289.972813	0.075	0.025
ΔE_{ST}		-0.032119	-0.013	-0.017
		Core Potential		
HF	$^3B_1$	-289.994255	0.002	0.01
HF	$^1A_1$	-290.003034	0.063	0.024
ΔE_{ST}		0.008779	-0.061	-0.014
GVB	$^3B_1$	-290.014773	0.001	0.004
GVB	$^1A_1$	-290.04802	0.063	0.024
ΔE_{ST}		0.033247	-0.061	-0.02

Stretched/twisted the experimental geometry with ϕ = 90°, R_{CC} = 2.676 Å, and all other quantities fixed.

For calculations on ethylene, the VDZ basis from methylene is used again. In these calculations the σ and π C-C bonds are correlated. Table 3.4 summarizes the calculations performed on ethylene. The first two columns tabulate the results from GVB2P5 (in hartrees) using standard methods to compute the molecular integrals, for both HF and GVB wave functions. The next four columns detail the errors (in kcal/mol) in the corresponding PS-GVB calculations. Columns three and four include results with 1C corrections, and columns five and six include results with 2C corrections.

With 1C corrections, all of the total energy calculations and relative energy quantities (singlet-triplet gaps, dissociation energies, rotational barriers) agree to within 0.25 kcal/mol. With 2C corrections the total energy calculations and relative energy quantities agree to within 0.05 kcal/mol.

The calculations reported in this section were performed using the original version of the PS-GVB program. Since these calculations were completed many more revisions of the program have been released, with improved accuracy, atomic corrections, speed, memory use and flexibility. But what these calculations show is still of crucial importance for the PS-GVB program: that it is possible, with the appropriate choice of grids, dealiasing functions, and atomic corrections, to create a numerical integration scheme that introduces only negligible errors to the formation of operators used in HF and GVB calculations. Moreover, holding all of these parameters fixed, this integration scheme can be applied to a wide range of basis sets, geometries, wave functions, and spin states, and a reliable degree of accuracy can be maintained throughout. These calculations demonstrated for the first time that the significant speed advantages of the PS-GVB program may be used for quantum chemical research without the need for constant worry about the accuracy of the algorithm, of whether the basic scheme still applies to the current system. These calculations showed that the numerical integration scheme used in PS-GVB is robust enough for practical applications in electronic structure theory.

3.9 Conclusion

The PS-GVB program presented in this section has significant advantages over the GVB2P5 program. By using the pseudospectral method to compute the two-electron operators, not only can PS-GVB run small molecules faster than GVB2P5, but PS-GVB can also run molecules much larger than the limits set in GVB2P5. Whereas GVB2P5 cannot compute the a molecule with more than 180 basis functions, PS-GVB can calculate molecules with up to 500 basis functions with roughly the same CPU, disk, and memory resources.

The PS-GVB program also presents substantial advantages over earlier implementations of the pseudospectral method. In particular, PS-GVB can compute molecules whose wave functions have arbitrary numbers of doubly-occupied core orbitals, singly occupied open-shell orbitals, and variably occupied GVB natural orbitals. This added flexibility comes without substantially increasing the disk storage, memory, or CPU time requirements of the program.

Table 3.4: Summary of energy differences for C_2H_4. See text for geometries. Calculations use VDZ basis. GVB2P5 energies are given in hartrees, PS-GVB errors are reported in kcal/mol. PS-GVB results are reported with both one center (1C) and two center (2C) corrections. A GVB (3/6) wave function is used for $^1A_1$ state, a GVB (2/4) wave function is used for $^3A_2$ state. The barriers reported for the twisted geometry are $\Delta E_\phi = E(\phi = 90°) - E(\phi = 0°)$. The bond energies ΔE_B reported for the stretched geometries are the energy required to double the bond length.

	GVB2P5		PS-GVB 1C		PS-GVB 2C	
	Total Energy (h)		Error (kcal/mol)		Error (kcal/mol)	
State	HF	GVB	HF	GVB	HF	GVB
			Experimental Geometry			
$^3A_2$	-77.931907	-77.942874	-0.137	-0.119	-0.036	-0.038
$^1A_1$	-78.060723	-78.09924	-0.243	-0.209	-0.045	-0.045
ΔE_{ST}	0.128816	0.156366	0.106	0.089	0.008	0.007
			Twisted Geometry			
$^3A_2$	-77.973417	-77.984305	-0.183	-0.022	0.003	0.004
$^1A_1$	-77.888273	-77.981006	0.016	-0.025	0.007	0.004
ΔE_{ST}	-0.085144	-0.003299	-0.199	0.003	-0.004	0
$\Delta E_\phi(^3A_2)$	-0.04151	-0.041431	0.046	-0.097	-0.039	-0.042
$\Delta E_\phi(^1A_1)$	-0.17245	0.118234	-0.259	-0.184	-0.053	-0.049
			Stretched Geometry			
$^3A_2$	-77.772934	-77.884587	-0.199	-0.196	-0.013	-0.013
$^1A_1$	-77.726946	-77.847384	-0.128	-0.209	-0.038	-0.016
ΔE_{ST}	-0.045988	0.002797	-0.07	0.013	-0.009	0.003
$\Delta E_B(^3A_2)$	0.158973	0.098287	0.062	0.077	0.023	0.025
$\Delta E_B(^1A_1)$	0.333777	0.251856	0.115	0	0.007	0.029
			Stretched/Twisted Geometry			
$^3A_2$	-77.773688	-77.845388	-0.128	-0.104	0.003	-0.013
$^1A_1$	-77.727351	-77.845284	-0.139	-0.104	0.012	0.013
ΔE_{ST}	-0.046337	-0.000104	0.011	0	-0.006	0

This chapter concludes with applications that demonstrate these advantages that PS-GVB introduces. Namely, molecules are run with GVB and open-shell wave functions, with larger and more accurate basis sets, with Si atoms, with Si atoms using effective core potentials. In these cases a wide variety of physical properties are reported, ranging from bond dissociation energies to singlet-triplet gaps. Over these examples, PS-GVB displays a remarkably constant accuracy, generally giving results within 0.1 kcal/mol of the experimental numbers. These applications demonstrate that the significant time advantages of the pseudospectral method for integral evaluation may be extended to a robust program that can be used to study real chemical problems.

Chapter 4

Pseudospectral Parameters for Calculations on Nickel Clusters

4.1 Introduction

The research presented in this chapter presents parameters for PS-GVB calculations on molecules containing Nickel atoms. By proper choice of these parameters, PS-GVB calculations run on Ni clusters can achieve the same accuracy as those on main group elements. A general procedure was used to optimize the parameters over a variety of geometries, so that when the same parameters were used on a different Ni cluster with a different wave function, the high degree of accuracy was maintained. The procedures and general lessons obtained from the Ni parameter optimization should be applicable for deriving PS-GVB parameter sets for other transition metal systems.

Chapter 3 describes the procedure by which the PS-GVB program [9, 10, 11, 12, 14, 13, 15, 16] constructs the operators required for *ab initio* electronic structure theory calculations. In addition to the basis sets required for standard *ab initio* calculations, PS-GVB requires grids and dealiasing sets for each atom type in the molecules.

The grids [12, 14, 13] for each atom type are composed of concentric shells of spherical grids. Each spherical shell is a Lebedev grid [17, 18] of a particular angular momentum. The Lebedev grids integrate the angular spherical harmonics exactly over the shell. For each atom type parameters must be determined for the radii at which to place the spherical shells, and for the angular momentum (which determines the number of gridpoints on the spherical grid) of each shell. Using the procedure described in Section 3.6, these atomic grids are patched together to form the molecular grid.

The dealiasing functions [10, 11] help remove the noise generated by inaccurate integration over finite grids, and, consequently, they are closely related to the particular nature of the grids. Because the grid is finite and therefore imperfect, the action of the Coulomb or exchange operator on a basis function contains an alias—character outside of the basis set. By employing a set of additional basis functions the alias can be expressed in the least squares fitting procedure and discarded. Thus, dealiasing functions are chosen that help complete the particular basis set.

PS-GVB has shown excellent results [15] for molecules composed of main group elements. Although main group elements are the most important elements for organic chemistry and biochemistry, a great deal of important chemistry occurs with metals and non-metals not in the main group. This chapter describes procedures for optimizing grids and dealiasing sets for one element—Nickel. Nickel was chosen because the bonding and the geometries it displays are strikingly different from those displayed by main group elements. At the outset of this research it was not clear that the 0.1 kcal/mol accuracy that PS-GVB achieves for main group elements could be extended to metals. This research shows that with judicious choices of grids and dealiasing functions the same accuracy obtained with main group elements can be obtained for metals.

It should be noted that the procedure for grid and dealiasing set generation presented here is slightly simplified for the sake of brevity and conciseness. The most important concepts and features are reported.

In this chapter, Section 4.2 describes some of the basic features of metal bonding that make the pseudospectral description of the bonding between these elements more difficult than for main group elements. Section 4.3 describes the nature of the parameters that form the pseudospectral atomic grids; in particular, it describes the Carbon atomic grid parameters, which are the most optimized of the main group element grid parameters, and the parameters from which consideration of Nickel atomic grid parameters began. Section 4.4 describes the nature of the parameters that determine the set of dealiasing functions. As with the atomic grid parameters, the Carbon dealiasing function parameters are the most optimized and the ones from which consideration of Nickel dealiasing set parameters began. Section 4.5 describes the optimization procedure through which the correct set of parameters for Nickel was determined. This section also presents the final values of the Nickel atomic grid and dealiasing function parameters, and draws some conclusions for deriving parameters for other elements from the nature of these parameters. Finally, Section 4.6 demonstrates that the parameters developed in Section 4.5 are general by applying them to a different Nickel cluster at a series of different geometries, and by using a correlated wave function. The optimized Nickel atomic grids and dealiasing functions show excellent agreement with the results from GVB2P5.

4.2 Nickel Cluster and Metal Bonding

Main group elements display chemical bonding behavior that is very regular. Orbitals are generally centered about the nucleus, and are composed of s and p hybrids. First row transition metals display strikingly different behaviour [24, 25]. The 3d orbitals are much smaller than the 4s orbitals in the valence shell. Consequently, the electrons in 3d orbitals stay largely localized on the atoms and do not participate in chemical bonding. The 4s electrons are for the most part responsible for the chemical bonding, but, in contrast to main group chemistry, the 4s electrons do not stay at the atom centers, but localize between atoms in metals. In linear chains of metal atoms electrons localize at bond midpoints. In two-dimensional sheets of atoms electrons localize at the center of triangles between three atoms, and in three-dimensional crystals electrons localize at the centers of octahedra and tetrahedra between three or more atoms [24].

Because metal molecular orbitals display such a different nature from main group molecular orbitals, it is not obvious that the same optimization techniques may be used to derive parameters for the grids and dealiasing functions used by PS-GVB in the numerical integration procedure. Clearly new parameters need to be determined to reflect the different bond angles, bond distances, basis sets, and bond character of Ni clusters. The issue with metals is whether the algorithm for choosing and optimizing parameters also needs to be changed. The research presented in this chapter demonstrates that essentially the same algorithms that were used to derive main group grids and dealiasing sets may be used to derive grids and dealiasing sets for Ni clusters. It is also presumed that these same techniques may be used to derive grids and dealiasing sets for other transition metals.

The research described in this chapter uses small Ni_3 clusters of atoms in different geometries to derive a set of grid and dealiasing set parameters that yield the high accuracy required for *ab initio* calculations. It is relatively easy to find a set of parameters that work for one geometry, but the constraint that the same set of parameters works for a wide variety of bond angles and radii was sought in the hope that the resulting parameters would work for arbitrary geometries.

Once such a set of grid and dealiasing set parameters is found that works for the various Ni_3 geometries, this set is applied to a system with a different geometry and wave function, and a calculation is made on a real physical property of that molecule to determine the accuracy of the parameter set. The idea is to test the parameters by running them on a molecule different from the ones for which the parameters were optimized. This presents a stiff test of the accuracy of the parameters. The final test system for the Ni parameters is the distortions of a Ni_4 cluster correlated with two GVB pairs, from the ground, rhombohedral geometry to a square geometry. The fact that the same accuracy was achieved on this system as was achieved for main group elements shows that the Ni parameters have broad applicability. This in turn shows that it is possible to optimize a set of grids and dealiasing functions with which PS-GVB calculate metal clusters with the same accuracy with which the program calculated molecules containing only main group elements.

4.3 Grid Parameters

Several parameters determine the structure of the atomic grids in the PS-GVB program. The radial space is divided into several regions. To each region is assigned a number of spherical shells, and an angular momentum for each shell. The angular momentum determines the number of points. Table 4.1 summarizes the number of grid points associated with each angular momentum level [17, 18].

PS-GVB uses a multi-grid algorithm [15] for the numerical integration. In this algorithm, grids of different densities—coarse, medium, and fine—are constructed for each molecule. The medium grid is used for the majority of the iterations. The highest quality grid is used for only one iteration, once the wave function has reached a certain level of convergence. After this iteration the medium grid is again used with Fock matrix updating procedures. The updating procedures integrate the difference in the orbitals over the grid, rather than the orbitals. The difference in the orbitals is smoother

Table 4.1: The number of points (N_{pts}) associated with the PS-GVB grid of a number (N). The points are arranged on a spherical shell. See text for other details.

N	N_{pts}	N	N_{pts}	N	N_{pts}
1	6	11	32	21	78
2	8	12	38	22	78
3	12	13	42	23	86
4	12	14	42	24	90
5	14	15	44	25	110
6	18	16	44	26	116
7	20	17	50	27	148
8	24	18	54	28	194
9	26	19	56	29	302
10	30	20	60		

and easier to integrate, so no loss of accuracy is obtained even though a less dense grid is used. The advantage to the multi-grid scheme is that even though the overall accuracy of the converged wave function is determined by the quality of the fine grid, this grid is only used for one iteration, and consequently the expense of the calculation is determined by the less dense medium grid.

In determining optimized grids for PS-GVB, a high quality grid that achieves good results is first obtained. Spherical shells are removed or made less dense to obtain medium and coarse grids. In the comparisons between the grids for different elements that follow, only the highest quality grids will be compared, because it is assumed that the lower quality grids can be obtained from the higher quality grids in a simple, straightforward manner.

The Carbon grid was the most optimized grid, and the work on determining Ni grid parameters began with the Carbon grid. For the placements of the radial grids, the highest quality C grid put 4 spherical shells below 0.4 bohr, another 3 shells between 0.4 and 1.173 bohr, another 5 shells between 1.173 and 3.2 bohr, another 3 shells between 3.2 and 4.765 bohr, and a final 3 shells between 4.765 and 8.0 bohr. All shells below 0.6 bohr used PS-GVB grid number 9 (26 points per shell), the shells between 0.6 and 4.5 bohr used grid number 26 (116 points per shell), and the shells beyond 4.5 bohr used grid number 3 (12 points per shell)9. Table 4.2 summarizes the results for the C fine grid.

Because the covalent radius of Ni is roughly twice that of C, the first attempt at a grid simply put another 2 spherical shells between 8 and 16 bohr, so that the spatial extent of the Ni grids would be roughly twice that of the C grids. The radial regions between 4.5 and 8 bohr were augmented with higher angular momenta shells. The reasoning behind these choices was to maintain the basic appearance of the C grids shifted out a bit. Care was taken to keep the total number of points from becoming too much larger than C, which had roughly 1000 gridpoints for the highest quality grids.

Table 4.2: PS-GVB C fine grid. The position of the spherical grids is given as the outer radius R_{out} of each region and the number of spherical grids N_{sphere} in the region. The density of the spherical grids is given as the outer radius R_{out} and the angular density N_{ang} of the grids in that region. Radii are in terms of bohr.

Position		Density	
R_{out}	N_{sphere}	R_{out}	N_{ang}
0.400	4	0.6	9
1.173	3	4.5	26
3.200	5	8.0	3
4.765	3		
8.000	3		

One unfortunate discovery of the optimization procedure was that grid and dealiasing function parameter optimization is tightly coupled. The result of this is that the grid cannot be optimized without the simultaneous optimization of the dealiasing functions. This made the optimization procedure much more time consuming. The particular form of the optimized Ni grid will be described after the discussion on the optimization procedure in Section 4.5

4.4 Dealiasing Function Parameters

While the grid parameters were being optimized it was also necessary to simultaneously optimize the dealiasing set parameters. The dealiasing function parameters are considerably more complex than those of the grid. Because of finite grid size, and therefore imperfect numerical integration, when the effect of J^k is computed on a basis function χ_η

$$J^k(r_g)R(r_g,\nu) = \left[\sum_{\sigma\eta} D^k_{\sigma\eta} A_{\sigma\eta}(r_g)\right] R(r_g,\nu) \tag{4.1}$$

it contains an alias [10, 11]—character outside of the basis set—that can cause errors in the integration if not removed. The dealiasing functions are a set of basis functions that express the alias so that it can be projected out of the integration procedure (see Section 3.6). Because the primary function of the dealiasing set is to complete the basis set, dealiasing functions are chosen with exponents between the basis set exponents, or with the same exponent and higher angular momentum. Again, because the C parameters are the most optimized, they are used as a starting point for Ni dealiasing set optimization.

The alias in the numerical integration procedure does not occur only on the atom on which the basis function cn is centered, but it also occurs on the neighboring atoms. Consequently dealiasing functions are also included on neighbors, next-nearest neighbors, and so on. Just as the medium and coarse grids are derived from the fine grids

Table 4.3: C 6-31G** basis set. The lines indicate groups of exponents contracted together via the coefficients in the third column.

Exponent	Type	Coefficient
3047	s	0.001835
457.4	s	0.01404
103.9	s	0.06884
29.21	s	0.2322
9.287	s	0.4679
3.164	s	0.3623
7.868	s	-0.1193
1.881	s	-0.1608
0.5442	s	1.143
7.868	p	0.06900
1.881	p	0.3164
0.5442	p	0.7443
0.1687	s	1.000
0.1687	p	1.000
0.8000	d	1.000

by simplifying them, the neighbor dealiasing functions are derived from the atoms dealiasing functions by removing some of the dealiasing functions.

Table 4.3 reports the C basis set 6-31G**, which is the basis set that PS-GVB primarily uses for C.

Generally, only the largest exponent in a contracted set is considered when choosing dealiasing functions. The guideline used in choosing exponents was that a factor of 2 between exponents is ideal. The smallest exponent in C 6-31G** is 0.1687. Optimization of C dealiasing sets showed that smaller exponents are not necessary. An additional exponent was included at 0.35 to span the space between 0.1687 and 0.5442, and an exponent of 1.6 was included to span the space between 0.8 and 3.164. Larger exponents were added at 6.4, 12.8, and 25.6 to span the rest of the space.

At each basis and dealiasing function exponent an angular momentum is also selected. The guideline used in choosing exponents is that one degree of angular momentum beyond the highest basis function angular momentum is required, and the angular momentum for dealiasing functions are chosen to be similar to the basis function angular momenta nearby. Table 4.4 shows the entire dealiasing set for C [16]. The guidelines are not absolutely followed because optimization shows that different choices might be better for a given basis set.

The Ni basis set is considerably different from the C 6-31G** basis set. The Ni basis set is a double-zeta basis derived by Hay and Wadt [23] with an effective core potential replacing the core electrons. This basis set is given in Table 4.5.

The most striking difference between the Ni basis set and that of C is that, just as

Table 4.4: C dealiasing set. Shown are the exponents of the basis functions, and the angular momenta at which dealiasing functions are created on the atom and neighboring atoms.

Exponent	Atom A.M.	Neighbor A.M.
0.1687	spdf	spd
0.3500	spdf	-
0.8000	spdf	spdf
1.600	spdf	spd
3.164	spd	-
6.400	spd	spd
12.80	sp	sp
25.60	sp	sp

Table 4.5: Ni Hay-Wadt basis set. The lines indicate groups of exponents contracted together via the coefficients in column three.

Exponent	Type	Coefficient
7.620	s	-0.4061
2.294	s	0.7423
0.8760	s	0.5330
2.294	s	-0.02643
0.8760	s	-0.1212
0.1153	s	0.5267
0.03960	s	1.000
23.66	p	-0.048019
2.893	p	0.6241
0.9435	p	0.4702
0.08600	p	0.02610
0.08600	p	0.5215
0.02400	p	0.5955
42.72	d	0.03236
11.76	d	0.1698
3.817	d	0.3960
1.169	d	0.4881
0.2836	d	1.000

the average bond distances are about twice as long for Ni as they are for C, the basis functions are more diffuse for Ni than they are for C.

The first guess of the Ni dealiasing set places exponents at 0.012 and 0.024 to span the space below 0.0396, an exponent to span the space between the exponents 0.0396 and 0.086 at their geometric mean, 0.0584, an exponent to span the space between the exponents 0.086 and 0.2836 at their geometric mean, 0.15, and exponents at 0.56, 1.12, 2.24, 4.48, 8.9, and 17.8 to span the rest of the functional space. The final optimized dealiasing set will be presented in the next section, after a discussion of the optimization procedure.

4.5 Optimization Procedure

The Ni_3 cluster was used to optimize the grid and dealiasing set parameters. Because PS-GVB uses two center atomic corrections, this was the smallest cluster that would include numerical integrals. Five geometries were selected, at a variety of angles and radii. It was desirable to have such a wide range of geometries to insure that the results were robust and not merely limited to a particular geometry. At each geometry calculations were run using a HF wave function on the quartet spin state.

The grids and dealiasing sets were optimized over a large number of different calculations. The final optimized highest quality Ni grid had 7 radial shells below 0.4 bohr, 8 radial shells between 0.4 and 1.173 bohr, 10 radial shells between 1.173 and 3.2 bohr, 5 radial shells between 3.2 and 4.765 bohr, 6 radial shells between 4.765 and 8.0 bohr, and 6 radial shells between 8.0 and 16.0 bohr11. These numbers were essential scaled from C results to the appropriate radii. Most of the grid optimization went into assigning appropriate angular momenta to each shell, on the assumption that new difficulties associated with Ni has more to do with the increased angular momentum of the d electrons than it has to do with increased complexity in the radial functions. Shells below 0.5 bohr use grid number 9, those between 0.5 and 1.0 bohr use grid number 20, those between 1.0 and 1.5 bohr use grid number 26, those between 1.5 and 4.5 bohr use grid number 28, those between 4.5 and 5.5 use grid number 26, and those between 5.5 and 16.0 bohr use grid number 22. These results are summarized in Table 4.6.

Many of these gridpoints are removed when the grids are patched together. Consequently, the central Ni atom in the Ni_3 clusters had 3000 gridpoints on it, compared to the roughly 1000 on C; more points were necessary to achieve the 0.1 kcal/mol accuracy for Ni.

Several conclusions can be drawn from the appearance of the Ni grid. Because the bonding in Ni clusters is delocalized from the atomic centers, higher densities of gridpoints are required farther away from the nucleus than were required with C. The C grids could fall off rapidly because most of the electron density was close to the nuclei. Not only do the grids have to extend farther out in space, due to the longer Ni bond lengths, but the density must be higher farther out, because of the delocalized electrons.

Table 4.7 displays the final dealiasing set for Ni.

The choice of the exponents is entirely determined from the basis set. The types of dealiasing functions at each exponent were optimized over a series of trials, until

Table 4.6: Ni fine grid. The position of the spherical grids is given as the outer radius R_{out} of each region and the number of spherical grids N_{sphere} in the region. The density of the spherical grids is given as the outer radius R_{out} and the angular momentum N_{ang} of the grids in that region. Radii are in terms of bohr.

Position		Density	
R_{out}	N_{sphere}	R_{out}	N_{ang}
0.4	7	0.5	9
1.17	8	1.0	20
3.2	10	1.5	26
4.77	5	4.5	28
8.0	6	5.5	26
16.0	3	16.0	22

Table 4.7: Ni dealiasing set. Shown are the exponents of the basis functions, and the angular momenta at which dealiasing functions are created on the atom and neighboring atoms.

Exponent	Atom A.M.	Neighbor A.M.
0.012	spd	spd
0.024	spd	spd
0.0396	spd	spd
0.0584	spdf	spdf
0.086	spd	spd
0.15	spdf	spdf
0.2836	spd	spd
0.56	spdf	spdf
1.12	sp	sp
2.24	sp	sp
4.48	sp	sp
8.9	sp	sp
17.8	spd	spd

Table 4.8: Ni_3 results. Shown are the total energies using GVB2P5 and PS-GVB in hartrees, and the error in kcal/mol, for a series of isosceles triangular Ni_3 clusters.

Geometry		Energy (h)		Error
θ	R (Å)	GVB2P5	PSGVB	(kcal/mol)
60°	1.74	-504.248096	-504.247943	0.096
60°	2.48	-504.628405	-504.628249	0.098
120°	2.04	-504.591164	-504.590973	0.120
180°	2.04	-504.598970	-504.598870	0.063
180°	2.48	-504.676823	-504.676809	0.009

the current set was found that could reproduce to within 0.1 kcal/mol the results of GVB2P5 calculations for a series of geometries.

Some conclusions may be drawn from the appearance of the Ni dealiasing set. The dealiasing functions have, in general, higher angular momentum, no doubt reflecting the higher angular momentum of the Ni 3d electrons. Moreover, the dealiasing set gives the most accurate results when the neighbor blocks have the same dealiasing functions as the central atom does. This is another result of the delocalized Ni bonding, similar to the grid requirement of higher density at greater radii.

The goal at the outset of the work on Ni clusters was to maintain the accuracy PS-GVB obtains on main group elements, 0.1 kcal/mol. Table 4.8 summarizes the results for Ni_3 clusters using the parameter sets reported in this section. These results meet the accuracy criteria of 0.1 kcal/mol.

The geometries for the Ni_3 clusters were all isosceles triangles, with the angles and bond lengths shown in Table 4.8. The geometries were chosen to span most of the geometries Ni would see in different metal clusters. By requiring the parameters apply to a wide range of geometries, a more physically relevant set of parameters is obtained. The quality of the parameters is confirmed in the next section when they are applied to a different type of Ni cluster.

4.6 Application to Ni_4 Clusters

To verify that the grid and dealiasing set parameters were general and did not only work for Ni_3 clusters, a set of calculations were run on Ni_4 clusters11. These clusters are described with two GVB pairs correlating the 4s orbitals localized at the interstices of the bonds. The ground state geometry for this cluster is a rhomboidal geometry, with acute angle 60°, obtuse angle 120°, and bond length 2.487 Å. The quintet spin state of the 3d electrons on the Ni atoms was used. From the ground state geometry, the rhomboid was distorted into a square, as shown in Figure 4.1.

Table 4.9 presents the results for this calculation. As the sixth column shows, the agreement of PS-GVB with GVB2P5 is excellent, once again to within roughly 0.1

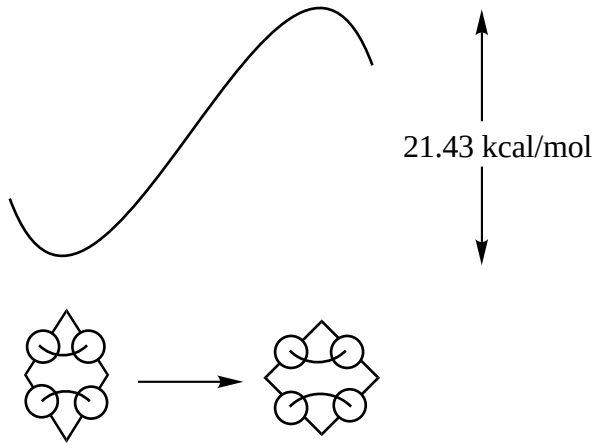

Figure 4.1: Distortion of Ni_4 from rhomboid to square.

kcal/mol.

The third and fifth columns show the distortion energy from the ground state energies. GVB2P5 calculates this barrier as 21.43 kcal/mol, and PS-GVB calculates the barrier as 21.26 kcal/mol. Figure 4.2 plots these values versus the angles, and shows that, compared to the magnitude of the quantities being calculated, whatever error PS-GVB introduces in negligible.

The Ni_4 case run in this section is a stringent test of the accuracy of the parameter set, because different geometries and wave functions are used than were used for any of the geometries for which the parameters were originally derived. That the same accuracy is achieved for a different system that was achieved for the Ni_3 clusters with which the parameters were obtained indicates that the parameters are general and do not apply only to the special cases used to derive them.

4.7 Conclusions

The work reported in this chapter shows that, with judicious choice of grid and dealiasing set parameters, it is possible to reproduce the results of standard method programs such as GVB2P5 using the PS-GVB program. A significant number of optimization runs are required and the two sets of parameters must be optimized simultaneously because of the tightly coupled nature of the grids and the dealiasing functions. Nonetheless, the fact that a high level of accuracy is possible with the PS-GVB program indicates that the significant speed advantages delivered by this program can be used for research on metallic systems.

The conclusions that can be drawn from the optimization work on Ni grids are: (i) because the bond lengths of Ni clusters are approximately twice as long as those for C containing molecules, the Ni grids must extend twice as far from the nucleus as the

Table 4.9: Ni_4 distortion energies. Ni_4 with a bond length of 2.487 Åand the acute angles shown in column one. Shown for each angle is the total energy in hartrees calculated via GVB2P5 and PS-GVB, and the distortion energy relative that program's minimum energy. Column 6 reports the error, in kcal/mol, between the two methods' total energies.

Angle	GVB2P5 (h)	ΔE_{GVB} (kcal/mol)	PS-GVB (h)	ΔE_{PS} (kcal/mol)	Error (kcal/mol)
60°	-672.902067	0.00	-672.901989	0.00	-0.04894
70°	-672.893097	5.63	-672.893090	5.58	-0.004392
80°	-672.880313	13.65	-672.880555	13.45	0.1518
90°	-672.867922	21.43	-672.868110	21.26	0.1180

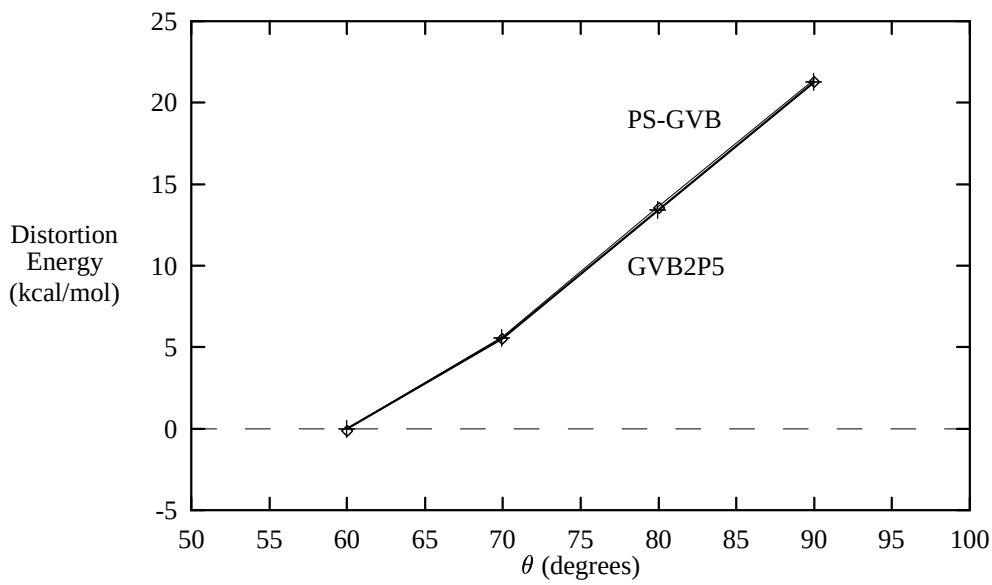

Figure 4.2: Distortion Energy of Ni_4 Cluster. Comparison of PS-GVB barrier to GVB2P5 barrier.

C grids; (ii) because the Ni orbitals are delocalized from the nucleus, in contrast to the atom-centered C orbitals, the Ni grids fall off more slowly than the C grids, and higher grid densities are required at large radius; (iii) that the factor of two spacing between dealiasing set exponents used for C again works for Ni; (iv) that the neighbor dealiasing functions are even more important for Ni than they were for C, and more functions are required on the neighbor atoms, another reflection of the delocalized Ni bonding. It is expected that these rules can be applied to derive parameter sets for other transition metal systems.

Chapter 5

Direct Inversion in the Iterative Subspace Convergence for Generalized Valence Bond Wave Functions

5.1 Introduction

The research presented in this chapter describes an improved method of converging Hartree-Fock and Generalized Valence bond wave functions. The most important advantage of this method is that wave functions converge in fewer iterations using this method than using standard convergence methods. Another advantage is that the method presented in this chapter is more reliable than standard convergence methods, almost always converging wave functions in 10-15 iterations; although in the best cases, standard methods can converge wave functions this quickly, they often require many more iterations. Finally, the method presented herein is automatic. Standard convergence methods often require user intervention to turn on or off orbital averaging or otherwise adjust the convergence procedure. This method is fully automatic and requires no input from the users to help the convergence.

Section 2.7 summarizes the orbital optimization equations [3, 6, 4] for a general wave function consisting of closed, open, and GVB pair orbitals. These optimal orbitals are solved in an iterative process. In each iteration the one- and two-electron operators are formed from the trial (or previous iteration's) orbitals, and the optimal occupied and unoccupied mixings are calculated, from which the set of improved orbitals is formed. The iterations proceed until the wave function stops changing.

Unfortunately, wave function optimization can be a very slow procedure, especially in cases with many open-shell or GVB orbitals. In these cases the orbital rotations between occupied shells can require many iterations to converge. Moreover, the rate of convergence for any type of wave function generally slows as the wave function be-

comes more converged, which makes attainment of a highly converged wave function an even more computationally expensive procedure than it would normally be.

For SCF calculations, quadratically convergent procedures [26, 27, 28] have been developed that require the Hessian matrix, whose elements represent the second derivative of the energy with respect to orbital variation. Although these methods show excellent convergence properties, they require a full transformation of the two-electron integrals—an $\mathcal{O}(N^5)$ process—to compute all of the elements for the optimization. General MC-SCF procedures require a full integral transformation, and so a negligible amount of additional work is required to use a quadratically convergent procedure. But one of the principal advantages of the general HF and GVB wave functions summarized in Section 2.7 is that they do not require a full integral transformation, and consequently the work required to compute the operators scales formally only as $\mathcal{O}(N^3)$ with the PS-GVB method. With such wave functions, computation of the Hessian matrix would be significantly more expensive than computation of the other operators, and therefore the quadratically convergent methods are not practical for HF and GVB wave functions.

To address these difficulties, Pulay introduced the direct inversion in the iterative subspace (DIIS) method [29, 30, 31] that has made a significant impact on SCF methods in quantum chemistry. The DIIS method allows wave functions to obtain convergence rates approaching quadratic convergence without any of the overhead associated with rigorous quadratically convergent methods (i.e., calculating and storing a Hessian matrix, which has N_{bf}^4 elements). DIIS methods extrapolate the Fock matrices from different iterations to obtain the most optimal Fock matrix. Pulay's DIIS methods have been applied to closed-shell HF, restricted open-shell HF (ROHF), and single-pair GVB wave functions, and have yielded impressive results [29, 30, 31].

The work described in this chapter reports the development of an improved DIIS scheme, generalized valence bond-direct inversion in the iterative subspace (GVB-DIIS) [32], which is valid for general wave functions having arbitrary numbers of doubly-occupied core orbitals, singly occupied open-shell orbitals, and variably occupied GVB natural orbitals (*vide supra* Section 2.7). The DIIS scheme presented here differs from previous schemes in several ways. Existing formulations of DIIS are only valid for special cases: closed-shell HF wave functions, ROHF wave functions, or one-pair GVB wave functions. GVB-DIIS is general, and can be applied to wave functions with arbitrary numbers of core, open, and GVB orbitals. Another limitation of the Pulay DIIS scheme is that it was only applicable for late-iteration convergence, when the wave function is already mostly converged. This implies that the Pulay scheme has a small radius of convergence. By introducing second-order terms into the Fock operator used in GVB-DIIS, the radius of convergence is significantly improved. With a sufficiently accurate initial guess [33], GVB-DIIS methods can be used for early iterations in addition to the late iteration convergence for which the methods were derived.

This chapter presents a description of the GVB-DIIS scheme and compares it to the Pulay DIIS scheme as well as another DIIS scheme in the GAMESS program suite [34]. This chapter also applies the GVB-DIIS method to a number of examples of wave functions with various numbers of core, open, and GVB pair orbitals; and it presents convergence results for GVB-DIIS as well as a number of the other standard methods of wave function convergence. For the limited types of wave functions for which the Pulay and GAMESS DIIS schemes, work the GVB-DIIS convergence is compared to

them. For more general wave functions we compare our convergence to the pseudo-second-order convergence used in GVB2P5 [5] as well as that in Gaussian90 [35].

5.2 Closed-Shell HF-DIIS

Using orbital optimization equations in Section 2.7, the wave function can be said to be converged if

$$\langle i|F^i|j\rangle = 0 \tag{5.1}$$

for all occupied orbitals ϕ_i, with Fock operator F^i, and all occupied and virtual orbitals ϕ_j. This is equivalent to saying that an orbital is converged if the Fock matrix for that orbital is diagonal in the space spanned by all other orbitals.

DIIS procedures [29, 30, 31] make use of this definition of wave function convergence to speed the convergence of the wave function. The error vector for the n-th iteration is given by

$$\epsilon_{ij}^n = \langle i|F^{i,n}|j\rangle \tag{5.2}$$

where $F^{i,n}$ is the Fock operator for the i-th orbital at the n-th iteration, and orbitals ϕ_i (ranging over the occupied orbitals) and ϕ_j (ranging over all orbitals) are also evaluated at the n-th iteration. The DIIS procedures use error vectors from various iterations to find an optimal combination

$$\sum_n^{N_{it}} q_n \epsilon^n = 0. \tag{5.3}$$

The next iteration uses the optimal Fock operator, $\mathbf{F}^{opt}$,

$$\mathbf{F}^{opt} = \sum_n^{N_{it}} q_n \mathbf{F}^n \tag{5.4}$$

where $\mathbf{F}^n$ now refers to the *general* (spanning all shells) Fock operator at iteration n. This is a single Fock operator that replaces the individual Fock operators $\mathbf{F}^{i,n}$. The particular nature of $\mathbf{F}^n$ is discussed below. Diagonalizing the optimal Fock operator $\mathbf{F}^{opt}$, rather than $\mathbf{F}^n$ (as in an eigenvalue method) leads to accelerated convergence.

The Fock operator in equation 5.4 and the error vector in equation 5.2 cannot be in an molecular orbital (MO) basis, as such a basis would be changing each iteration as the orbitals are optimized. In practice an symmetrically orthonormalized atomic basis, hereafter referred to as *canonical orbitals* (CO), is generally used. Alternatively, the initial guess molecular orbitals could instead be used as an unchanging basis.

For closed shell HF cases it is convenient to write the error vector en as simply

$$\epsilon^n = \sum_i^{N_{core}} [F^c|i\rangle\langle i| - |i\rangle\langle i|F^c] \tag{5.5}$$

in terms of the N_{core} doubly occupied molecular orbitals. This definition of ϵ^n has the property that

$$\epsilon_{ij}^n \quad = 0 \qquad \text{if } \phi_i \text{ and } \phi_j \text{ are both occupied,} \tag{5.6}$$

$$
\begin{aligned}
\epsilon^n_{ij} &= -F^c_{ij} && \text{if } \phi_i \text{ is occupied and } \phi_j \text{ is unoccupied,} \\
\epsilon^n_{ij} &= F^c_{ij} && \text{if } \phi_i \text{ is unoccupied and } \phi_j \text{ is occupied,} \\
\epsilon^n_{ij} &= 0 && \text{if } \phi_i \text{ and } \phi_j \text{ are both unoccupied.}
\end{aligned}
$$

In terms of the atomic orbital basis

$$\epsilon^n_{\mu\nu} = \sum_i [\langle\mu|F^c|i\rangle\langle i|\nu\rangle - \langle\mu|i\rangle\langle i|F^c|\nu\rangle] \tag{5.7}$$

or, in matrix notation,

$$\epsilon^n = \mathbf{F}^n\mathbf{D}^n\mathbf{S} - \mathbf{S}\mathbf{D}^n\mathbf{F}^n \tag{5.8}$$

where

$$S_{\mu\nu} = \langle\chi_\mu|\chi_\nu\rangle \tag{5.9}$$

is the overlap matrix, and

$$D_{\mu\nu} = \sum_i^{N_{core}} c_{\mu i}c_{\nu i} \tag{5.10}$$

is the core density matrix with orbital coefficients $c_{\mu i}$ given in equation 2.37.

Equation 5.5 is normally written as $(\mathbf{FD} - \mathbf{DF})$ for a closed-shell system. Because the canonical orbital basis is also an orthogonal basis, the error vector is also defined as $(\mathbf{FD} - \mathbf{DF})$ in that basis. In practice, for closed shell systems, the Fock matrix $\mathbf{F}$ and the density matrix $\mathbf{D}$ are formed in the atomic orbital basis (over the basis functions χ_μ) and transformed to canonical orbitals to form the error vector.

For multi-shell systems the choice of the error vector is no longer straightforward. Section 5.4 presents a general approach for such systems.

Once an error vector has been defined, the q_n iteration coefficients are determined by minimizing [29, 30, 31]

$$\sum_{ij}\left[\sum_n q_n e^n_{ij}\right]^2 \tag{5.11}$$

under the constraint that

$$\sum_n^{N_{it}} q_n = 1. \tag{5.12}$$

This leads to the equations

$$\mathbf{Pq} = \mathbf{f} \tag{5.13}$$

of order $N_{it} + 1$, where

$$P_{ij} = \epsilon^i\epsilon^j \quad \text{for } i, j > 0, \tag{5.14}$$

$$P_{i0} = P_{0i} = -1 \quad \text{for } i > 0, \tag{5.15}$$

$$P_{00} = 0, \tag{5.16}$$

and

$$f_i = 0 \quad i > 0, \tag{5.17}$$

$$f_0 = -1 \tag{5.18}$$

and the q_i coefficients are used in equation 5.4 to obtain the orbitals of the new iteration, and where q_0 is a Lagrange multiplier corresponding to half the norm of the new error vector.

5.3 General Fock Operators

The Fock operator in equation 2.121 represents the first-order change in the energy with respect to orbital variation. Normally, one Fock matrix, $\mathbf{F}^c$, is constructed for the core orbitals, and other Fock matrices, $\mathbf{F}^i$, are constructed for each open or GVB pair orbital ϕ_i. But in order for the DIIS method to work, all orbital optimizations take place as the diagonalization of a single Fock operator. This section describes a variety of methods for replacing the separate Fock operators ($\mathbf{F}^c$, $\mathbf{F}^i$) with a single Fock operator $\mathbf{F}$. Traditionally, orbital optimization schemes that performed all orbital optimization with a single diagonalization (pure diagonalization or eigenvalue methods) for multi-shell cases generally give slow convergence because only first-order changes in the energy are considered. One of the major advantages to a DIIS method is that through extrapolation it can provide the fast convergence generally only seen in second-order methods. The goal in this section is how to combine the speed of the DIIS method with a Fock operator that can express all of the open-shell and GVB orbital optimization in a single diagonalization.

5.3.1 Simplest Approach: Combine Separate Fock Operators

The simplest definition of a multi-shell Fock operator that satisfies the convergence criteria in equation 5.1 is

$$\begin{aligned} F_{ij} &= F^I_{ij} && i,j \text{ are orbitals in shell } I \\ F_{ij} &= F^I_{ij} - F^J_{ij} && i,j \text{ are in different occupied shells } I,J \\ F_{ij} &= F^I_{ij} && i \text{ is an orbital in shell } I,\ j \text{ is unoccupied} \\ F_{ij} &= F^c_{ij} && i,j \text{ are unoccupied orbitals.} \end{aligned} \tag{5.19}$$

This is the algorithm that the GAMESS program suite [34] uses for DIIS convergence for open shell and GVB wave functions. We have found that DIIS methods based on such a Fock operator work well when the wave function is sufficiently close to convergence, but have difficulty with less optimal starting guesses. Moreover, this method is inherently unsuited to cases with multiple GVB pairs because very often two or more pairs are degenerate (e.g. the two OH bonds in water); with this Fock operator the diagonal elements for degenerate pairs are equivalent, and diagonalization will delocalize the GVB natural orbitals over the equivalent pair.

Further difficulties with this Fock operator can be seen by examining the mixing due to off-diagonal elements in a matrix diagonalization, which is proportional to

$$\frac{M_{ij}}{M_{jj} - M_{ii}} \tag{5.20}$$

for an arbitrary matrix $\mathbf{M}$, where

$$M_{ij} << |M_{jj} - M_{ii}|. \tag{5.21}$$

With the Fock matrix definition from equation 5.20, this yields for the mixing between two occupied orbitals

$$\frac{F_{ij}^J - F_{ij}^I}{F_{jj}^J - F_{ii}^I} \tag{5.22}$$

where $\mathbf{F}^I$ is the Fock operator for orbital ϕ_i, and $\mathbf{F}^J$ is the Fock operator for orbital ϕ_j. Recalling equations 2.116–2.119, the correct second-order form for the mixing between two occupied orbitals is

$$\frac{F_{ij}^J - F_{ij}^I}{F_{ii}^J - F_{ii}^I - F_{jj}^J + F_{jj}^I + \gamma_{ij}}. \tag{5.23}$$

The most striking part of equation 5.22 is that it gets the sign wrong for the mixing of F_{jj}^J and F_{ii}^I in the denominator. In equation 5.22 these elements have opposite signs, whereas the correct mixing term from equation 5.23 has the same signs for these two terms. This can cause the denominator to be small (or even zero) and the mixing terms consequently to become very large and unstable. Moreover, the lack of the γ_{ij} terms prevents the wave function from converging with two degenerate orbitals: as ϕ_i approaches ϕ_j all of the terms in equation 5.23 approach zero except γ_{ij}, which is large for localized orbitals. The γ_{ij} term causes equation 5.23 to go to zero, because the denominator remains non-zero while the numerator goes to zero. The mixing in equation 5.22 is unstable for degenerate orbitals because both the numerator and the denominator go to zero. The absence of F_{jj}^I and F_{ii}^J terms in equation 5.22 is yet another example of how the mixing described there does not reproduce the actual orbital mixing in equation 5.23.

5.3.2 The Pulay Multi-shell Fock Operator

Other methods, e.g., Pulay's5, have used as the Fock operator

$$\begin{aligned} F_{ij} &= F_{ij}^c && i,j \text{ both in shell } I \text{ or both unoccupied orbitals} \\ F_{ij} &= F_{ij}^I - F_{ij}^J && i,j \text{ are in different occupied shells } I \text{ and } J \\ F_{ij} &= F_{ij}^I && i \text{ is occupied, } j \text{ is unoccupied.} \end{aligned} \tag{5.24}$$

The advantage to the Pulay Fock operator is that the denominator of the mixing term from equation 5.20 is $F_{jj}^c - F_{ii}^c$ rather than $F_{jj}^J - F_{ii}^I$, which is a somewhat better approximation. The Pulay Fock operator is intended only for wave functions with a single GVB pair, and, indeed, is inappropriate for wave functions with more pairs, as degenerate orbitals would still produce the instabilities discussed above.

5.3.3 The Page and McIver Fock Operator

Page and McIver suggest [36] that many of the problems associated with the Fock matrix of the type in equations 5.20 or 5.25 may be avoided by incorporating the proper

orbital mixing terms into the Fock operator and scaling those elements by the difference in the diagonal elements so that the proper mixing terms are obtained when the matrix is diagonalized. A further improvement is made when pseudo-canonical orbitals are used by diagonalizing each shell individually before forming the Fock operator. Such a formulation allows an artificial diagonal term, generally $F_{ii}^D = i$, to be used as the diagonal element and divided out when the matrix is diagonalized. Page and McIver use this Fock operator in a scaled eigenvalue method. GVB-DIIS uses the Page and McIver method to incorporate the proper orbital mixing into a DIIS procedure for multiple shells.

5.3.4 The GVB-DIIS Multi-shell Fock Operator

GVB-DIIS, following Page and McIver, uses the following form for the multi-shell Fock operator:

$$\begin{aligned}
F_{ij} &= F_{ii}^D \delta_{ij} && i,j \text{ are in shell } I \text{ or unoccupied} \\
F_{ij} &= -\tfrac{A_{ij}}{B_{ij}}(F_{jj}^D - F_{ii}^D) && i,j \text{ are in different shells } I \text{ and } J \\
F_{ij} &= -\tfrac{F_{ij}^I}{F_{jj}^J - F_{ii}^I}(F_{jj}^D - F_{ii}^D) && i \text{ is occupied, } j \text{ is unoccupied.}
\end{aligned} \tag{5.25}$$

This definition requires that pseudo-canonical orbitals be used. Transforming to pseudo-canonical orbitals is easily done: essentially the core Fock operator is diagonalized in the space spanned by the closed shell orbitals. Although such a transformation does not change the energy, it does rotate the core orbitals into their canonical orientations. In equation 5.26, A_{ij} and B_{ij} are defined as in Section 2.7, leading to an off-diagonal matrix element of

$$F_{ij} = \frac{(F_{ij}^I - F_{ij}^J)(F_{jj}^D - F_{ii}^D)}{F_{jj}^J + F_{ii}^I - F_{ij}^J - F_{ij}^I + \gamma_{ij}} \tag{5.26}$$

Multiplying the off-diagonal blocks by $(F_{jj}^D - F_{ii}^D)$ removes the effect of the division by this term when the matrix is diagonalized (see equation 5.20). This allows the inclusion in equation 5.26 of the correct second-order terms from Section 2.7. This approach has the additional advantage that it reduces exactly to the standard approach in the limit where all the off-diagonal elements of equation 5.26 go to zero. It should be emphasized that the multiplication by $(F_{jj}^D - F_{ii}^D)$ in equation 5.26 is not included to scale the mixing in the off-diagonal elements, but rather to ensure that the correct second-order mixing strength is included when the matrix is diagonalized.

5.4 Choice of the Error Vector

Section 5.2 describes the choice of the error vector ϵ^n at iteration n. In particular, equation 5.7 describes the error vector in terms of off-diagonal elements of the Fock matrix for that iteration. Using this definition it is easy to see how DIIS algorithms work. The orbitals are converged when the off-diagonal elements of the Fock matrix are

all zero. DIIS find the linear combination of Fock operators that is closest to diagonal, and takes the eigenvalues of that matrix as the next iteration's orbitals.

Our original approach for a multi-shell error vector built on the definition in equation 5.5. That is, $(\mathbf{FD} - \mathbf{DF})$ is taken as the error vector, and a general definition of the multi-shell density matrix is sought. Using the definition for $\mathbf{F}$ given in equation 5.26, the multi-shell density matrix is defined in terms of molecular orbitals as

$$D_{ii} = f_i \tag{5.27}$$

$$D_{ij} = 0 \quad i \neq j. \tag{5.28}$$

This definition corresponds to transforming the standard atomic orbital definition of the density matrix from equation 2.48 into a molecular orbital basis. $\mathbf{D}$ thus defined is transformed into the canonical orbital basis, and the error vector is formed as $(\mathbf{FD} - \mathbf{DF})$.

Using the definition iin equation 5.28 of the multi-shell density matrix and forming the error vector as $(\mathbf{FD} - \mathbf{DF})$ has the unfortunate effect of minimizing the importance of GVB second natural orbitals, where f_i can be very small. With such a formulation of the error vector the core and first natural orbitals converge well, but the second natural orbitals converged more slowly. Correcting this problem leads to the modified definition

$$D_{ii} = f_i \quad f_i > 1/2 \tag{5.29}$$

$$D_{ii} = 1/2 \quad fi < 1/2 \tag{5.30}$$

$$D_{ij} = 0 \quad i \neq j. \tag{5.31}$$

Although equation 5.31 is an *ad hoc* definition and lacks the physical rigor of definition 5.28, it leads to reliable convergence for all orbitals when $(\mathbf{FD} - \mathbf{DF})$ is used as the definition of the error vector.

At this point it is noted that although the definition $(\mathbf{FD} - \mathbf{DF})$ is a convenient method of implementing the conditions for the error vector defined in equation 5.7, it is by no means the only definition of the error vector. In particular, because the definition of the multi-shell density matrix is not straightforward, $(\mathbf{FD} - \mathbf{DF})$ may be abandoned in favor of a more direct method of forming the error vector that preserves the spirit of equation 5.7. The essence of the DIIS method is that the off-diagonal elements of the Fock matrix be zero for convergence, and that the linear combination of past and present iterations' Fock matrices be chosen that form the most diagonal Fock matrix. Thus the error vector for iteration n is defined as the super-vector

$$\epsilon_{ij}^{n} = F_{ij} \tag{5.32}$$

where ϕ_i ranges over the occupied orbitals, and $\phi_j < \phi_i$ and that ϕ_i and ϕ_j cannot also be in the same type of shell (e.g., both core orbitals). This matrix is constructed over the current iteration's molecular orbitals, and transformed to the canonical orbital basis so that it is in the same basis as the error vectors from other iterations.

In practice, this definition of the error vector leads to essentially the same convergence behavior as the definition using equation 5.31 and forming the error vector as $(\mathbf{FD} - \mathbf{DF})$. The definition in equation 5.32 is used in GVB-DIIS because of its conceptual and computational simplicity.

5.5 Related Convergence Issues

Pulay has found [29, 30, 31] the use of level shifting and off-diagonal element scaling useful in improving DIIS convergence. Level shifting is a method of insuring that the wave function converges to the proper root. Recalling equation 2.116 for the rotation angle Δ

$$\Delta = \begin{bmatrix} 0 & \frac{A_{ij}}{B_{ij}} \\ -\frac{A_{ij}}{B_{ij}} & 0 \end{bmatrix} \tag{5.33}$$

and further recalling that the A_{ij} terms are related to the first derivative of the energy with respect to orbital mixing, and the B_{ij} terms are related to the second derivative of the energy with respect to orbital variations, for a wave function to converge to a minimum the denominator must be positive. When the wave function is far away from convergence it is often the case that many of the B_{ij} terms are negative. Level shifting calculates an amount δ to add to all of the B_{ij} terms to make them all positive, and forms the rotation angle as

$$\Delta = \begin{bmatrix} 0 & \frac{A_{ij}}{B_{ij}+\delta} \\ -\frac{A_{ij}}{B_{ij}+\delta} & 0 \end{bmatrix} \tag{5.34}$$

Typically, δ is taken as twice the amount of the most negative value of B_{ij}, which has the effect of making the new minimum value of B_{ij} as much positive as it had been negative, and shifting all of the other values upward accordingly. If excited states are desired, a value of δ can be chosen that makes all but one of the values of B_{ij} positive. The second-order terms introduced in the GVB-DIIS Fock operator in equation 5.26 give excellent convergence for a wide variety of cases without needing to resort to such methods. Indeed, no improvement is seen when such methods are introduced, but these methods may be important in future applications to metals or excited states.

The DIIS extrapolation scheme in equations 5.4 and 5.11–5.18 require Fock matrices and error vectors to be saved every iteration. This can result in large values of the q_n coefficients in equation 5.4 if the number of iterations becomes large. Pulay scales the diagonal elements of the $\mathbf{P}$ matrix in 5.11–5.18 to resolve this problem. GVB-DIIS has implemented a scheme that saves only ten iterations. Past algorithms that save only a fixed number of iterations use an expensive process of discarding the oldest iteration, moving the matrices around in memory to save the newest iteration's information. In contrast, for each iteration past the tenth GVB-DIIS overwrites the matrix that had the lowest q_n coefficient in the previous extrapolation. The GVB-DIIS scheme amounts to discarding the least important information rather than the oldest information; the scheme that older methods employ assumes that the oldest information is the least important for convergence, but this is not necessarily the case. The GVB-DIIS scheme decreases the storage requirements and has little impact on the efficiency of the GVB-DIIS convergence.

Although the introduction of second-order terms greatly increases the radius of convergence for GVB-DIIS, and although quality initial guesses most often put the starting point of a calculation within this radius of convergence, it is still possible to find a system for which the initial guess is outside the radius of convergence of GVB-DIIS. Defining a threshold limit of the error vector, above which standard convergence

methods (such as those defined in Section 2.7) are used, can make the algorithm more robust. The results presented here use $\max(\epsilon) = 1.0$ as this threshold, which is found to be optimal for overall computation time. In contrast, the Pulay DIIS method uses a threshold error vector value of 0.05, which reflects the smaller radius of convergence of the Pulay DIIS scheme. GAMESS DIIS scheme uses a threshold of the energy change being less than 0.5 hartree, which is also generally closer to convergence than the threshold used by GVB-DIIS. The difficulty with using a lower value is that very often non-DIIS convergence methods take a long time to reach the lower value; the difficulty with a higher value is that there is a chance the wave function will still be outside of the radius of convergence of the DIIS method. Generally such a threshold definition, with a quality initial guess, leads to no more than one non-DIIS iteration.

Once the calculation is within the DIIS radius of convergence, the sequence of operations within a GVB-DIIS iteration is: (i) calculation of the two-electron operators; (ii) calculation of GVB-CI coefficients; (iii) formation of the general Fock operator via equation 5.26 and error vector via equation 5.32; (iv) determination of the iteration coefficients via equations 5.11–5.18; (v) diagonalization of the composite Fock operator in equation 5.4 to obtain the new orbitals. If the wave function is not converged, the calculation proceeds back to (i) for another iteration.

5.6 Results

The GVB-DIIS method [32] described above provides excellent convergence for a wide variety of wave functions. For one-pair GVB wave functions we compare our results to both GVB2P5 [5] and GAUSSIAN90 [35] convergence methods and to the DIIS convergence in GAMESS [34]. The DIIS scheme in GAMESS can be unstable for more than one GVB pair or for open shell orbitals in addition to a GVB pair. GAUSSIAN90 only uses DIIS for HF wave functions. Thus, the GVB-DIIS results for more complex wave functions are compared to GVB2P5 and GAUSSIAN90 standard (i.e., non-DIIS) convergence.

One of the important lessons of the work reported here is that reliable convergence does require a reliable automatic procedure for initial guesses. GVB-INIT [33] is a fast, automatic method of generating the localized initial guesses for GVB orbitals, and is used as the starting guess for the examples reported here.

In the following examples we compare results between different programs. We begin all programs from the same initial guess. The convergence criteria we use in the following examples requires the SQCDF, the sum of the squares of the difference in the wave function between two iterations, to be less than 10^{-9} (it should be noted than this is often a much more stringent requirement than the more commonly used criteria of energy variation between iterations being less than 10^{-9}). We report the number of iterations from trial guess to convergence in all cases.

Table 5.1: Number of iterations to converge the one-pair GVB wave function for H_2O as one OH bond is dissociated. The starting geometry ($R_{OH} = 0.94$ Å, $\theta_{HOH} = 105.98°$) is the optimum geometry for the HF wave function using a STO-3G basis. For the SCF, a 6-31G** basis set is used with the GVB-INIT initial guess.

		Number of iterations			
ΔR_{OH} (Å)	Energy (h)	GVBDIIS	GVB2P5	GAMESS	G90
0.0	-76.043561	13	24	†	41
0.2	-76.023038	13	23	†	26
0.5	-75.963830	11	23	22	24
1.0	-75.904616	12	19	20	22
2.0	-75.883588	11	20	22	26

† Did not converge

5.6.1 One pair GVB wave functions

H2O, one bond stretched

The first example demonstrates the ability of GVB-DIIS to converge a wave function with a single correlated s bond. Table 5.1 summarizes a series of electronic structure calculations on H2O using a GVB pair for one of the O-H σ bonds and a 6-31G** basis set. The equilibrium geometry is obtained from a STO-3G minimization. The correlated O-H bond is stretched to a variety of distances past the equilibrium geometry, the electronic structure is calculated using GVB-DIIS, GVB2P5, GAUSSIAN90 and GAMESS, starting from the same initial guess and geometry for all three programs.

Table 5.1 presents data starting from our standard initial guess, described above. GVB-DIIS displays typically excellent behavior, converging in 11 to 13 iterations in the cases reported. GVB2P5 takes significantly longer in every case. The GAMESS DIIS convergence scheme does about as well as GVB2P5 for the three most stretched cases, but does not converge for the two cases closer to the equilibrium geometry. This is due to mixing between the first GVB natural orbital and the uncorrelated O-H bond, which results from using the Fock operator defined in equation 5.20, which would have near-identical matrix elements along the diagonal for these two orbitals. The use of pseudo-canonical orbitals and the Fock matrix defined in equation 5.26 allows GVB-DIIS to use an artificial diagonal element of the Fock operator with no loss of accuracy. As the results in Table 5.1 show, GVB-DIIS has no difficulty whatsoever with these degeneracies. GAUSSIAN90, whose GVB convergence is based upon a similar scheme to that in GVB2P5, follows the same general trends as GVB2P5 but takes slightly longer for each case; its convergence is much slower than that seen in GVB-DIIS.

In Table 5.2, the effect of using a guess that involves a HF SCF calculation before generating the GVB orbitals is investigated. These guesses are significantly more computationally intensive than the guesses used in Table 5.1. In every case GVB-DIIS runs

Table 5.2: The same sequence as in Table 5.1 but with initial guesses based on localizing the orbitals of the HF wave function rather than GVB-INIT.

		Number of iterations			
ΔR_{OH} (Å)	Energy (h)	GVBDIIS	GVB2P5	GAMESS	G90
0.0	-76.043561	13	22	†	34
0.2	-76.023038	12	21	†	26
0.5	-75.963830	11	19	†	24
1.0	-75.904616	11	37	19	46
2.0	-75.883588	10	107	27	392

† Did not converge

as fast or faster with these guesses, but the one or two iterations saved hardly justifies the expense of obtaining the guess. On the other hand, although GVB2P5 does work slightly better for some of the less distorted geometries, for the more distorted ones it behaves very poorly. This is no doubt due to the fact that HF orbitals are poor descriptions for chemical bonds at very distorted geometries, and that they therefore provide a poor basis for initial guesses here. GAUSSIAN's convergence is also moderately better for the less distorted geometries and rather poorly for the more distorted geometries. GAMESS failed to converge 3 of the cases. The general conclusion is that the potential added accuracy of the guesses that involve a HF SCF calculation before generating the GVB orbitals certainly does not justify the added expense. The remainder of this chapter uses GVB-INIT, the less expensive standard initial guess method used in Table 5.1.

Twisted ethylene

Table 5.3 reports data obtained from twisting the π bond in ethylene from $0°$ to $90°$. The geometry of Krisnan et al. [37] is used as the equilibrium geometry. The π bond is correlated with a GVB pair. The total number of iterations required to converge the wave function from the trial guess to a SQCDF $< 10^{-9}$ is reported.

At the equilibrium geometry all methods display acceptable convergence, but as the bond twists further GVB2P5, GAUSSIAN90, and GAMESS have increasing difficulty. GVB2P5 and GAUSSIAN take a large number of iterations for the $90°$ geometry, and GAMESS does not converge at all. In contrast, GVB-DIIS shows rapid convergence in every example. All of the wave functions have the most difficult time converging the wave function for the geometry that has the dissociated p bond. GVB-DIIS maintains reasonable convergence properties even for this wave function. The fact that the GAMESS DIIS convergence scheme cannot converge a number of the geometries used so far casts doubts on the general applicability and reliability of its algorithm. In contrast, GVB-DIIS demonstrates excellent convergence for all of the geometries.

Table 5.3: Number of iterations for the one-pair GVB wave function for C_2H_4 as a function of torsional twisting about the C-C bond. Starting geometry: $R_{CC} = 1.334$ Å, $R_{CH} = 1.081$ Å, $\theta_{HCH} = 117.4°$. The 6-31G** basis set is used with the GVB-INIT initial guess.

		Number of iterations			
Twist	Energy (h)	GVBDIIS	GVB2P5	GAMESS	G90
0°	-78.066047	7	11	13	27
30°	-78.022104	12	19	21	23
60°	-77.906403	12	29	25	31
90°	-77.748431	21	46	†	74

† Did not converge

Formaldehyde, one pair

Figure 5.1 graphically illustrates the convergence advantages of GVB-DIIS using an electronic structure calculation on formaldehyde with a GVB pair correlating the p bond. An STO-3G minimized geometry and a 6-31G** basis set is used with all methods. The figure plots the convergence, -log10(SQCDF), versus iteration number for GVB-DIIS, GVB2P5, GAUSSIAN90, and GAMESS methods. GVB-DIIS has the fastest convergence of the four programs. GAMESS also displays the rapid convergence typical of DIIS methods. GVB2P5 takes much longer than either of the DIIS methods to converge, and GAUSSIAN90 takes even longer; the run illustrates how this type of scheme can often slow down close to convergence. In contrast the DIIS methods continue their rapid rate of convergence for the entire sequence.

Figure 5.1 demonstrates how the convergence of standard methods (GVB2P5 and GAUSSIAN90) slows as the wave function becomes increasingly converged. In contrast, both DIIS methods show rapid convergence properties that remain relatively constant as the wave function converges.

5.6.2 Multiple GVB pair wave functions

Dissociating both bonds of H2O

An example of wave functions with multiple GVB pairs is reported in Table 5.4, where the electronic structure of H_2O is calculated with a 6-31G** basis set using two GVB pairs to correlate both OH bonds. The equilibrium geometry is obtained from an STO-3G minimization. The bonds are stretched from equilibrium (0.94 Å) to over three times the equilibrium distance (2.94 Å). GVB-INIT is again used for the trial wave function. Table 5.4 reports the total number of iterations from trial guess to SQCDF $< 10^{-9}$.

Although in one case GVB2P5 converges in fewer iterations than GVB-DIIS, for other cases the convergence using GVB2P5 can be quite poor. In contrast, GVB-DIIS

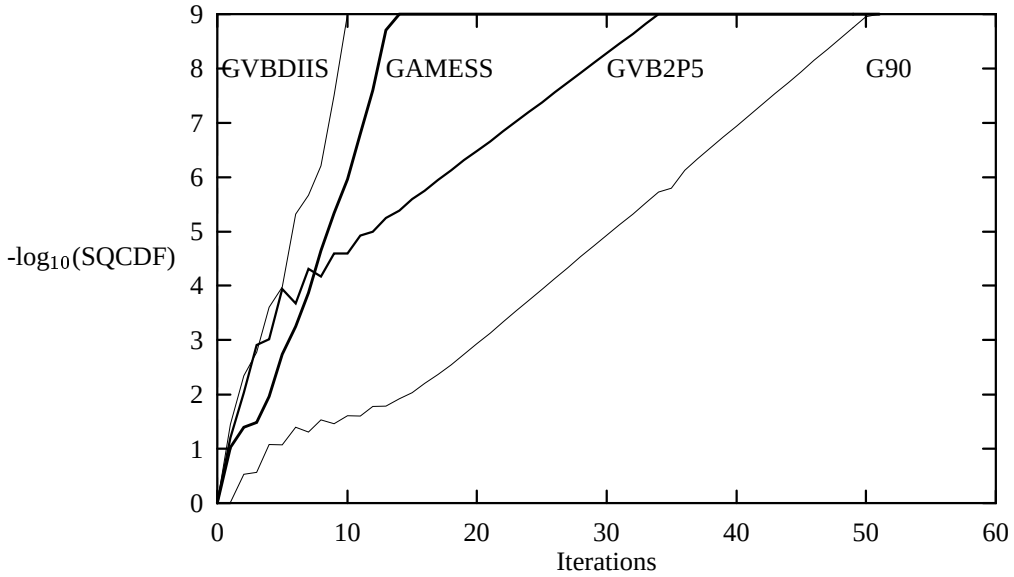

Figure 5.1: Comparison of convergence with GVB-DIIS, GVB2P5, GAMESS/diis, and GAUSSIAN90 for formaldehyde with a one-pair GVB wave function.

Table 5.4: Same as Table 5.1, except that both bonds are simultaneously dissociated and a two-pair GVB wave function is used to correlate both OH σ bonds.

			Number of Iterations		
ΔR_{OH1} (Å)	ΔR_{OH2} (Å)	Energy (h)	GVBDIIS	GVB2P5	G90
0.0	0.0	-76.063303	14	24	89
0.0	1.0	-75.925219	15	31	36
1.0	1.0	-75.799411	14	17	61
0.0	2.0	-75.904235	14	32	40
1.0	2.0	-75.778726	15	56	65
2.0	2.0	-75.756784	18	13	†

† Did not converge

converges quickly (14 to 18 iterations) for every case reported; GVB2P5 requires from 13 to as many as 56 iterations to converge the same cases. GAUSSIAN90, again, does significantly worse than either of the other programs for all cases here.

The fact that GVB2P5 does better for one of these cases is very curious, because the GVB-DIIS Fock operator should reproduce all of the orbital optimization characteristics of GVB2P5 convergence methods. The approximation

$$\frac{M_{ij}}{M_{jj} - M_{ii}} \tag{5.35}$$

made for the mixing when an arbitrary matrix M is diagonalized only holds when

$$M_{ij} << |M_{jj} - M_{ii}|. \tag{5.36}$$

This is not the case for large changes in the orbitals during optimization steps. Thus, standard methods for orbital optimization can still work better for unconverged wave functions. This is why non-DIIS iterations are still necessary at the beginning of the convergence sequence. It should be emphasized that even though the standard methods work better in this one instance, GVB-DIIS at its worst converges wave functions much more rapidly than the majority of examples using standard methods.

Dissociation of the double bond in ethylene

Dissociating a double bond is a stiff test of the convergence method. The next example, summarized in Table 5.5, reports the dissociation of C-C double bond in C_2H_4. The σ and π bonds are correlated with two GVB pairs. The planar geometry from Table 5.3 is used as the equilibrium geometry here. GVB-DIIS is dramatically faster than the other two programs for every geometry, requiring no more than 15 iterations from initial guess to SQCDF $< 10^{-9}$ for any case. GVB2P5, on the other hand, takes no less than 14 and as many as 54 iterations, whereas GAUSSIAN90 requires from 26 to 126 iterations for these same geometries.

Methyl dissociation

The next example, in Table 5.6, examines the effect of an open-shell orbital on the convergence rate of GVB-DIIS. One of the advantages of GVB-DIIS is that it can handle general wave functions that mix open-shell and GVB natural orbitals. The CH_3 radical is a good test of the convergence for such a wave function; the wave function is calculated using a planar geometry with $\theta_{HCH} = 120°$. The C-H bond distances are varied from 1 to 2.6 Å, and the electronic structure of the doublet state is calculated at that geometry using both GVB-DIIS and GVB2P5. Once again, GVB-DIIS requires fewer iterations than does GVB2P5, and GAUSSIAN90 has increasing difficulty as the molecule dissociates.

Glycine with different numbers of GVB pairs

In the final example the number of iterations required to converge a glycine wave function with up to ten GVB pairs is examined. An STO-3G minimized geometry is used

Table 5.5: Number of iterations for the two-pair GVB wave function for ethylene, as a function of displacement of the bond from equilibrium. The GVB pairs correlate both the C-C σ and π bonds. This study uses the same equilibrium geometry as was used in Table 5.3 uses.

		Number of Iterations		
ΔR_{CC} (Å)	Energy (h)	GVBDIIS	GVB2P5	G90
0.0	-78.075751	10	15	26
0.5	-77.975870	13	36	40
1.0	-77.862122	8	14	70
2.0	-77.800986	15	54	74
3.0	-77.798767	15	39	125

Table 5.6: Number of iterations for converging the three-pair GVB wave function of CH_3 radical for symmetric dissociation of the three C-H bonds. The geometry is kept planar with bond angles of 120°. The 6-31G** basis set is used with a GVB-INIT guess.

		Number of Iterations		
R_{CH} (Å)	Energy (h)	GVBDIIS	GVB2P5	G90
1.0	-39.585824	14	17	28
1.2	-39.583762	12	15	28
1.4	-39.492389	11	18	30
1.6	-39.382916	11	21	39
1.8	-39.281492	11	22	41
2.0	-39.196612	10	21	67
2.2	-39.127903	12	20	111
2.4	-39.072965	12	18	191
2.6	-39.029350	14	17	249

Table 5.7: Number of iterations for converging GVB wave functions for glycine. The 6-31G** basis set is used with GVB-INIT. The geometry was from an STO-3G minimization: $R_{NH} = 1.03$ Å, $R_{NC} = 1.48$ Å, $R_{CH} = 1.09$ Å, $R_{CC} = 1.55$ Å, $R_{CO} = 1.22$ Å, $R_{C-OH} = 1.37$ Å, $R_{OH} = 0.99$ Å, $\theta_{HNH} = 104.25°$, $\theta_{HCH} = 107.54°$, $\theta_{HNC} = 107.24°$, $\theta_{NCC} = 113.59°$, $\theta_{CCO} = 125.67°$, $\theta_{OCO} = 122.44°$, $\theta_{COH} = 104.75°$, $\phi_{HNCC} = 55.98°$, $\phi_{HCCO} = -122.00°$, all heavy atoms and the hydroxyl H are coplanar.

		Number of Iterations		
N_{pair}	Energy (h)	GVBDIIS	GVB2P5	G90
0	-282.837281	12	48	16†
1	-282.864831	13	26	30
5	-282.932640	20	162	111
6	-282.953850	17	42	42
10	-283.019396	20	90	75

†HF DIIS convergence used.

for glycine. Table 5.7 reports results with 0 GVB pairs (the regular HF wave function), 1 GVB pair (correlating the C-O π bond), 5 GVB pairs (correlating all the heavy atom-heavy atom bonds: 4 σ and 1 π bonds), 6 GVB pairs (correlating the C-O π bond, the 3 C-H σ bonds, and the 2 N-H σ bonds), and 10 GVB pairs (correlating all bonds). GVB-DIIS requires from 12 to 20 iterations to converge these wave functions, whereas GVB2P5 requires from 26 to 162 iterations, and GAUSSIAN90 from 16 to 75 iterations.

Particularly interesting in this example is that GVB-DIIS converges the HF wave function faster than GAUSSIAN90, which uses the Pulay DIIS scheme. This demonstrates that the additional equations required to make the GVB-DIIS scheme consistent with general wave functions does not impede its behavior on closed-shell HF wave functions, and, in fact, improves the convergence behavior.

Figures 5.2 and 5.3 illustrate some of these cases graphically. The convergence, -Log10(SQCDF), is plotted versus the iteration number for the wave functions with 1 and 10 GVB pairs for GVB-DIIS, GVB2P5 and GAUSSIAN90. We see consistently rapid convergence for GVB-DIIS. GVB2P5 and GAUSSIAN90 show similar behavior, each requiring many more iterations, and the rate of convergence slows as the iterations increase.

Although GVB-DIIS has one iteration where the convergence does not monotonically increase, the wave function converges rapidly, and the convergence behavior does not degrade as the wave function converges. In contrast, the standard convergence methods slow down significantly as the wave functions converge, and the wave functions take much longer to reach convergence.

The same trend continues with the ten pair example. GVB-DIIS converges rapidly, whereas the convergence of the standard methods slows as the wave functions become

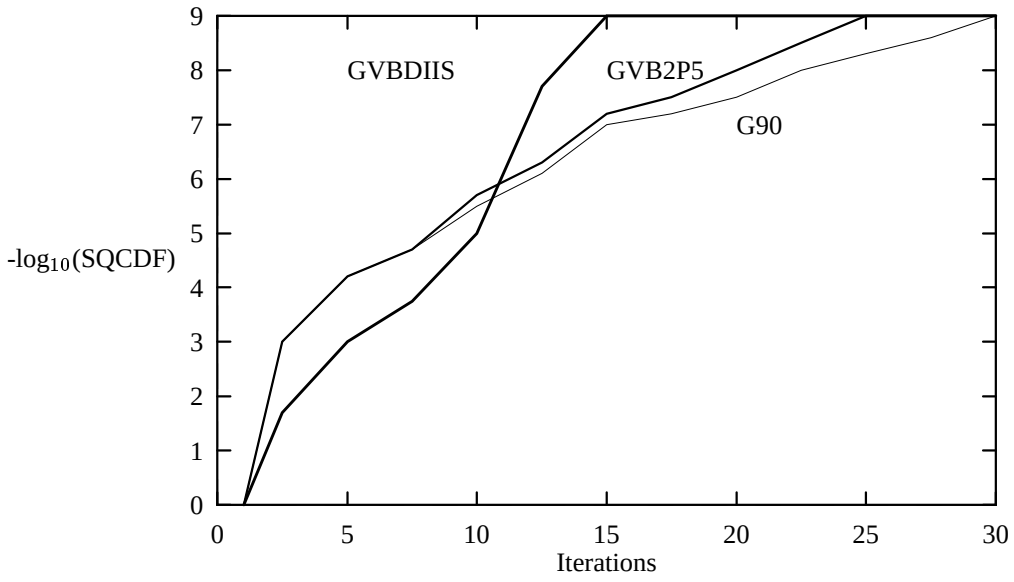

Figure 5.2: Comparison of convergence of GVB-DIIS, GVB2P5 and Gaussian90 for Glycine wave functions with the C-O π-bond correlated using one GVB pair.

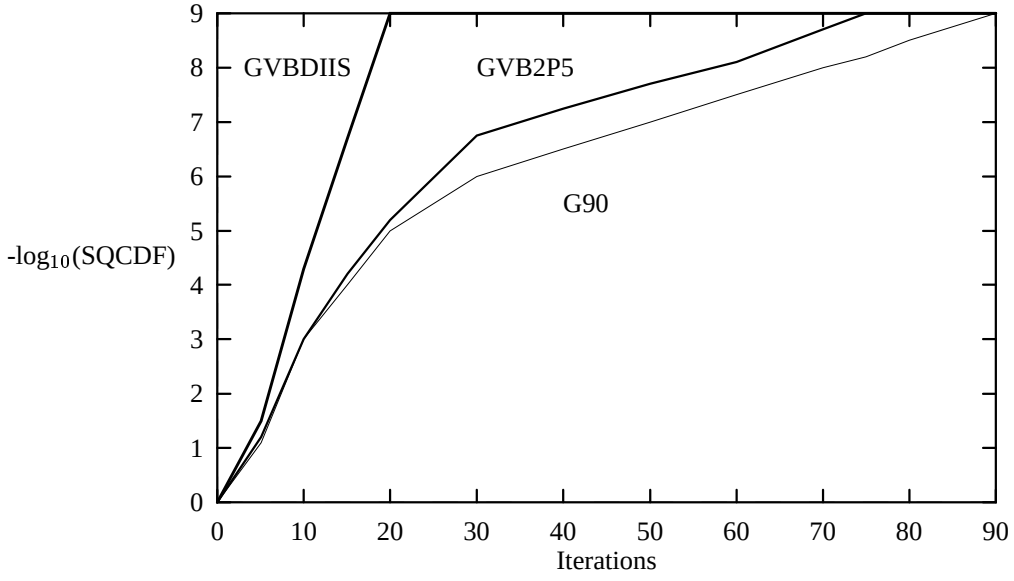

Figure 5.3: Comparison of convergence of GVB-DIIS, GVB2P5 and Gaussian90 for Glycine wave functions with all 10 bonds correlated using GVB pairs.

more converged.

The results presented in Section 5.6 reflect a number of significant points. GVB-DIIS in general converges much more quickly than GVB2P5 does. Moreover, pathological cases, where the program takes an inordinate number of iterations or does not converge, are much rarer in GVB-DIIS than in GVB2P5. GAUSSIAN90 convergence follows the same general trends as does GVB2P5, but generally takes longer for a given case; this convergence is far inferior to that seen in GVB-DIIS. Finally, the radius of convergence for GVB-DIIS, although perhaps not as wide as that of GVB2P5, is a significant improvement over that in the DIIS scheme in GAMESS.

The most important advantage gained by the GVB-DIIS algorithm comes from the reliability it brings to wave function convergence. As the examples in this section demonstrate, GVB-DIIS converges wave functions in 10-15 iterations, often a few more or a few less, but almost always in this range. The behavior of other convergence algorithms varies from cases where they do as well as GVB-DIIS, to cases where they take several times as many iterations to converge. It is this reliability that makes GVB-DIIS an extremely reliable option for converging HF and GVB wave functions.

5.7 Conclusions

The GVB-DIIS method makes converging wave functions that include arbitrary numbers of core, open, and GVB orbitals fast and reliable. This method makes it now possible to use physically accurate wave functions to calculate force-fields, to describe bond distortion and dissociation processes, and to obtain highly converged wave functions for the purpose of calculating more exact molecular properties such as charges and dipole moments.

The GVB-DIIS convergence scheme has already been implemented in the PS-GVB electronic structure program [16]. The pseudospectral approach, when combined with the methods detailed here, should allow GVB calculations on much larger systems than have been possible before.

Chapter 6

Ab Initio Calculation of Porphyrin Excited States

6.1 Introduction

The research presented in this section develops two new methods of calculating the energy and wave functions for porphyrin excited states using *ab initio* electronic structure theory methods. These methods involve frozen core approximations and the self-consistent optimization of the excited states. Results are presented for porphine, the simplest porphyrin, using both methods. In addition, the flexibility of the second method allows calculation of chlorin and bacteriochlorin, two reduced porphyrins. These methods may be used to evaluate the accuracy of some of the common assumptions made on porphyrin excited states.

Porphyrin molecules are ubiquitous in biology and chemistry, appearing in, among other places, photosynthetic pigments [38], hemoglobin [39], cyctochrome P-450 [40], and a variety of synthetic catalysts [41, 42]. One of the reasons porphyrins are so common in biology and chemistry is that they can be modified and substituted in a variety of ways, and these variations can have a profound effect on the chemistry they perform. Figure 6.1 shows porphine, the simplest porphyrin. The two hydrogens can be removed from the center of the ring yielding the porphyrin dianion, and a series of metals can coordinate with the four nitrogen atoms. The outer ring hydrogens may also be replaced with organic groups, which can affect the ring geometry, changing it from the planar porphine geometry to a non-planar geometry. Finally, double bonds on the pyrrole groups may be reduced.

Because porphyrins are primarily characterized by their absorption spectrum, and because the absorption spectrum varies greatly with substitution of the ring and center positions on the porphyrin, analysis of the excited states of the molecule has long been a subject of intense experimental and theoretical effort. The spectra of porphyrins are characterized by an intense UV absorption known as the *Soret* or *B* band, and several weak visible absorptions known as the *visible* or *Q* bands [43]. The four-orbital model [44, 45] arose from 18-electron circular wire models of porphyrins, and was later re-

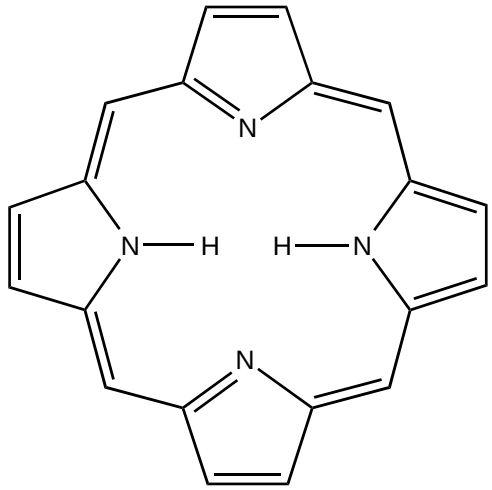

Figure 6.1: Structure of Porphine

fined with semi-empirical calculations. The four-orbital model explains the qualitative appearance of the absorption spectrum, and the qualitative shift of the absorption spectrum with substitution, and has been an invaluable tool in the analysis of porphyrin spectra.

Unfortunately, attempts to put the four-orbital model on firmer theoretical ground have been hindered by the difficulty of an *ab initio* calculation on a porphyrin molecule. This difficulty is partially due to the size of the porphyrin molecule. With 24 heavy atoms and 14 hydrogens, porphine requires 430 basis functions when using a double-zeta plus polarization basis set. Moreover, the multi-configurational nature of the excited states predicted by the four-orbital model contribute to the difficulty of the calculation. In general, description of multi-configurational states requires an $\mathcal{O}(N_{bf}^5)$—where N_{bf} is the number of basis functions—transformation of the two-electron integrals that is prohibitively expensive for a molecule with 430 basis functions. Descriptions of the excited states of porphyrins have thus lacked the rigor of *ab initio* quantum chemistry.

This chapter describes two methods, both based on *ab initio* quantum chemistry, of calculating the four orbital excited states (FOES) of porphyrins that correct these shortcomings. The first, frozen core four orbital excited states (FC-FOES) uses frozen core corrections to freeze the σ interactions in the porphyrin and performs MC-SCF calculations on the FOES. These calculations are followed by CI calculations (FC-FOES-CI) at the single excitation level to correct for the approximations made by the Gouterman model. The FC-FOES and FC-FOES-CI methods are used to calculate the excited state for porphine, the simplest porphyrin. The second method, self-consistent four orbital excited states (SC-FOES), calculates the FOES self-consistently, using the appropriate Hamiltonian for each state. The SC-FOES calculations use the PS-GVB program to describe the electronic structure of porphyrin molecules. This program makes it pos-

sible to directly calculate the matrix elements necessary to describe the energy and the orbital optimization of the multi-configurational states, so that a transformation of the two-electron integrals is not necessary. The flexibility of the SC-FOES method allows it to calculate the excited states of not only porphine, but also those of chlorin and bacteriochlorin, two reduced porphyrins. Both FC- and SC-FOES methods show excellent agreement with experimental results. The accuracy of the FOES method can be improved by combining it with the frozen core method, which allows the incorporation of single excitations from the FOES states into the unoccupied orbitals. This combined method, SC-FOES-CI, is used to correct the limitations of the four orbital approximation in porphine. The high degree of accuracy attained with these methods indicates that they are well suited to describing the absorption spectrum of other porphyrins.

6.2 The Four-Orbital Model and Four-Orbital Excited States

The four-orbital model considers the occupied orbitals with the highest energies, ϕ_a and ϕ_b, and the two virtual orbitals with the lowest energies, ϕ_c and ϕ_d. From 18-electron circular wire models a and b are degenerate, as are c and d. In porphine with D_{2h} symmetry orbital a has b_{1u} symmetry, orbital b has a_u symmetry, orbital c has b_{3g} symmetry, and orbital d has b_{2g} symmetry, as shown in Figure 6.2.

Thus, the optically allowed transitions consist of

$$\begin{aligned} a \rightarrow \quad & c \quad b_{2u} \text{ symmetry} \\ b \rightarrow \quad & d \quad b_{2u} \text{ symmetry} \\ a \rightarrow \quad & d \quad b_{3u} \text{ symmetry} \\ b \rightarrow \quad & c \quad b_{3u} \text{ symmetry.} \end{aligned} \tag{6.1}$$

Transitions of like symmetry combine to form the following coupled transitions

$$\begin{aligned} Q_y &= (a \rightarrow c) + (b \rightarrow d) \\ B_y &= (a \rightarrow c) - (b \rightarrow d) \\ Q_x &= (a \rightarrow d) - (b \rightarrow c) \\ B_x &= (a \rightarrow d) + (b \rightarrow c). \end{aligned} \tag{6.2}$$

These states will hereafter be referred to as the four-orbital excited states, or FOES. These transitions are shown schematically in Figure 6.3.

In D_{4h} symmetry orbital a has symmetry a_{2u}, orbital b has symmetry a_{1u}, and c and d form a degenerate pair of e_g orbitals. Even though the transitions are all now of symmetry e_u and may freely mix, the four-orbital model assumes that they still retain the general form of equation 6.3.

The four-orbital model predicts the shift of the absorption spectrum with substitution by predicting that the relative strength of the individual transitions in each of the coupled transitions in equation 6.3 will shift, causing a shift in intensity. Thus the *pure* FOES described by equation 6.3 are no longer the exact wave functions but are only

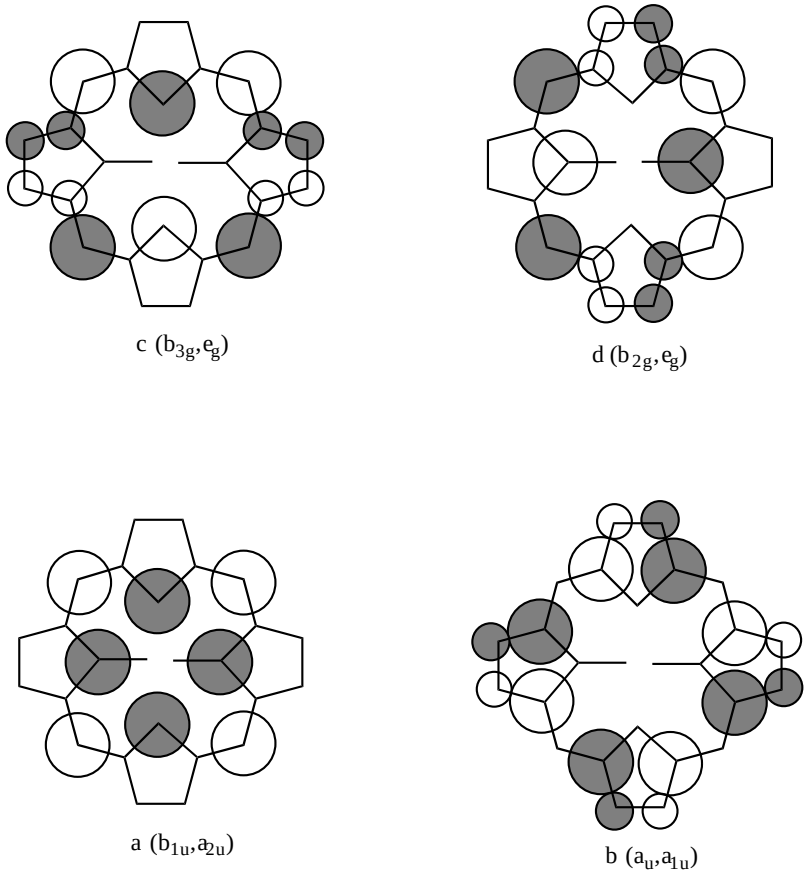

Figure 6.2: Schematic representation of the p-density of the highest two occupied molecular orbitals and the lowest two unoccupied molecular orbitals of porphine. Shown are the tops of the π basis functions that compose the orbitals, filled circles representing negative phase, open circles representing positive phase. Symmetry labels are given for each orbital in the D2h and D4h symmetries.

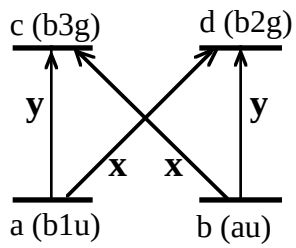

Figure 6.3: Schematic representation of transitions between idealized, degenerate four orbitals.

approximate. The pure FOES remain an excellent approximation to the real excited states that would be obtained by allowing the single excitations in equation 6.3 to mix arbitrarily by comparing our calculated excitation energies to experimental spectra.

6.3 The Multi-Configurational Nature of FOES

Wave functions whose energy expression can be written in the form of equation 2.105 can form all of the terms required to calculate the energy and to optimize the orbitals from h, J, and K operators. Thus, rather than a complete transformation of the two-electron integrals only the partial transformation to compute J and K operators is required. This reduces the formal scaling of the problem from $\mathcal{O}(N_{bf}^5)$ to $\mathcal{O}(N_{bf}^4)$, where N_{bf} is the number of basis functions (cf. discussions in Chapters 1 and 2).

Unfortunately, more complex wave functions do require a full transformation of the two electron integrals. The four-orbital states described in equation 6.3 are multi-configurational. For example, consider the four-orbital Q_y state:

$$\Psi_{Q_y} = \frac{1}{\sqrt{2}} \left| \{Core\}[a^2(bd+db) + b^2(ac+ca)] \right\rangle \tag{6.3}$$

The energy of this wave function is given by

$$\begin{aligned} E_{Q_y} \quad = \quad & \sum_i^{N_{Core}} (2h_{ii} + 2J_{ik} - K_{ik}) + \frac{3}{2}h_{aa} + \frac{3}{2}h_{bb} + \frac{1}{2}h_{cc} + \frac{1}{2}h_{dd} \\ & +3J_{ak} - \frac{3}{2}K_{ak} + 3J_{bk} - \frac{3}{2}K_{bk} + J_{ck} - \frac{1}{2}K_{ck} + J_{dk} - \frac{1}{2}K_{dk} \\ & +\frac{1}{2}J_{aa} + \frac{1}{2}J_{bb} + 2J_{ab} - K_{ab} + \frac{1}{2}J_{ac} + \frac{1}{2}K_{ac} + J_{ad} - \frac{1}{2}K_{ad} \\ & +J_{bc} - \frac{1}{2}K_{bc} + \frac{1}{2}J_{bd} + \frac{1}{2}K_{bd} + 2(ac|bd) - (ab|cd) \end{aligned} \tag{6.4}$$

where k signifies a core orbital. Most of the terms in equation 6.5 are simple h, J, and

K matrix elements, but the terms

$$(ac|bd) = \int \frac{\phi_a^*(1)\phi_c(1)\phi_b^*(2)\phi_d(2)}{r_{12}} d^3r_2 d^3r_1 \tag{6.5}$$

and

$$(ac|bd) = \int \frac{\phi_a^*(1)\phi_b^*(1)\phi_c(2)\phi_d(2)}{r_{12}} d^3r_2 d^3r_1 \tag{6.6}$$

cannot be formed from matrix elements of h, J, or K operators.

The situation is made even more difficult when the orbital optimization equations are considered. Recalling the procedure described in Chapter 2, given a set of trial orbitals $\{\phi_i^{Old}\}$, the optimal set of orbitals $\{\phi_i^{New}\}$ are obtained via the transformation

$$[\phi^{New}] = \exp(\Delta)[\phi^{Old}] \tag{6.7}$$

where $[\phi^{New}]$ and $[\phi^{Old}]$ are the matrices whose columns are the orbitals ϕ_i^{New} and ϕ_i^{Old}, respectively. Δ is the anti-symmetric matrix with zero diagonal defined by

$$\Delta = \begin{bmatrix} 0 & \frac{A_{ij}}{B_{ij}} \\ -\frac{A_{ij}}{B_{ij}} & 0 \end{bmatrix} \tag{6.8}$$

where A_{ij} contains terms of first-order in orbital mixing, and B_{ij} contains terms of second-order in orbital mixing.

For general HF or GVB wave functions of the form of equation 2.101, all of the A_{ij} and B_{ij} terms are formed from the J and K operators. The energy expressions for the wave functions which describe the FOES contain terms of the types in equations 6.5 and 6.6 that cannot be constructed from J and K operators. Consequently, the orbital mixing terms A_{ij} and B_{ij} contain terms which cannot be computed from J and K operators, and a full transformation of the two-electron integrals is needed to update the orbitals and form the energy expression.

Because of the size of porphyrin molecules, the required integral transformation is impossible. Consequently, methods must be determined which can calculate the excited states without requiring a transformation of the two-electron integrals. Section 6.4 describes a method which transforms only a small subset of the two-electron integrals, thus reducing the problem to one of manageable size, and Section 6.6 describes a method where the orbitals are not transformed at all, but where additional terms are calculated using the pseudospectral program for the orbital optimization equations and the energy expression.

6.4 The Frozen Core Four Orbital Excited State Method

One method of making *ab initio* calculations on porphyrin excited states tractable is the frozen core approximation. The electronic energy in equation 2.105 may be expressed as a sum of orbital energies

$$E = \sum_i^{N_{occ}} E_i \tag{6.9}$$

where

$$E_i = f_i h_{ii} + \sum_j^{N_{occ}} (a_{ij} J_{ij} + b_{ij} K_{ij}) \tag{6.10}$$

The σ and π orbitals in planar molecules are of different symmetry types and do not mix with each other. We can therefore rewrite E_i as

$$E_i = f_i h_{ii} + \sum_j^{\sigma} (a_{ij} J_{ij} + b_{ij} K_{ij}) + \sum_j^{\pi} (a_{ij} J_{ij} + b_{ij} K_{ij}) \tag{6.11}$$

Taking

$$V_\sigma = + \sum_j^{\sigma} (a_{ij} J_{ij} + b_{ij} K_{ij}) \tag{6.12}$$

allows us to rewrite E_i as

$$E_i = f_i h_{ii} + V_\sigma + \sum_j^{\pi} (a_{ij} J_{ij} + b_{ij} K_{ij}) \tag{6.13}$$

The frozen core approximation assumes that V_σ remains constant while the π-orbitals are optimizing, being excited, and so on. This assumption allows us to perform a calculation only in the π-space of the molecule, which is much smaller than the full $\sigma + \pi$ space. In the case of porphine the $\sigma + \pi$ space contains 430 basis functions and 81 occupied orbitals whereas the π space contains only 110 basis functions and 13 occupied orbitals. The π space is small enough to allow a full transformation of the two-electron integrals, which allows standard methods such as Configuration Interactions (CI) and Multi-Configurational SCF (MC-SCF) to be used to describe the excited states.

In practice, the FC-FOES method uses PS-GVB [16] to calculate the V_σ term. As outlined in Chapters 2–4, the combination of a grid and basis functions for integral evaluation enables PS-GVB to handle calculations with very large basis sets. Porphine has 24 heavy atoms and 14 hydrogens, and requires 430 basis functions using the 6-31G** basis set. PS-GVB makes possible calculations of this size even on simple laboratory workstations. The V_σ term is evaluated via equation 6.12 and output over the basis set of 110 π basis functions.

Using the MQM program suite, the two-electron integrals are constructed in a modified 6-31G** basis that contains only π basis functions, and V_σ is added to the one-electron integrals. The π space is only 110 basis functions, small enough to allow a full transformation of the two-electron integrals. After the integral transformation, MC-SCF calculations are performed to optimize the FOES in the four orbital active space using the MQM program GVBTHREE. These FC-FOES approximations subsequently can be corrected by performing a single-excitation CI (CI-S) calculation. The FC-FOES-CI calculation allows the excited states to relax from the FOES structure.

The frozen core approximation thus described can break down in two ways. First, if the molecule is not planar the σ and π spaces are no longer orthogonal and can mix. In such a case V_σ is no longer constant and cannot be included as a parameter. Secondly,

excitations or other perturbations of the π orbitals can cause the s core to relax, which again causes V_σ to change.

In the present work we use the frozen core approximation in two applications. First, we calculate V_σ from a HF ground state. The V_σ potential can be included in a π only calculation of the porphyrin excited states. The relaxation of the σ core that occurs when the π orbitals are excited is not included, which leads to errors in the calculation. Later, in Section 6.10, the SC-FOES calculations are used to obtain improved V_σ. In this case the σ core already has adjusted to the excited π orbitals, and our results are much more accurate. Such a calculation is valuable because it allows the CI-S calculation to estimate the error introduced by the FOES assumption in the SC-FOES.

6.5 Results of FC-FOES Porphine Calculations

This section reports the results of FC-FOES and FC-FOES-CI calculations on porphine, where the V_σ term is calculated from ground state calculations porphine calculations. In FC-FOES calculations, V_σ is calculated with the PS-GVB program, and is incorporated into the MQM program suite, where HF and MC-SCF calculations are performed. The active space in our MC-SCF calculations is confined to the four orbitals; excitations amongst the four orbitals are allowed to mix in arbitrary amounts. Table 6.1 reports the accuracy of the V_σ potential. For a ground state calculation, virtually the same orbital energies are obtained with a frozen core as with an active core. The error reported in the last column is no higher than 0.03 eV—which is the same order of magnitude of error that the numerical grid itself introduces to PS-GVB calculations. This indicates that, for ground state calculations, no additional error is introduced when the V_σ term is introduced to the energy.

In these calculations the porphine geometry is taken from the crystal structure given in reference [46]. Slight modifications to this geometry are made so that the porphine molecule has overall D_{2h} symmetry.

Table 6.2 reports the accuracy of FC-FOES and FC-FOES-CI calculations, again using a V_σ derived from a ground state wave function. The first four columns of Table 6.2 compare the FC-FOES energies to experimental numbers. The FC-FOES results agree with experimental results to within 1.29 to 1.78 eV for the Soret and visible band of porphine. This error—roughly 1.5 eV—comes from three sources. The first comes from the four orbital approximation itself, limiting the excited states to the form of equation 6.3. The second comes from freezing the electrons represented by the V_σ potential in the same states that they occupied in the ground state calculations. Although the σ and π orbitals do not mix in planar molecules, the π electron density changes when the electron in the four orbitals go from their ground to their excited configurations. Consequently, the σ electron density would normally readjust, but being represented by a potential rather than explicit active electrons, it cannot, which introduces another source of error. Section 6.6 presents a method of correcting for the σ relaxation upon π excitation.

With the frozen core calculations it is possible to correct for the errors introduced by the FOES structure. By following the FC-FOES calculations with a single-excitation CI (CI-S) calculation even greater accuracy may be obtained. The final two columns of

Table 6.1: Comparison of ground state frozen core and active core orbital energies for porphine. Active core energies calculated using PS-GVB, frozen core energies calculated using GVB2P5 and V_σ from PS-GVB active core calculation. See text for other details.

Symmetry	Active Core (h)	Frozen Core (h)	Error (h)	Error (eV)
1 b_{2g}	-0.539384	-0.539370	-0.000014	-0.000381
2 b_{2g}	-0.375437	-0.375329	-0.000108	-0.002939
3 b_{2g}	-0.324257	-0.324189	-0.000068	-0.001850
1 b_{3g}	-0.582523	-0.582513	-0.000010	-0.000272
2 b_{3g}	-0.374731	-0.374622	-0.000109	-0.002966
3 b_{3g}	-0.366131	-0.366372	0.000241	0.006558
1 a_u	-0.437340	-0.437228	-0.000112	-0.003048
2 a_u	-0.219526	-0.219372	-0.000154	-0.004190
1 b_{1u}	-0.589291	-0.589152	-0.000139	-0.003782
2 b_{1u}	-0.522173	-0.522011	-0.000162	-0.004408
3 b_{1u}	-0.377294	-0.377387	0.000093	0.002531
4 b_{1u}	-0.333696	-0.333601	-0.000095	-0.002585
5 b_{1u}	-0.238392	-0.238227	-0.000165	-0.004490

Table 6.2: Comparison of theoretical and experimental porphine excited state energies using ground state V_σ. FC-FOES and FC-FOES-CI results are reported. All energies in eV.

State	Experiment†	FC-FOES	Error	FC-FOES-CI	Error
Q_x	2.03	3.45	1.42	2.26	0.23
Q_y	2.46	3.71	1.25	2.75	0.29
B_x	3.33	5.07	1.74	4.01	0.68
B_y	3.33	5.11	1.78	4.37	1.04

† Reference [47, 48]

Table 6.2 report the improvement of these FC-FOES calculations when a CI calculation is performed at the single excitation level in the 110 orbital π-space—the FC-FOES-CI method. The single excitations improve the agreement with experiment to from 0.29 to 1.04 eV. We therefore estimate that the FOES structure introduces roughly 1 eV of error to the porphyrin excited state energies, and that the remaining 0.5 eV of error in the FC-FOES-CI calculations is due to the lack of σ relaxation in this model.

Later, Section 6.10 again uses frozen σ cores, but there V_σ is derived from the excited state calculations. These calculations should combine the strengths of the frozen core calculations with a potential that has already relaxed to the excited π electrons.

6.6 Self-Consistent Orbital Optimization in FOES

The FC-FOES and FC-FOES-CI methods show excellent agreement with experimental results. In an effort to obtain better agreement with experiment, this section describes a method that describes all σ and π electrons self-consistently. Such a description of the porphyrin excited states is made possible by assuming that the excited states are of the form of equation 6.3 with equal components of the two excitations in each excited state.

The SC-FOES method is the method that solves for the FOES, by calculating the energy and the optimum orbitals of the excited state self-consistently and without an integral transformation. The SC-FOES method accomplishes this by analytically calculating the orbital optimization equations for each of the FOES. The equations that result are expressed in terms not only of h, J, and K operators (as is the case for simpler energy expressions of the form of equation 2.101), but also general two electron integrals that cannot be expressed as matrix elements of h, J or K. These terms are normally calculated by a full transformation of the two-electron integrals, but, as porphine is too big to allow a full integral transformation without resorting to either a poor basis set or a frozen core description, a different method of obtaining these terms must be found. SC-FOES uses PS-GVB is used to calculate all of the terms required for the orbital optimization and the energy expressions and to use these terms to optimize the orbitals for each state self-consistently. SC-FOES uses the standard PS-GVB procedure of calculating the h, J, and K operators required in the optimization equations, and explicitly calculates the additional general two electron integrals required.

The energies of the wave functions for the four states are given by

$$\begin{aligned} E_{Q_y/B_y} \quad = \quad & \sum_i^{N_{Core}} (2h_{ii} + 2J_{ik} - K_{ik}) + \frac{3}{2}h_{aa} + \frac{3}{2}h_{bb} + \frac{1}{2}h_{cc} + \frac{1}{2}h_{dd} \quad (6.14) \\ & +3J_{ak} - \frac{3}{2}K_{ak} + 3J_{bk} - \frac{3}{2}K_{bk} + J_{ck} - \frac{1}{2}K_{ck} + J_{dk} - \frac{1}{2}K_{dk} \\ & +\frac{1}{2}J_{aa} + \frac{1}{2}J_{bb} + 2J_{ab} - K_{ab} + \frac{1}{2}J_{ac} + \frac{1}{2}K_{ac} + J_{ad} - \frac{1}{2}K_{ad} \\ & +J_{bc} - \frac{1}{2}K_{bc} + \frac{1}{2}J_{bd} + \frac{1}{2}K_{bd} \pm 2(ac|bd) \mp (ab|cd) \end{aligned}$$

where the Q_y state comes from the top part of the $\pm$ or $\mp$ operators and the B_y state

comes from the bottom part, and

$$
\begin{aligned}
E_{B_x/Q_x} &= \sum_i^{N_{Core}} (2h_{ii} + 2J_{ik} - K_{ik}) + \frac{3}{2}h_{aa} + \frac{3}{2}h_{bb} + \frac{1}{2}h_{cc} + \frac{1}{2}h_{dd} \quad (6.15)\\
&+3J_{ak} - \frac{3}{2}K_{ak} + 3J_{bk} - \frac{3}{2}K_{bk} + J_{ck} - \frac{1}{2}K_{ck} + J_{dk} - \frac{1}{2}K_{dk}\\
&+\frac{1}{2}J_{aa} + \frac{1}{2}J_{bb} + 2J_{ab} - K_{ab} + J_{ac} - \frac{1}{2}K_{ac} + \frac{1}{2}J_{ad} + \frac{1}{2}K_{ad}\\
&+\frac{1}{2}J_{bc} + \frac{1}{2}K_{bc} + J_{bd} - \frac{1}{2}K_{bd} \pm 2(ad|bd) \mp (ab|cd)
\end{aligned}
$$

where the B_x state comes from the top part of the $\pm$ or $\mp$ operators and the Q_x state comes from the bottom part.

There are two methods of obtaining the orbital optimization equations from the energy expressions 6.15 and 6.16. The first and most general method is that of Yaffe and Goddard [6]. This is a method consists of writing the energy expression in the form

$$E_{YG} = \sum_{ij} f_{ij}h_{ij} + \sum_{ijkl} c_{ijkl}(ij|kl) \quad (6.16)$$

The Yaffe-Goddard method obtains the A_{ij} and B_{ij} terms for use in the Δ matrix in 2.116 from the coefficients f_{ij} and c_{ijkl}.

A simpler method is to take pairwise mixings of all of the orbitals. Pairwise mixings of the form

$$\phi_i' = \frac{\phi_i + \lambda\phi_j}{\sqrt{1+\lambda^2}} \quad (6.17)$$

and

$$\phi_j' = \frac{\phi_j - \lambda\phi_i}{\sqrt{1+\lambda^2}} \quad (6.18)$$

are inserted into an energy expression such as equation 6.15 or 6.16. By expanding the energy expression in terms of powers of λ, the terms that are first-order in λ lead to the A_{ij} terms, and the terms that are second-order in λ lead to the B_{ij} terms.

For the derivation of the SC-FOES equations presented below, both the Yaffe-Goddard method and the pairwise mixing method were applied, and both yield the same set of equations.

The FOES wave functions have three types of orbitals: *core*, the doubly occupied orbitals; *active*, the fractionally occupied Four Orbitals; and *virtual*, the unoccupied orbitals. This section categorizes the equations as core-active mixings, active-active mixings, and active-virtual mixings.

In this section, the label k will signify a core orbital, labels a, b, c, and d signify the active orbitals, and the label v will signify a virtual orbital. We also define the following modified Fock operators, which are useful in simplifying the equations

$$
\begin{aligned}
F^k &= 4h + 8J^k - 4K^k + 6J^a - 3K^a + 6J^b - 3K^b \quad (6.19)\\
&\quad +2J^c - K^c + 2J^d - K^d\\
F^a &= 3h + 6J^k - 3K^k + 4J^a - 2K^a + 4J^b - 2K^b \quad (6.20)
\end{aligned}
$$

$$
\begin{aligned}
& & & +J^c + K^c + 2J^d - K^d \\
F^b & = & & 3h + 6J^k - 3K^k + 4J^a - 2K^a + 4J^b - 2K^b & (6.21)\\
& & & +2J^c - K^c + J^d + K^d & (6.22)\\
F^c & = & & h + 2J^k - K^k + J^a + K^a + 2J^b - K^b & (6.23)\\
F^d & = & & h + 2J^k - K^k + 2J^a - K^a + J^b + K^b. & (6.24)
\end{aligned}
$$

There is an appealing similarity between the modified Fock operators, as described above, and the normal Fock operators from standard Hartree-Fock theory, which is why the name is retained even though the derivative of an orbital's energy with respect to mixing with other orbitals also depends upon inhomogeneous terms, as shown below. All of the operators required to optimize the orbitals and calculate the energy of the wave functions can be constructed from the matrix elements h_{xy}, J^k_{xy}, K^k_{xy}, J^a_{xy}, K^a_{xy}, J^b_{xy}, K^b_{xy}, J^c_{xy}, K^c_{xy}, J^d_{xy}, K^d_{xy}, $(ab|xy)$, $(ac|xy)$, $(ad|xy)$, $(bc|xy)$, and $(bd|xy)$, where x and y range over all occupied and virtual orbitals. We use the PS-GVB program to form these operators.

The following equations are the orbital mixing equations for the Q_y (the top combination of the $\pm$ operators) and the B_y FOES. The corresponding equations for the B_x and Q_x states are obtained by switching the c and d labels in the equations.

6.6.1 Core-Active Mixing

$$
\begin{aligned}
A_{ka} & = & & \langle k|F^k - F^a|a\rangle \pm (kb|cd) \mp 2(kc|bd) & (6.25)\\
B_{ka} & = & & \langle k|F^k - F^a|k\rangle - \langle a|F^k - F^a|a\rangle & (6.26)\\
& & & \mp(ab|cd) \pm 2(ac|bd) & \\
A_{kb} & = & & \langle k|F^k - F^b|b\rangle \pm (ka|cd) \mp 2(kd|ac) & (6.27)\\
B_{kb} & = & & \langle k|F^k - F^b|k\rangle - \langle b|F^k - F^b|b\rangle & (6.28)\\
& & & \mp(ab|cd) \pm 2(ac|bd) & \\
A_{kc} & = & & \langle k|F^k - F^c|c\rangle \pm (kd|ab) \mp 2(ka|bd) & (6.29)\\
B_{kc} & = & & \langle k|F^k - F^c|k\rangle - \langle c|F^k - F^c|c\rangle & (6.30)\\
& & & +2J_{kc} - 6K_{kc} \mp (ab|cd) \pm 2(ac|bd) & \\
A_{kd} & = & & \langle k|F^k - F^d|d\rangle \pm (kc|ab) \mp 2(kb|ac) & (6.31)\\
B_{kd} & = & & \langle k|F^k - F^d|k\rangle - \langle d|F^k - F^d|d\rangle & (6.32)\\
& & & +2J_{kd} - 6K_{kd} \mp (ab|cd) \pm 2(ac|bd) &
\end{aligned}
$$

6.6.2 Active-Active Mixing

$$
\begin{aligned}
A_{ab} & = & & \langle a|F^a - F^b|b\rangle \pm \langle c|J^a - 2K^a - J^b - 2K^b|d\rangle & (6.33)\\
B_{ab} & = & & \langle a|F^a - F^b|a\rangle - \langle b|F^a - F^b|b\rangle & (6.34)\\
& & & \pm 4(ab|cd) \mp 4(ac|bd) \mp 4(ad|bd) & \\
A_{ac} & = & & \langle a|F^a - F^c|c\rangle \pm \langle b|2J^a - K^a - 2J^c + K^c|d\rangle & (6.35)
\end{aligned}
$$

$$
\begin{aligned}
B_{ac} &= \langle a|F^a - F^c|a\rangle - \langle c|F^a - F^c|c\rangle && (6.36)\\
&\quad +2J_{ac} - 6K_{ac} \pm 2(ab|cd) \pm 2(ad|bc) \mp 8(ac|bd) \\
A_{ad} &= \langle a|F^a - F^d|d\rangle \pm \langle b|K^a - K^d|c\rangle && (6.37)\\
B_{ad} &= \langle a|F^a - F^d|a\rangle - \langle d|F^a - F^d|d\rangle && (6.38)\\
&\quad \mp 2(ab|cd) \pm 2(ac|bd) \\
A_{bc} &= \langle b|F^b - F^c|c\rangle \pm \langle a|K^b - K^c|d\rangle && (6.39)\\
B_{bc} &= \langle b|F^b - F^c|b\rangle - \langle c|F^b - F^c|c\rangle && (6.40)\\
&\quad - \mp 2(ab|cd) \pm 2(ac|bd) \\
A_{bd} &= \langle b|F^b - F^d|d\rangle \pm \langle a|2J^b - K^b - 2J^d + K^d|c\rangle && (6.41)\\
B_{bd} &= \langle b|F^b - F^d|b\rangle - \langle d|F^b - F^d|d\rangle && (6.42)\\
&\quad +2J_{bd} - 6K_{bd} \pm 2(ab|cd) \pm 2(ad|bc) \mp 8(ac|bd) \\
A_{cd} &= \langle c|F^c - F^d|d\rangle \pm \langle a|J^c - 2K^c - J^d + 2K^d|b\rangle && (6.43)\\
B_{cd} &= \langle c|F^c - F^d|c\rangle - \langle d|F^c - F^d|d\rangle && (6.44)\\
&\quad \pm 4(ab|cd) \mp 4(ac|bd) \mp 4(ad|bc)
\end{aligned}
$$

6.6.3 Occupied-Virtual Mixing

$$
\begin{aligned}
A_{kv} &= \langle k|F^k|v\rangle && (6.45)\\
B_{kv} &= \langle k|F^k|k\rangle - \langle v|F^k|v\rangle && (6.46)\\
&\quad -4J_{kv} + 12K_{kv} \\
A_{av} &= \langle a|F^a|v\rangle \pm 2(bd|cv) \mp (bv|cd) && (6.47)\\
B_{av} &= \langle a|F^a|a\rangle - \langle v|F^a|v\rangle && (6.48)\\
&\quad -4K_{av} \mp (ab|cd) \pm 2(ac|bd) \\
A_{bv} &= \langle b|F^b|v\rangle \pm 2(ac|dv) \mp (av|cd) && (6.49)\\
B_{bv} &= \langle b|F^b|b\rangle - \langle v|F^b|v\rangle && (6.50)\\
&\quad -4K_{bv} \mp (ab|cd) \pm 2(ac|bd) \\
A_{cv} &= \langle c|F^c|v\rangle \pm 2(av|bd) \mp (ab|dv) && (6.51)\\
B_{cv} &= \langle c|F^c|c\rangle - \langle v|F^c|v\rangle && (6.52)\\
&\quad \mp (ab|cd) \pm 2(ac|bd) \\
A_{dv} &= \langle d|F^d|v\rangle \pm 2(ac|bv) \mp (ab|cv) && (6.53)\\
B_{dv} &= \langle d|F^d|d\rangle - \langle v|F^d|v\rangle && (6.54)\\
&\quad \mp (ab|cd) \pm 2(ac|bd)
\end{aligned}
$$

6.7 PS-GVB Calculation of Multi-Configurational Operators for SC-FOES

The last section lists the operators required for the four-orbital state orbital optimization and energy calculation. Most of the operators, the ones in standard J or K form, can be formed using the standard PS-GVB program as described in Chapter 2. The other operators, those of the form $(ij|xy)$, where ij is the pair of active orbitals in the set ab, ac, ad, bc, bd, and x and y range over all occupied and virtual orbitals. These operators are also formed using the PS-GVB program. Replacing the density matrix D^k in equation 3.25 with the two-orbital effective density matrix Dij given by

$$D^{ij}_{\mu\nu} = \frac{1}{2}(c_{\mu i}c_{\nu j} + c_{\mu j}c_{\nu i}) \tag{6.55}$$

yields

$$(ij|\mu\nu) = \sum_{g} Q_{\mu} \left[\sum_{\sigma\eta} A_{\sigma\eta}(g) D^{ij}_{\sigma\eta} \right] R(g,\nu) \tag{6.56}$$

The matrix elements $(ij|xy)$ can be formed via the transformation

$$(ij|xy) = \sum_{\mu\nu} c_{\mu x} c_{\nu y} (ij|\mu\nu) \tag{6.57}$$

The program forms the density matrices D^k, D^a, D^b, D^c, D^d, D^{ab}, D^{ac}, D^{ad}, D^{bc}, and D^{bd}. With each density matrix it forms the associated J and K matrices, which it stores on disk. After all of the two-electron matrices have been formed, the program optimizes the orbitals, calculates the energy, and, if the program is not converged, goes to the beginning. The process repeats until the program converges.

Because each four-orbital excited state Q_x, Q_y, B_x, and B_y has a different Hamiltonian, this sequence is repeated for each of the four-orbital excited states for each molecule studied.

6.8 Convergence Acceleration in SC-FOES

The B_{ij} matrix described in equation 6.6 as the denominator of Δ_{ij}, the rotation matrix, is actually just the diagonal elements of $B_{ij,kl}$, a tensor that describes the full second derivative of the electronic energy with respect to orbital variations. When the molecule is small enough to permit a full transformation of the two-electron integrals, quadratic convergence may be achieved by forming all elements of the $B_{ij,kl}$ tensor (according to the equations in reference [6]) and solving

$$0 = A_{kl} + \Delta_{ij} B_{ij,kl} \tag{6.58}$$

For most equations the advantages obtained from using the full $B_{ij,kl}$ tensor are negligible when compared to the amount of computational effort that is required for a full integral transformation, primarily because the $B_{ij,kl}$ tensor is diagonally dominant. Consequently, only the diagonal elements $B_{ij,ij}$ are used, resulting in equation 6.6.

Unfortunately, in cases where the B_{ij} matrix alone is not sufficient to achieve reliable convergence, methods to improved convergence must be used. Such methods include scaling down the size of the Δ matrix, orbital averaging, level shifting, and Direct Inversion in the Iterative Subspace (DIIS) [32] convergence acceleration. Here the SC-FOES method implements a level shifting scheme, primarily for its computational simplicity. Noting that the curvature of a function is positive at a local minimum, all B_{ij} values are shifted by an amount equal to twice the most negative value. The result of such a shift is that the smallest value of the matrix is now positive by as much as it had previously been negative.

It might be questioned here why, if excited states are sought, are positive values of the second derivative matrix desired? Excited states are generally characterized as having one negative eigenvalue. But because of the nature of the FOES wave function, each state is the ground state of its particular Hamiltonian, and consequently the lowest state of that particular Hamiltonian is sought.

The use of the level shifting allows the rapid convergence of the wave functions that otherwise would require many more iterations.

6.9 SC-FOES Results for Porphine

In this section we present calculations on the FOES of porphine. The greater freedom of the SC-FOES description of the electronic structure allows the different porphyrins to be described, and Section 6.11 reports for two reduced porphyrins, chlorin and bacteriochlorin. The porphine molecule is calculated using a 6-31G** basis set. The porphine geometry is obtained from a crystal structure symmetrized to D_{2h} symmetry from reference [46], the same geometry used in the FC-FOES and FC-FOES-CI calculations in Section 6.5.

The first part of this section presents the orbital energies for porphine and demonstrates that even though the energies of the pairs of orbitals in the Four Orbitals are not exactly degenerate, they remain sufficiently close to degeneracy compared to the energy of the orbitals higher and lower than the Four Orbitals. This near-degeneracy justifies the structure of the FOES wave functions used in this section. The second part of this section reports the actual excited state energies using the FOES model.

6.9.1 Orbital Energies

As was noted in Section 6.2, because the four-orbital model assumes the two HOMOs and the two LUMOs are each degenerate pairs of orbitals, the FOES assume an even mixing of the single excitations from the HOMOs into the LUMOs. In real systems these orbitals are not degenerate. For metalloporphyrins with D4h symmetry the two LUMOs form a pair of degenerate eg orbitals, but the two HOMOs are no longer degenerate. For porphyrins of lower symmetry neither the HOMOs nor the LUMOs form degenerate pairs. This section shows that although the active orbitals no longer form degenerate pairs, they are still close enough in energy to justify the FOES structure.

Table 6.3 shows the orbital energies for porphine. The column marked RVO contain the energies of the regular virtual orbitals that are obtained from the eigenvalues of the

Table 6.3: RVO and IVO orbital energies in eV for porphine calculated using PS-GVB. See text and Figure 6.4 for other details.

Orbital	RVO Energy	IVO Energy
HOMO-2	-8.82	-8.82
b_{1u}	-6.48	-6.48
a_u	-5.98	-5.98
b_{3g}	0.36	-1.93
b_{2g}	0.50	-1.80
LUMO+2	3.30	0.46

Fock operator. The difficulty with these orbitals and the accompanying orbital energies is that the virtual orbitals are generated in the field generated by the N electrons in the core, rather than the field from $(N-1)$ electrons that an electron in such an orbital would interact with if the orbital corresponded roughly to an excited orbital. Because of this the energy of the RVOs is unnaturally high. To correct this discrepancy the Improved Virtual Orbital (IVO) [49] energies are also displayed in Table 6.3. These are the virtual orbitals from the cation of the molecule, and correspond much more closely to experimental excitation energies. Whereas the RVO energies predict excitation energies of roughly 6.5 eV, the IVO energies predict excitation energies of roughly 4.0 eV, significantly closer to the theoretical and experimental results presented in the next section.

Figure 6.4 represents the RVO and IVO data from Table 6.3 pictorially. It is evident from this figure that although the pairs of active orbitals are not perfectly degenerate, their energies are still much closer to each other than to that of any other nearby orbitals, suggesting that the structure of the FOES is still accurate.

The RVO energies shown in Figure 6.4 have the correct qualitative appearance, but the actual energies are unnaturally high, due to the extra electrons contained in the core. The use of the IVOs presents a more realistic picture of the orbital energies. Although the energies cannot be used to estimate excitation energies accurately (via Koopman's theorem) because they ignore the resonance between the multiple configurations involved in the excitation, they present a reasonably accurate model of the excitations.

6.9.2 SC-FOES Porphine Calculations

Table 6.4 describes the results of the SC-FOES calculations for porphine. The excited state energies range from 2.73 to 4.03 eV above the ground state energy. The experimental numbers [47, 48] correspond well with these numbers. The last column of Table 6.4 gives the error in the calculation relative to the experimental number; this error ranges from 0.32 to 0.76 eV.

By comparing the FC-FOES, FC-FOES-CI, and SC-FOES calculations, several conclusions can be made. On the average, the FC-FOES method makes an error of

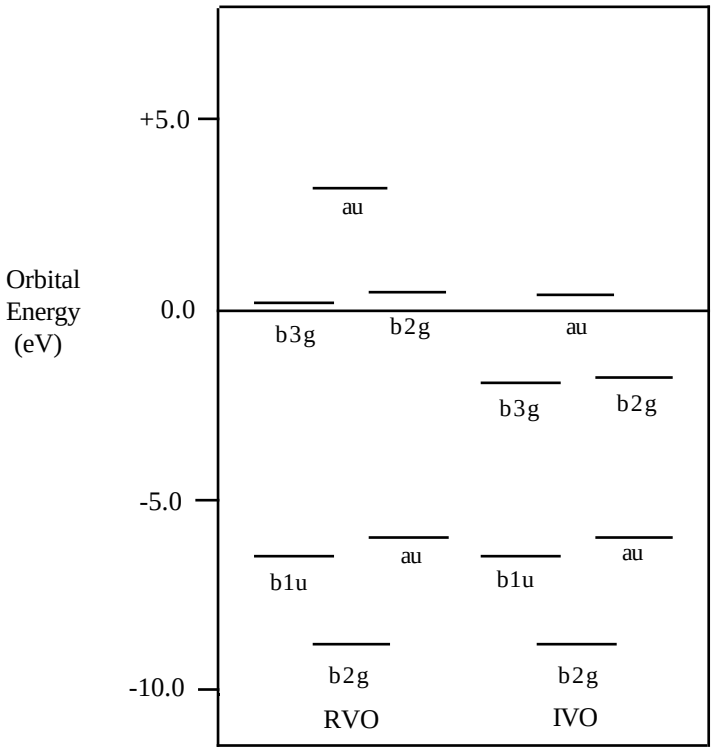

Figure 6.4: Orbital energies and symmetry labels for porphine IVOs and RVOs. Shown are the four active orbitals, the next lowest occupied orbital, and the next highest unoccupied orbital. Orbital energies in eV.

Table 6.4: Excited State Energies for Porphine. Excited states calculated via SC-FOES procedure. Experimental energies as in Table 6.2.

State	Total E (h)	Excit. E (h)	Excit. E (eV)	Exp. (eV)	Error (eV)
Ground	-983.219088	-	-	-	-
Q_x	-983.118662	0.100426	2.73	2.03	0.70
Q_y	-983.111192	0.107896	2.94	2.46	0.48
B_x	-983.071054	0.148034	4.03	3.33	0.70
B_y	-983.084791	0.134297	3.65	3.33	0.32

Table 6.5: Porphine excitation energies in eV, using a frozen V_σ core from SC-FOES calculations. Experimental energies as in Table 6.2. See text for other details.

	Excitation Energy		
State	SC-FOES-CI	Experiment	Error
Q_x	2.21	2.03	0.18
Q_y	2.74	2.46	0.28
B_x	-	3.33	-
B_y	-	3.33	-

1.55 eV, the FC-FOES-CI method makes an error of 0.56 eV, and the SC-FOES method makes an error of 0.55 eV, relative to the experimental results. The FC-FOES and SC-FOES methods are the most similar of the three. The methods differ in that (i) the FC-FOES method allows the excited configurations to mix in arbitrary amounts, and (ii) the SC-FOES method allows the σ orbitals to relax in response to the excited π orbitals. Table 6.3 shows that the pairs of HOMOs and LUMOs are roughly degenerate in porphine, so that the stabilization gained by allowing the different configurations to mix arbitrarily is minimal. Consequently, the 1.0 eV difference in the accuracy of the FC-FOES and SC-FOES methods can be taken as the effect of σ orbital relaxation.

The FC-FOES-CI method reproduces experimental results more accurately than the FC-FOES method by 0.98 eV. As Section 6.5 noted, this amount is taken as the magnitude of the error introduced by limiting the excited states to the Gouterman FOES form.

The FC-FOES/FC-FOES-CI methods are limited because they do not include s relaxation. The SC-FOES method is limited because the excited states are restricted to the FOES form. These methods can be combined to one which has none of these limitations, as detailed in the next section.

6.10 Frozen Core Corrections to SC-FOES: SC-FOES-CI

By combining the SC-FOES methodology with the frozen core technique we can take advantage of the best aspects of both approaches. Here the V_σ potentials are calculated from the converged wave functions from the FOES, and perform the MC-SCF and the CI calculations using a V_σ where the σ core has already relaxed in response to the π excitations. The resulting method is called SC-FOES-CI.

Table 6.5 details the result of these calculations. As the table shows, by using a V_σ where the σ core has relaxed in response to the excited π orbitals improves the accuracy of the visible bands by roughly 0.05 eV, a significant portion of the error in these states. For the Soret bands, where the error is larger, the calculations are still underway, but a similar improvement is expected.

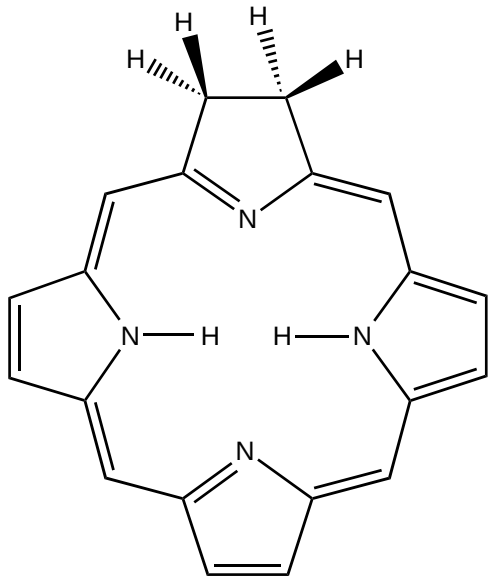

Figure 6.5: Structure of Chlorin

For the visible Q bands the SC-FOES-CI method shows excellent agreement with experimental results. Future studies will complete the analysis of porphine excited states by determining the SC-FOES-CI excitation energies for the B_x and B_y bands.

6.11 Reduced Porphyrins

One important advantage to the SC-FOES method mentioned in earlier sections is that the method does not depend upon symmetry to make the calculation tractable. As a consequence, calculations on porphyrins which do not have D_{2h} symmetry are possible with the SC-FOES method. One important porphyrin which does not have D_{2h} symmetry is chlorin, the porphyrin part of the chlorophyll molecule. The bacterial analog of chlorin is bacteriochlorin. The SC-FOES energies for these molecules are presented in this section.

The chlorin and bacteriochlorin geometries are obtained from the porphine crystal structure by reducing the relevant double bonds and minimizing using a molecular mechanics program; this method is chosen for ease of comparison with the porphine calculations. For chlorin and bacteriochlorin the axis of reduction is perpendicular to the axis of the protons in the porphyrin ring; this choice was made to be consistent with earlier calculations [50] that show it to be slightly lower in energy. Figures 6.5–6.6 show the structures of these molecules.

As with porphine, an important issue for SC-FOES calculations on chlorin and bacteriochlorin is whether the orbitals are degenerate enough for the FOES model of

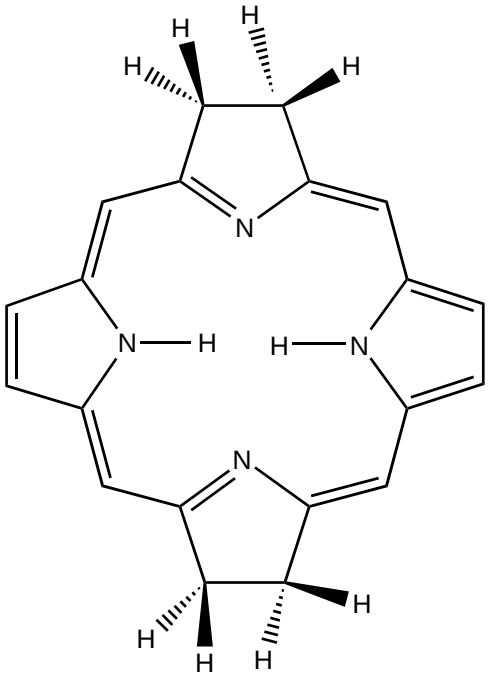

Figure 6.6: Structure of Bacteriochlorin

Table 6.6: RVO and IVO energies in eV for chlorin and bacteriochlorin. See text and Figure 6.7 for details.

	Chlorin		Bacteriochlorin	
Orbital	RVO Energy	IVO Energy	RVO Energy	IVO Energy
HOMO-2	-8.27	-8.27	-8.82	-8.82
b_{1u}	-6.45	-6.45	-6.26	-6.26
a_u	-5.89	-5.89	-4.92	-4.92
b_{3g}	0.40	-2.16	0.18	-1.61
b_{2g}	1.34	-1.18	2.48	-0.99
LUMO+2	4.07	1.12	4.77	1.91

Table 6.7: Excited State Energies for Chlorin. Excited states calculated via FOES procedure.

State	Total E (h)	Excit. E (h)	Excit. E (eV)	Exp.† (eV)	Error (eV)
Ground	-984.350401	-	-	-	-
Q_x	-984.244819	0.105582	2.87	1.90	0.97
Q_y	-984.244813	0.105588	2.87	2.28	0.59
B_x	-984.214517	0.135884	3.70	2.96	0.74
B_y	-984.215089	0.135312	3.68	3.03	0.65

† Reference [51]

the excited states to apply. Table 6.6 reports the RVO and IVO orbital energies for these two molecules.

Figure 6.7 pictorially displays the RVO energies for chlorin and bacteriochlorin. Shown are the four active orbitals, the next lowest occupied orbital, and the next highest unoccupied orbital. Orbital energies are presented in eV.

As Table 6.6 and Figure 6.7 show, the HOMOs and LUMOs are not as degenerate in chlorin and bacteriochlorin as they are in porphine. The orbital energies only differ by an eV, and consequently, the SC-FOES energies should be a good approximation to the excited state energies.

Table 6.7 details SC-FOES calculations for chlorin. The excited state energies range from 2.87 eV to 3.70 eV. Again, experimental results are reported, and the errors relative to these results range from 0.59 to 0.97 eV.

Table 6.8, finally, describes the calculations of the FOES energies for bacteriochlorin. The energies here range from 2.94 to 3.99 eV.

Whereas the average SC-FOES error in porphine is 0.55 eV relative to the experimental results, the average SC-FOES error for chlorin is 0.74 eV and that of bacte-

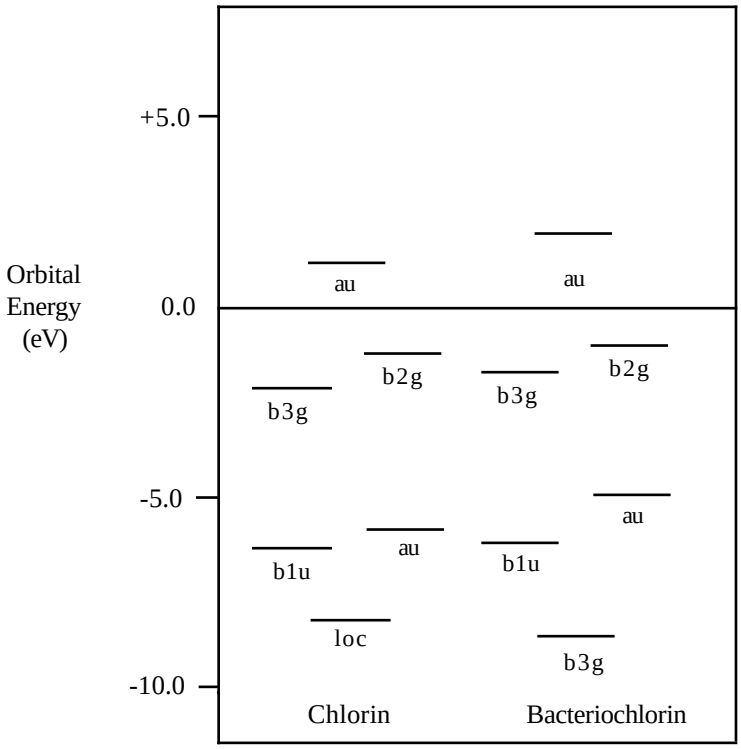

Figure 6.7: Orbital energies and symmetry labels for chlorin and bacteriochlorin RVOs.

Table 6.8: Excited State Energies for Bacteriochlorin. Excited states calculated via FOES procedure.

State	Total E (h)	Excit. E (h)	Excit. E (eV)	Exp.† (eV)	Error (eV)
Ground	-985.484634	-	-	-	-
Q_x	-985.376757	0.107877	2.94	1.66	1.28
Q_y	-985.368262	0.116372	3.17	2.36	0.81
B_x	-985.351625	0.133009	3.62	3.23	0.39
B_y	-985.337881	0.146753	3.99	3.47	0.52

† Reference [51]

riochlorin is 0.75 eV. Because the only additional source of error in the chlorin and bacteriochlorin results is the lack of approximate degeneracy between the two HOMOs and between the two LUMOs, this discrepancy is taken to be the source of the increased error in the chlorin and bacteriochlorin results.

The CI corrections to the SC-FOES calculations via the frozen core approximation described for porphine in the previous section are also possible for the reduced porphyrins in this section. Such SC-FOES-CI calculations for reduced porphins are currently underway. These calculations will correct the restriction imposed by the FOES structure, and it is expected that the results of these calculations will yield the same accuracy relative to experiment as did the SC-FOES-CI calculations on porphine.

6.12 Conclusion

The methods described in this chapter can reproduce porphine excited states quantitatively. These methods employ a variety of techniques to make the calculation of porphine excited states computationally tractible. The first of these techniques is the frozen core approximation, which uses the planarity of the porphine molecule to separate the σ and π parts of the calculations. This separation enables a potential to be substituted for the σ orbitals, and a full MC-SCF and CI calculations to be performed in the π space. The limitation to the frozen core method is that it does not describe the relaxation of the σ orbitals as the π orbitals are excited. The second method described in this section explicitly calculates the resonance wave functions in the Gouterman Four Orbital model for porphyrin excited states. The limitation to this method is that the excited state structure is restricted to the form with equal contributions from the two excited configurations in each state. These two techniques can be combines, and the frozen core MC-SCF and CI calculations are performed using a frozen core potential consistent with the excited π configuration. This hybrid method produces results which agree with experiemental results to within 0.18 eV.

Appendix A

A Technique for Evaluating Hamiltonian Matrix Elements

A.1 Introduction

At various times in this thesis it has been necessary to evaluate matrix elements of the form

$$H_{ij} = \langle \Psi_i | H | \Psi_j \rangle \tag{A.1}$$

where Ψ_i and Ψ_j are two wave functions consisting of singly or doubly occupied spin orbitals, or linear combinations of such wave functions. Among other places, these terms occur in evaluating the energy of ground and excited state wave functions, in calculating the resonance between different configurations, and in calculating CI matrix elements.

This appendix will describe a simple technique [1] for evaluating these terms. The technique involves transforming the wave functions into spin orbitals, evaluating the matrix element there, and transforming back to spatial orbitals.

A.2 The Method

A.2.1 Break Into Individual Determinants

The first step in the method is to break the matrix element down into matrix elements between single determinants or configurations. The GVB wave function with one correlated pair [3]

$$\begin{aligned} \Psi_{GVB1} &= \mathcal{A}[\phi_k^2(c_g\phi_g^2 + c_u\phi_u^2)\alpha\beta\alpha\beta] \\ &= |kk(c_g gg + c_u uu)\rangle \\ &= |c_g kkgg + c_u kkuu\rangle \end{aligned} \tag{A.2}$$

has energy given by

$$E_{GVB1} = \langle c_g kkgg + c_u kkuu | H | c_g kkgg + c_u kkuu \rangle. \tag{A.3}$$

Equation A.3 is then separated into a linear combination of matrix elements between individual determinants

$$\begin{aligned} E_{GVB1} &= c_g^2\langle kkgg|H|kkgg\rangle + c_u^2\langle kkuu|H|kkuu\rangle \\ &\quad +2c_g c_u\langle kkgg|H|kkuu\rangle \end{aligned} \tag{A.4}$$

A.2.2 Transform to Spin Orbitals

The next step is to transform from spatial orbitals to spin orbitals. For the wave function in equation A.3, the spin orbitals are:

$$\begin{aligned} \phi_k\alpha &\rightarrow \psi_1 \\ \phi_k\beta &\rightarrow \psi_2 \\ \phi_g\alpha &\rightarrow \psi_3 \\ \phi_g\beta &\rightarrow \psi_4 \\ \phi_u\alpha &\rightarrow \psi_5 \\ \phi_u\beta &\rightarrow \psi_6 \end{aligned} \tag{A.5}$$

This transforms the energy expression into

$$E_{GVB1} = c_g^2\langle 1234|H|1234\rangle + c_u^2\langle 1256|H|1256\rangle + 2c_g c_u\langle 1234|H|1256\rangle \tag{A.6}$$

It is often useful to write spin orbital indices using Arabic numerals, and spatial orbital indices using letters to avoid confusion.

A.2.3 Order and Classify Determinants

The next step is to order the determinants in each matrix element so that they are in the order of maximum coincidence. There should be three types of determinant relationships: identical determinants, determinants that differ by one spin orbital, and determinants that differ by two spin orbitals. Because the electronic Hamiltonian has only one and two electron operators, a matrix element containing determinants that differ by more than two determinants are zero.

When the determinants have to be rearranged, the sign of a determinant flips whenever two of the orbitals are interchanged. An example of putting a matrix element in the order of maximum coincidence follows.

$$\begin{aligned} \langle 2135|H|4321\rangle &= -\langle 2135|H|2341\rangle \\ &= \langle 2135|H|2143\rangle \\ &= -\langle 2135|H|2134\rangle \end{aligned} \tag{A.7}$$

Thus, this matrix element is classified as one that differs by one spin orbital.

A.2.4 Evaluate Matrix Elements between Operators

In this section the rules are given for evaluating matrix operators between the two types of operators in the Hamiltonian

$$\mathcal{O}_1 = \sum_{i=1}^{N_{occ}} h(i) \tag{A.8}$$

$$\mathcal{O}_2 = \sum_{i>j}^{N_{occ}} r_{ij}^{-1} \tag{A.9}$$

Identical determinants

$$|K\rangle = |123 \cdots N_{occ}\rangle \tag{A.10}$$

$$\langle K|\mathcal{O}_1|K\rangle = \sum_{i}^{N_{occ}} h_{ii} \tag{A.11}$$

$$\langle K|\mathcal{O}_2|K\rangle = \sum_{ij}^{N_{occ}} (ii|jj) - (ij|ij) \tag{A.12}$$

Determinants differing by one spin orbital

$$|K\rangle = |123 \cdots a \cdots N_{occ}\rangle \tag{A.13}$$

$$|L\rangle = |123 \cdots b \cdots N_{occ}\rangle \tag{A.14}$$

$$\langle K|\mathcal{O}_1|L\rangle = h_{ab} \tag{A.15}$$

$$\langle K|\mathcal{O}_2|L\rangle = \sum_{i}^{N_{occ}} (ab|ii) - (ai|bi) \tag{A.16}$$

Determinants differing by two spin orbitals

$$|K\rangle = |123 \cdots ab \cdots N_{occ}\rangle \tag{A.17}$$

$$|L\rangle = |123 \cdots mn \cdots N_{occ}\rangle \tag{A.18}$$

$$\langle K|\mathcal{O}_1|L\rangle = 0 \tag{A.19}$$

$$\langle K|\mathcal{O}_2|L\rangle = (am|bn) - (an|bm) \tag{A.20}$$

A.2.5 Transform Back to Spatial Orbitals

Once the matrix elements have been evaluated, all that remains is to transform back to spatial orbitals. The two-electron integrals $(ab|cd)$ are zero unless orbitals a and b have the same spin and c and d have the same spin.

A.2.6 Example: One Pair GVB Energy

The one GVB pair wave function was already given in equation A.3, and transformed into spin orbitals in equation A.6:

$$\begin{aligned} \Psi_{GVB1} &= |c_g kkgg + c_u kkuu\rangle \\ &= |c_g 1234 + c_u 1256\rangle \end{aligned} \tag{A.21}$$

The energy of the GVB wave function is given by

$$\begin{aligned} E_{GVB1} &= \langle c_g 1234 c_u 1256|H|c_g 1234 c_u 1256\rangle \\ &= c_g^2\langle 1234|H|1234\rangle + c_u^2\langle 1256|H|1256\rangle \\ &\quad +2c_g c_u\langle 1234|H|1256\rangle \end{aligned} \tag{A.22}$$

Using the rules from the previous section, the matrix elements are:

$$\begin{aligned} \langle kkgg|H|kkgg\rangle &= \langle 1234|H|1234\rangle \\ &= h_{11} + h_{22} + h_{33} + h_{44} + J_{12} + J_{13} - K_{13} \\ &\quad +J_{14} + J_{23} + J_{24} - K_{24} + J_{34} \\ &= 2h_{kk} + 2h_{gg} + J_{kk} + J_{gg} + 4J_{kg} - 2K_{kg} \end{aligned} \tag{A.23}$$

$$\begin{aligned} \langle kkuu|H|kkuu\rangle &= \langle 1256|H|1256\rangle \\ &= h_{11} + h_{22} + h_{55} + h_{66} + J_{12} + J_{15} - K_{15} \\ &\quad +J_{16} + J_{25} + J_{26} - K_{26} + J_{56} \\ &= 2h_{kk} + 2h_{uu} + J_{kk} + J_{uu} + 4J_{ku} - 2K_{ku} \end{aligned} \tag{A.24}$$

$$\begin{aligned} \langle kkgg|H|kkuu\rangle &= \langle 1234|H|1256\rangle \\ &= (35|46) \\ &= K_{gu} \end{aligned} \tag{A.25}$$

The total energy of the one GVB pair wave function is given by

$$\begin{aligned} E_{GVB1} &= 2h_{kk} + c_g^2(2h_{gg} + J_{gg} + 2J_{kg} - K_{kg}) \\ &\quad +c_u^2(2h_{uu} + J_{uu} + 2J_{ku} - K_{ku}) \\ &\quad +2c_g c_u K_{gu} \end{aligned} \tag{A.26}$$

A.3 Conclusion

One common task in electronic structure theory is the evaluation of matrix elements of the Hamiltonian operator between different determinants. The method presented in this appendix may be used to obtain wave function energy expressions, resonance energies, and CI matrix elements for a variety of wave functions. The evaluation method is

made easier by transforming the wave function into spin orbitals from the more commonly used spatial orbitals, evaluating the matrix elements, and transforming back. Although the extra transformations introduce additional work, orbital interchanges and other manipulations of the Slater determinants are much easier using spin orbitals. Consequently, the method is relatively simple, and presents a reliable method of Hamiltonian matrix element evaluation with minimal room for error.

Appendix B

The Self-Consistent Optimization of Restricted Configuration Interaction Wave Functions: Two-Pair, Closed-Shell Special Case

B.1 Introduction

As an extension of the methods in Chapter 5 and Appendix A, this appendix presents the equations for the self-consistent optimization of a two-pair, closed-shell restricted configuration interaction wave function. The equations and techniques presented here should able to be generalized to a method with an arbitrary number of RCI pairs, to provide an accurate method of correlated ground state wave functions that does not require a full transformation of the two-electron integrals and thus can be applied to large molecules.

The Generalized Valence Bond–Perfect Pairing (GVB-PP or GVB) wave function [3] for a single GVB pairs is given by

$$\begin{aligned} \Psi_{GVB} &= \left|\phi_k^2[c_g\phi_g^2 + c_u\phi_u^2]\right\rangle \\ &= c_g|k^2g^2\rangle + c_u|k^2u^2\rangle \end{aligned} \tag{B.1}$$

with the constraint that

$$c_g^2 + c_u^2 = 1, \tag{B.2}$$

and where the brackets indicate an antisymmetrized wave function. As in earlier sections, orbital label k refers to a core orbital, and orbital labels g and u refer to the *gerade* and *ungerade* natural orbitals. The energy for this wave function is given by

$$E_{GVB} = c_g^2\langle k^2g^2|H|k^2g^2\rangle + c_u^2\langle k^2u^2|H|k^2u^2\rangle + 2c_gc_u\langle k^2g^2|H|k^2u^2\rangle \tag{B.3}$$

The c_g and c_u coefficients are the GVB CI coefficients, which are determined by solving a 2x2 CI. Section 2.6 presents the GVB wave function in greater detail.

The advantage of a GVB wave function over HF wave functions is that GVB introduces electron correlation that is not present in HF wave functions. This way GVB includes electron correlations yields wave functions that can accurately reproduce dissociation energies, vibrational frequencies, bond lengths, bond angles, and many other physical properties of molecules without being significantly more expensive than HF wave functions. Unlike more complete correlated methods such as CI or MC-SCF, GVB does not require a full transformation of the two-electron integrals (see Sections 2.8 and 2.9 for more details), and thus GVB wave functions can be applied to much larger wave functions than can CI or MC-SCF wave functions.

Can the approach GVB-PP uses for electron correlation be extended and improved upon to yield an even more accurate MC-SCF? Can more electron correlation be included while still not requiring an integral transformation? This appendix presents such a method. The next level of correlated valence bond wave function is the GVB-Restricted Configuration Interaction (GVB-RCI or RCI) wave function [52], that includes $|gu\rangle$ terms representing single occupation of each of the g and u natural orbitals in addition to the $|gg\rangle$ and $|uu\rangle$ terms:

$$\Psi_{RCI} = c_g|k^2g^2\rangle + c_u|k^2u^2\rangle + c_r|k^2[gu]\rangle \tag{B.4}$$

with the constraint that

$$c_g^2 + c_u^2 + c_r^2 = 1, \tag{B.5}$$

and where the brackets around the $[gu]$ term represents the particular spin pairing that will be addressed later. For a single correlated pair, as written above, the cg and cu coefficients are chosen such that cr is zero with no loss of accuracy; the wave function is identical to the GVB wave function. For greater numbers of pairs the cr terms are no longer negligible.

This appendix will outline the energy expression and orbital optimization equations required for a self consistent GVB-RCI wave function without a full integral transformation. Indeed, with appropriate restrictions, the GVB-RCI wave function is only minimally more computationally expensive than the GVB-PP wave function.

B.2 The GVB-RCI Wave Function

We first consider which terms should be included in a self consistent RCI wave function. A wave function containing two GVB-RCI pairs has the form

$$\begin{aligned}\Psi_{RCI} &= |k^2(c_{g_1}g_1^2 + c_{u_1}u_1^2 + c_{r_1}[g_1u_1]) \\ &\quad \times(c_{g_2}g_2^2 + c_{u_2}u_2^2 + c_{r_2}[g_2u_2])\rangle\end{aligned} \tag{B.6}$$

where the brackets around the $[gu]$ terms again indicate that we will wait until later to consider the exact spin pairing of these terms. Expanding this expression yields

$$\Psi_{RCI} = \Psi_{GVB-GVB} + \Psi_{RCI-RCI} + \Psi_{RCI-GVB} \tag{B.7}$$

$$\begin{aligned}
\Psi_{GVB-GVB} &= c_{g_1}c_{g_2}|k^2g_1^2g_2^2\rangle + c_{g_1}c_{u_2}|k^2g_1^2u_2^2\rangle \\
&\quad + c_{u_1}c_{g_2}|k^2u_1^2g_2^2\rangle + c_{u_1}c_{u_2}|k^2u_1^2u_2^2\rangle \qquad \text{(B.8)}\\
\Psi_{RCI-RCI} &= c_{r_1}c_{r_2}|k^2[g_1u_1][g_2u_2]\rangle \qquad \text{(B.9)}\\
\Psi_{RCI-GVB} &= c_{g_1}c_{r_2}|k^2g_1^2[g_2u_2]\rangle + c_{u_1}c_{r_2}|k^2u_1^2[g_2u_2]\rangle \\
&\quad + c_{r_1}c_{g_2}|k^2[g_1u_1]g_2^2\rangle + c_{r_1}c_{u_2}|k^2[g_1u_1]u_2^2\rangle \qquad \text{(B.10)}
\end{aligned}$$

The terms in the wave function marked GVB-GVB are the terms from the GVB-PP wave function and must be retained. The most important terms from those that remain are the ones marked RCI-RCI, which represent the effect of one of the $[gu]$ terms on the other $[gu]$ term. Ignoring the terms marked RCI-GVB is consistent with the fact that, as was explained for a one-pair case, the GVB-CI coefficients are chosen so that there is no interaction between the $|gu\rangle$ term of one pair and any of the other $|gg\rangle$ or $|uu\rangle$ terms. There can, of course, still be interaction between the $|gu\rangle$ terms of different pairs, and, consequently, the terms marked RCI-RCI are retained. Thus, the simplest wave function we can derive that includes the effect of the $[gu]$ terms includes only the terms marked GVB-GVB and RCI-RCI. This wave function is of the form

$$\begin{aligned}
\Psi_{RCI} &= c_{g_1}c_{g_2}|k^2g_1^2g_2^2\rangle + c_{g_1}c_{u_2}|k^2g_1^2u_2^2\rangle \\
&\quad + c_{u_1}c_{g_2}|k^2u_1^2g_2^2\rangle + c_{u_1}c_{u_2}|k^2u_1^2u_2^2\rangle \\
&\quad + c_{r_1}c_{r_2}|k^2[g_1u_1][g_2u_2]\rangle \qquad \text{(B.11)}
\end{aligned}$$

B.3 RCI Spin Coupling

This section considers the exact spin couplings represented by the $[gu]$ notation in earlier sections. Four open shell orbitals can be combined into a singlet in two different ways: two singlet pairs of orbitals paired as a singlet overall, and two pairs of triplet orbitals, paired as a singlet overall.

The singlet-singlet spin coupling has the form

$$\Psi_{00} = \frac{1}{2}\left(|k\bar{k}a\bar{s}r\bar{b}\rangle + |k\bar{k}a\bar{r}s\bar{b}\rangle + |k\bar{k}r\bar{a}b\bar{s}\rangle + |k\bar{k}s\bar{a}b\bar{r}\rangle\right) \qquad \text{(B.12)}$$

and the triplet-triplet spin coupling has the form

$$\begin{aligned}
\Psi_{11} &= \frac{1}{\sqrt{12}}(2|k\bar{k}r\bar{a}s\bar{b}\rangle + 2|k\bar{k}a\bar{r}b\bar{s}\rangle - |k\bar{k}a\bar{s}r\bar{b}\rangle \\
&\quad + |k\bar{k}a\bar{r}s\bar{b}\rangle + |k\bar{k}r\bar{a}b\bar{s}\rangle - |k\bar{k}s\bar{a}b\bar{r}\rangle) \qquad \text{(B.13)}
\end{aligned}$$

Combining these two spin couplings with the GVB-PP spin-coupling yields the RCI wave function of the form

$$\Psi_{RCI} = C_g\Psi_{PP} + C_0\Psi_{00} + C_1\Psi_{11} \qquad \text{(B.14)}$$

with YPP the two-pair GVB-PP wave function from equation B.2. Expanding Ψ_{RCI} gives

$$\Psi_{RCI} = C_g(c_ac_b|k\bar{k}a\bar{a}b\bar{b}\rangle + c_ac_s|k\bar{k}a\bar{a}s\bar{s}\rangle \qquad \text{(B.15)}$$

$$
\begin{aligned}
& +c_r c_b|k\bar{k}r\bar{r}b\bar{b}\rangle + c_r c_s|k\bar{k}r\bar{r}s\bar{s}\rangle) \\
+ \quad & \frac{C_0}{2}(|k\bar{k}a\bar{s}r\bar{b}\rangle + |k\bar{k}a\bar{r}s\bar{b}\rangle \\
& +|k\bar{k}r\bar{a}b\bar{s}\rangle + |k\bar{k}s\bar{a}b\bar{r}\rangle) \\
+ \quad & \frac{C_1}{\sqrt{12}}(2|k\bar{k}r\bar{a}s\bar{b}\rangle + 2|k\bar{k}a\bar{r}b\bar{s}\rangle \\
& -|k\bar{k}a\bar{s}r\bar{b}\rangle + |k\bar{k}a\bar{r}s\bar{b}\rangle \\
& +|k\bar{k}r\bar{a}b\bar{s}\rangle - |k\bar{k}s\bar{a}b\bar{r}\rangle)
\end{aligned}
$$

B.4 Determinants in the GVB-RCI Wave Function

For the GVB-RCI wave function optimization and energy calculation, we must calculate coupling between the following determinants:

$$
\begin{aligned}
|d1\rangle &= |k\bar{k}a\bar{a}b\bar{b}\rangle \\
|d2\rangle &= |k\bar{k}a\bar{a}s\bar{s}\rangle \\
|d3\rangle &= |k\bar{k}r\bar{r}b\bar{b}\rangle \\
|d4\rangle &= |k\bar{k}r\bar{r}s\bar{s}\rangle \\
|d5\rangle &= |k\bar{k}a\bar{s}r\bar{b}\rangle \\
|d6\rangle &= |k\bar{k}a\bar{r}s\bar{b}\rangle \\
|d7\rangle &= |k\bar{k}r\bar{a}b\bar{s}\rangle \\
|d8\rangle &= |k\bar{k}s\bar{a}b\bar{r}\rangle \\
|d9\rangle &= |k\bar{k}r\bar{a}s\bar{b}\rangle \\
|d10\rangle &= |k\bar{k}a\bar{r}b\bar{s}\rangle
\end{aligned}
\tag{B.16}
$$

given core orbital k, g-type natural orbitals a and b, and u-type natural orbitals r and s. Using these determinants, we may rewrite the Ψ_{RCI}

$$
\begin{aligned}
\Psi_{RCI} = \; & C_g\,(c_a c_b|d1\rangle + c_a c_s|d2\rangle + c_r c + b|d3\rangle + c_r c_s|d4\rangle) \\
& +\frac{C_0}{2}\,(|d5\rangle + |d6\rangle + |d7\rangle + |d8\rangle) \\
& +\frac{C_1}{\sqrt{12}}\,(2|d9\rangle + 2|d10\rangle - |d5\rangle + |d6\rangle + |d7\rangle - |d8\rangle)
\end{aligned}
\tag{B.17}
$$

or, grouping terms of the same determinant together,

$$
\begin{aligned}
\Psi_{RCI} = \; & |d1\rangle(C_g c_a c_b) + |d2\rangle(C_g c_a c_s) + |d3\rangle(C_g c_r c_b) \\
& +|d4\rangle(C_g c_r c_s) + |d5\rangle(\frac{C_0}{2} - \frac{C_1}{\sqrt{12}}) + |d6\rangle(\frac{C_0}{2} + \frac{C_1}{\sqrt{12}}) \\
& +|d7\rangle(\frac{C_0}{2} + \frac{C_1}{\sqrt{12}}) + |d8\rangle(\frac{C_0}{2} - \frac{C_1}{\sqrt{12}}) + |d9\rangle(\frac{C_1}{\sqrt{3}}) + |d10\rangle(\frac{C_1}{\sqrt{3}})
\end{aligned}
\tag{B.18}
$$

B.5 Matrix Elements Between Determinants in the GVB-RCI Wave Function

The matrix elements between these determinants are given below. They are evaluated by transforming to spin orbitals, evaluating the determinant there using the technique discussed in Appendix A, and transforming the result back to spatial orbitals. This technique yields for the matrix elements:

$$
\begin{aligned}
H_{11} &= \langle d1|H|d1\rangle && \text{(B.19)}\\
&= 2h_{kk} + 2h_{aa} + 2h_{bb} + J_{kk} + J_{aa} + J_{bb} \\
&\quad +4J_{ka} - 2K_{ka} + 2J_{kb} - 2K_{kb} + 4J_{ab} - 2K_{ab} \\
H_{12} &= K_{bs} && \text{(B.20)}\\
H_{13} &= K_{ar} && \text{(B.21)}\\
H_{14} &= 0 && \text{(B.22)}\\
H_{15} &= (as|br) && \text{(B.23)}\\
H_{16} &= (ar|bs) && \text{(B.24)}\\
H_{17} &= (ar|bs) && \text{(B.25)}\\
H_{18} &= (as|br) && \text{(B.26)}\\
H_{19} &= (ar|bs) - (as|br) && \text{(B.27)}\\
H_{1,10} &= (ar|bs) - (as|br) && \text{(B.28)}\\
H_{22} &= 2h_{kk} + 2h_{aa} + 2h_{ss} + J_{kk} + J_{aa} + J_{ss} && \text{(B.29)}\\
&\quad +4J_{ka} - 2K_{ka} + 4J_{ks} - 2K_{ks} + 4J_{as} - 2K_{as} \\
H_{23} &= 0 && \text{(B.30)}\\
H_{24} &= K_{ar} && \text{(B.31)}\\
H_{25} &= -(ab|rs) && \text{(B.32)}\\
H_{26} &= (ar|bs) - (ab|rs) && \text{(B.33)}\\
H_{27} &= (ar|bs) - (ab|rs) && \text{(B.34)}\\
H_{28} &= -(ab|rs) && \text{(B.35)}\\
H_{29} &= (ar|bs) && \text{(B.36)}\\
H_{2,10} &= (ar|bs) && \text{(B.37)}\\
H_{33} &= 2h_{kk} + 2h_{rr} + 2h_{bb} + J_{kk} + J_{rr} + J_{bb} && \text{(B.38)}\\
&\quad +4J_{kr} - 2K_{kr} + 4J_{kb} - 2K_{kb} + 4J_{br} - 2K_{br} \\
H_{34} &= K_{bs} && \text{(B.39)}\\
H_{35} &= -(ab|rs) && \text{(B.40)}\\
H_{36} &= (ar|bs) - (ab|rs) && \text{(B.41)}\\
H_{37} &= (ar|bs) - (ab|rs) && \text{(B.42)}\\
H_{38} &= -(ab|rs) && \text{(B.43)}\\
H_{39} &= (ar|bs) && \text{(B.44)}
\end{aligned}
$$

$$H_{3,10} = (ar|bs) \tag{B.45}$$

$$\begin{aligned} H_{44} &= 2h_{kk} + 2h_{rr} + 2h_{ss} + J_{kk} + J_{rr} + J_{ss} \\ &\quad +4J_{kr} - 2K_{kr} + 4J_{ks} - 2K_{ks} + 4J_{rs} - 2K_{rs} \end{aligned} \tag{B.46}$$

$$H_{45} = (as|br) \tag{B.47}$$

$$H_{46} = (ar|bs) \tag{B.48}$$

$$H_{47} = (ar|bs) \tag{B.49}$$

$$H_{48} = (as|br) \tag{B.50}$$

$$H_{49} = (ar|bs) - (as|br) \tag{B.51}$$

$$H_{4,10} = (ar|bs) - (as|br) \tag{B.52}$$

$$\begin{aligned} H_{55} &= 2h_{kk} + h_{aa} + h_{bb} + h_{rr} + h_{ss} + h_{kk} + J_{kk} \\ &\quad +2J_{ka} - K_{ka} + 2J_{kb} - K_{kb} + 2J_{kr} - K_{kr} \\ &\quad +2J_{ks} - K_{ks} + J_{ab} + J_{ar} - K_{ar} \\ &\quad +J_{as} + J_{br} + J_{bs} - K_{bs} + J_{rs} \end{aligned} \tag{B.53}$$

$$H_{56} = K_{rs} \tag{B.54}$$

$$H_{57} = K_{ab} \tag{B.55}$$

$$H_{58} = 0 \tag{B.56}$$

$$H_{59} = -K_{as} \tag{B.57}$$

$$H_{5,10} = -K_{br} \tag{B.58}$$

$$\begin{aligned} H_{66} &= 2h_{kk} + h_{aa} + h_{bb} + h_{rr} + h_{ss} + h_{kk} + J_{kk} \\ &\quad +2J_{ka} - K_{ka} + 2J_{kb} - K_{kb} + 2J_{kr} - K_{kr} + 2J_{ks} - K_{ks} \\ &\quad +J_{ab} + J_{ar} + J_{as} - K_{as} + J_{br} - K_{br} + J_{bs} + J_{rs} \end{aligned} \tag{B.59}$$

$$H_{67} = 0 \tag{B.60}$$

$$H_{68} = K_{ab} \tag{B.61}$$

$$H_{69} = K_{ar} \tag{B.62}$$

$$H_{6,10} = K_{bs} \tag{B.63}$$

$$\begin{aligned} H_{77} &= 2h_{kk} + h_{aa} + h_{bb} + h_{rr} + h_{ss} + h_{kk} + J_{kk} \\ &\quad +2J_{ka} - K_{ka} + 2J_{kb} - K_{kb} + 2J_{kr} - K_{kr} + 2J_{ks} - K_{ks} \\ &\quad +J_{ab} + J_{ar} + J_{as} - K_{as} + J_{br} - K_{br} + J_{bs} + J_{rs} \end{aligned} \tag{B.64}$$

$$H_{78} = K_{rs} \tag{B.65}$$

$$H_{79} = K_{bs} \tag{B.66}$$

$$H_{7,10} = K_{ar} \tag{B.67}$$

$$\begin{aligned} H_{88} &= 2h_{kk} + h_{aa} + h_{bb} + h_{rr} + h_{ss} + h_{kk} + J_{kk} \\ &\quad +2J_{ka} - K_{ka} + 2J_{kb} - K_{kb} + 2J_{kr} - K_{kr} + 2J_{ks} - K_{ks} \\ &\quad +J_{ab} + J_{ar} - K_{ar} + J_{as} + J_{br} + J_{bs} - K_{bs} + J_{rs} \end{aligned} \tag{B.68}$$

$$H_{89} = -K_{br} \tag{B.69}$$

$$H_{8,10} = -K_{as} \tag{B.70}$$

$$H_{99} = 2h_{kk} + h_{aa} + h_{bb} + h_{rr} + h_{ss} + h_{kk} + J_{kk} \tag{B.71}$$

$$
\begin{aligned}
& +2J_{ka} - K_{ka} + 2J_{kb} - K_{kb} + 2J_{kr} - K_{kr} + 2J_{ks} - K_{ks} \\
& +J_{ab} - K_{ab} + J_{ar} + J_{as} + J_{br} + J_{bs} + J_{rs} - K_{rs} \\
H_{9,10} &= 0 \qquad \text{(B.72)} \\
H_{10,10} &= 2h_{kk} + h_{aa} + h_{bb} + h_{rr} + h_{ss} + h_{kk} + J_{kk} \qquad \text{(B.73)} \\
& +2J_{ka} - K_{ka} + 2J_{kb} - K_{kb} + 2J_{kr} - K_{kr} + 2J_{ks} - K_{ks} \\
& +J_{ab} - K_{ab} + J_{ar} + J_{as} + J_{br} + J_{bs} + J_{rs} - K_{rs}
\end{aligned}
$$

B.6 The GVB-RCI Energy Expression

Using the matrix elements defined in the previous section, the energy of the two-pair closed-shell RCI wave function may be defined as

$$
\begin{aligned}
E_{RCI} &= C_g^2 c_a^2 c_g^2 H_{11} + 2C_g^2 c_a^2 c_b c_s H_{12} \qquad \text{(B.74)} \\
& +2C_g^2 c_a c_b^2 c_r H_{13} + 2C_g^2 c_a c_b c_r c_s H_{14} \\
& +C_g c_a c_b \left(C_0 - \frac{C_1}{\sqrt{3}}\right) H_{15} + C_g c_a c_b \left(C_0 + \frac{C_1}{\sqrt{3}}\right) H_{16} \\
& +C_g c_a c_b \left(C_0 + \frac{C_1}{\sqrt{3}}\right) H_{17} + C_g c_a c_b \left(C_0 - \frac{C_1}{\sqrt{3}}\right) H_{18} \\
& +\frac{2}{\sqrt{3}} C_1 C_g c_a c_b H_{19} + \frac{2}{\sqrt{3}} C_1 C_g c_a c_b H_{1,10} \\
& +C_g^2 c_a^2 c_s^2 H_{22} + 2C_g^2 c_a c_b c_r c_s H_{23} + 2C_g^2 c_a c_b c_s^2 H_{24} \\
& +C_g c_a c_s \left(C_0 - \frac{C_1}{\sqrt{3}}\right) H_{25} + C_g c_a c_s \left(C_0 + \frac{C_1}{\sqrt{3}}\right) H_{26} \\
& +C_g c_a c_s \left(C_0 + \frac{C_1}{\sqrt{3}}\right) H_{27} + C_g c_a c_s \left(C_0 - \frac{C_1}{\sqrt{3}}\right) H_{28} \\
& +\frac{2}{\sqrt{3}} C_1 C_g c_a c_s H_{29} + \frac{2}{\sqrt{3}} C_1 C_g c_a c_s H_{2,10} \\
& +C_g^2 c_b^2 c_r^2 H_{33} + 2C_g^2 c_b c_r^2 c_s H_{34} \\
& +C_g c_r c_b \left(C_0 - \frac{C_1}{\sqrt{3}}\right) H_{35} + C_g c_r c_b \left(C_0 + \frac{C_1}{\sqrt{3}}\right) H_{36} \\
& +C_g c_r c_b \left(C_0 + \frac{C_1}{\sqrt{3}}\right) H_{37} + C_g c_r c_b \left(C_0 - \frac{C_1}{\sqrt{3}}\right) H_{38} \\
& +\frac{2}{\sqrt{3}} C_1 C_g c_r c_b H_{39} + \frac{2}{\sqrt{3}} C_1 C_g c_r c_b H_{3,10} \\
& +C_g^2 c_r^2 c_s^2 H_{44} \\
& +C_g c_r c_s \left(C_0 - \frac{C_1}{\sqrt{3}}\right) H_{45} + C_g c_r c_s \left(C_0 + \frac{C_1}{\sqrt{3}}\right) H_{46} \\
& +C_g c_r c_s \left(C_0 + \frac{C_1}{\sqrt{3}}\right) H_{47} + C_g c_r c_s \left(C_0 - \frac{C_1}{\sqrt{3}}\right) H_{48}
\end{aligned}
$$

$$
\begin{aligned}
&+\frac{2}{\sqrt{3}}C_1C_gc_rc_sH_{49}+\frac{2}{\sqrt{3}}C_1C_gc_rc_sH_{4,10}\\
&+\frac{1}{4}\left(C_0^2-\frac{2C_0C_1}{\sqrt{3}}+\frac{C_1^2}{3}\right)H_{55}+\frac{1}{2}\left(C_0^2-\frac{C_1^2}{3}\right)H_{56}\\
&+\frac{1}{2}\left(C_0^2-\frac{C_1^2}{3}\right)H_{57}+\frac{1}{2}\left(C_0^2-\frac{2C_0C_1}{\sqrt{3}}+\frac{C_1^2}{3}\right)H_{58}\\
&+\left(\frac{C_0C_1}{\sqrt{3}}-\frac{C_1^2}{3}\right)H_{59}+\left(\frac{C_0C_1}{\sqrt{3}}-\frac{C_1^2}{3}\right)H_{5,10}\\
&+\frac{1}{4}\left(C_0^2-\frac{2C_0C_1}{\sqrt{3}}+\frac{C_1^2}{3}\right)H_{66}+\frac{1}{2}\left(C_0^2+\frac{C_1^2}{3}\right)H_{67}\\
&+\frac{1}{2}\left(C_0^2-\frac{C_1^2}{3}\right)H_{68}+\left(\frac{C_0C_1}{\sqrt{3}}+\frac{C_1^2}{3}\right)H_{69}\\
&+\left(\frac{C_0C_1}{\sqrt{3}}+\frac{C_1^2}{3}\right)H_{6,10}+\frac{1}{4}\left(C_0^2+\frac{2C_0C_1}{\sqrt{3}}+\frac{C_1^2}{3}\right)H_{77}\\
&+\frac{1}{2}\left(C_0^2-\frac{C_1^2}{3}\right)H_{78}+\left(\frac{C_0C_1}{\sqrt{3}}+\frac{C_1^2}{3}\right)H_{79}\\
&+\left(\frac{C_0C_1}{\sqrt{3}}+\frac{C_1^2}{3}\right)H_{7,10}+\frac{1}{4}\left(C_0^2-\frac{2C_0C_1}{\sqrt{3}}+\frac{C_1^2}{3}\right)H_{88}\\
&+\left(\frac{C_0C_1}{\sqrt{3}}-\frac{C_1^2}{3}\right)H_{89}+\left(\frac{C_0C_1}{\sqrt{3}}-\frac{C_1^2}{3}\right)H_{8,10}\\
&+\frac{C_1^2}{3}H_{99}+frac2C_1^23H_{9,10}+\frac{C_1^2}{3}H_{10,10}
\end{aligned}
$$

Inserting definitions for the matrix elements and simplifying gives

$$
\begin{aligned}
E_{RCI} \quad = \quad & h_{kk}(2C_g^2+2C_0^2+2C_1^2)+h_{aa}(2C_g^2c_a^2+2C_0^2+2C_1^2) \qquad \text{(B.75)}\\
&+h_{bb}(2C_g^2c_b^2+2C_0^2+2C_1^2)+h_{rr}(2C_g^2c_r^2+2C_0^2+2C_1^2)\\
&+h_{ss}(2C_g^2c_s^2+2C_0^2+2C_1^2)+J_{kk}(C_g^2+C_0^2+C_1^2)\\
&+J_{aa}C_g^2c_a^2+J_{bb}C_g^2c_b^2+J_{rr}C_g^2c_r^2+J_{ss}C_g^2c_s^2\\
&+(2J_{ka}-K_{ka})(2C_g^2c_a^2+C_0^2+C_1^2)+(2J_{kb}-K_{kb})(2C_g^2c_b^2+C_0^2+C_1^2)\\
&+(2J_{kr}-K_{kr})(2C_g^2c_r^2+C_0^2+C_1^2)+(2J_{ks}-K_{ks})(2C_g^2c_s^2+C_0^2+C_1^2)\\
&+J_{ab}(4C_g^2c_a^2c_b^2+C_0^2+C_1^2)+K_{ab}(-2C_g^2c_a^2c_b^2+C_0^2-C_1^2)\\
&+J_{ar}(C_0^2+C_1^2)+K_{ar}(C_g^2c_ac_r-\frac{1}{2}C_0^2+\frac{1}{2}C_1^2+\sqrt{3}C_0C_1)\\
&+J_{as}(4C_g^2c_a^2c_s^2+C_0^2+C_1^2)+K_{ar}(-C_g^2c_ac_s-\frac{1}{2}C_0^2+\frac{1}{2}C_1^2-\sqrt{3}C_0C_1)\\
&+J_{br}(4C_g^2c_b^2c_r^2+C_0^2+C_1^2)+K_{br}(-C_g^2c_bc_r-\frac{1}{2}C_0^2+\frac{1}{2}C_1^2-\sqrt{3}C_0C_1)\\
&+J_{bs}(C_0^2+C_1^2)+K_{bs}(C_g^2c_bc_s-\frac{1}{2}C_0^2+\frac{1}{2}C_1^2+\sqrt{3}C_0C_1)\\
&+J_{rs}(4C_g^2c_r^2c_s^2+C_0^2+C_1^2)+K_{rs}(-2C_g^2c_r^2c_s^2+C_0^2-C_1^2)
\end{aligned}
$$

$$
\begin{aligned}
&+(ab|rs)(-4C_0C_gc_aC_s - 4C_0C_gc_rc_b)\\
&+(ar|bs)(2C_0C_gc_ac_b + 2C_0C_gc_ac_s + 2C_0C_gc_bc_r + 2C_0C_gc_rc_s\\
&+2\sqrt{3}C_1C_gc_ac_b + 2\sqrt{3}C_1C_gc_ac_s + 2\sqrt{3}c_1C_gc_bc_r + 2\sqrt{3}C_1C_gc_rc_s)\\
&+(as|br)(2C_0C_gc_ac_b + 2C_0C_gc_rc_s - 2\sqrt{3}C_1C_gc_ac_b - 2\sqrt{3}C_1C_gc_rc_s)
\end{aligned}
$$

B.7 Energy Coefficients and the Yaffe-Goddard Form

We may simplify the energy expression in the preceding section by grouping together the coefficients of like matrix elements:

$$E_{RCI} = \sum_{ij}^{N_{occ}} 2f_{ij}h_{ij} + \sum_{ijkl}^{N_{occ}} C_{ijkl}(ij|kl) \tag{B.76}$$

The Yaffe-Goddard equations take an energy expression of the form B.76 and generate the A_{ij} and B_{ij} matrices used to update the orbitals in equations 2.116–2.119. The f_{ij} coefficients are all zero, except:

$$f_k = f_{kk} = C_g^2 + C_0^2 + C_1^2 \tag{B.77}$$

$$f_a = f_{aa} = C_g^2c_a^2 + \frac{1}{2}C_0^2 + \frac{1}{2}C_1^2 \tag{B.78}$$

$$f_b = f_{bb} = C_g^2c_b^2 + \frac{1}{2}C_0^2 + \frac{1}{2}C_1^2 \tag{B.79}$$

$$f_r = f_{rr} = C_g^2c_r^2 + \frac{1}{2}C_0^2 + \frac{1}{2}C_1^2 \tag{B.80}$$

$$f_s = f_{ss} = C_g^2c_s^2 + \frac{1}{2}C_0^2 + \frac{1}{2}C_1^2 \tag{B.81}$$

Similarly, the Cijkl coefficients are all zero, except:

$$a_{kk} = C_{kkkk} = C_g^2 + C_0^2 + C_1^2 \tag{B.82}$$

$$a_{aa} = C_{aaaa} = C_g^2c_a^2 \tag{B.83}$$

$$a_{bb} = C_{bbbb} = C_g^2c_b^2 \tag{B.84}$$

$$a_{rr} = C_{rrrr} = C_g^2c_r^2 \tag{B.85}$$

$$a_{ss} = C_{ssss} = C_g^2c_s^2 \tag{B.86}$$

$$a_{ka} = C_{kkaa} = C_{aakk} = 2C_g^2c_a^2 + C_0^2 + C_1^2 \tag{B.87}$$

$$\begin{aligned} b_{ka} &= C_{kaka} = C_{akka} = C_{kaak} = C_{akak} \qquad \text{(B.88)}\\ &= -\frac{1}{2}C_g^2c_a^2 - \frac{1}{4}C_0^2 - \frac{1}{4}C_1^2 \end{aligned}$$

$$a_{kb} = C_{kkbb} = C_{bbkk} = 2C_g^2c_b^2 + C_0^2 + C_1^2 \tag{B.89}$$

$$\begin{aligned} b_{kb} &= C_{kbkb} = C_{bkka} = C_{kbbk} = C_{bkbk} \qquad \text{(B.90)}\\ &= -\frac{1}{2}C_g^2c_b^2 - \frac{1}{4}C_0^2 - \frac{1}{4}C_1^2 \end{aligned}$$

$$
\begin{aligned}
a_{kr} &= C_{kkrr} = C_{rrkk} = 2C_g^2 c_r^2 + C_0^2 + C_1^2 && \text{(B.91)}\\
b_{kr} &= C_{krkr} = C_{rkkr} = C_{krrk} = C_{rkrk} && \text{(B.92)}\\
&= -\frac{1}{2}C_g^2 c_r^2 - \frac{1}{4}C_0^2 - \frac{1}{4}C_1^2 \\
a_{ks} &= C_{kkss} = C_{sskk} = 2C_g^2 c_s^2 + C_0^2 + C_1^2 && \text{(B.93)}\\
b_{ks} &= C_{ksks} = C_{skks} = C_{kssk} = C_{sksk} && \text{(B.94)}\\
&= -\frac{1}{2}C_g^2 c_s^2 - \frac{1}{4}C_0^2 - \frac{1}{4}C_1^2 \\
a_{ab} &= C_{aabb} = C_{bbaa} = 2C_g^2 c_a^2 c_b^2 + \frac{1}{2}C_0^2 + \frac{1}{2}C_1^2 && \text{(B.95)}\\
b_{ab} &= C_{abab} = C_{abba} = C_{baab} = C_{baba} && \text{(B.96)}\\
&= -\frac{1}{2}C_g^2 c_a^2 c_b^2 - \frac{1}{4}C_0^2 - \frac{1}{4}C_1^2 \\
a_{ar} &= C_{aarr} = C_{rraa} = \frac{1}{2}C_0^2 + \frac{1}{2}C_1^2 && \text{(B.97)}\\
b_{ar} &= C_{arar} = C_{arra} = C_{raar} = C_{rara} && \text{(B.98)}\\
&= \frac{1}{4}C_g^2 c_a^2 c_r^2 - \frac{1}{8}C_0^2 + \frac{1}{8}C_1^2 + \frac{\sqrt{3}}{4}C_0 C_1 \\
a_{as} &= C_{aass} = C_{ssaa} = 2C_g^2 c_a^2 c_s^2 + \frac{1}{2}C_0^2 + \frac{1}{2}C_1^2 && \text{(B.99)}\\
b_{as} &= C_{asas} = C_{assa} = C_{saas} = C_{sasa} && \text{(B.100)}\\
&= -\frac{1}{2}C_g^2 c_a^2 c_s^2 - \frac{1}{8}C_0^2 + \frac{1}{8}C_1^2 - \frac{\sqrt{3}}{4}C_0 C_1 \\
a_{br} &= C_{bbrr} = C_{rrbb} = 2C_g^2 c_b^2 c_r^2 + \frac{1}{2}C_0^2 + \frac{1}{2}C_1^2 && \text{(B.101)}\\
b_{br} &= C_{brbr} = C_{brra} = C_{rbbr} = C_{rbrb} && \text{(B.102)}\\
&= -\frac{1}{2}C_g^2 c_r^2 c_b^2 - \frac{1}{8}C_0^2 + \frac{1}{8}C_1^2 - \frac{\sqrt{3}}{4}C_0 C_1 \\
a_{bs} &= C_{bbss} = C_{ssbb} = \frac{1}{2}C_0^2 + \frac{1}{2}C_1^2 && \text{(B.103)}\\
b_{bs} &= C_{bsbs} = C_{bssb} = C_{sbbs} = C_{sbsb} && \text{(B.104)}\\
&= \frac{1}{4}C_g^2 c_b^2 c_s^2 - \frac{1}{8}C_0^2 + \frac{1}{8}C_1^2 + \frac{\sqrt{3}}{4}C_0 C_1 \\
a_{rs} &= C_{rrss} = C_{ssrr} = 2C_g^2 c_r^2 c_s^2 + \frac{1}{2}C_0^2 + \frac{1}{2}C_1^2 && \text{(B.105)}\\
b_{rs} &= C_{rsrs} = C_{rssr} = C_{srrs} = C_{srsr} && \text{(B.106)}\\
&= -\frac{1}{2}C_g^2 c_r^2 c_s^2 - \frac{1}{4}C_0^2 - \frac{1}{4}C_1^2 \\
C_{abrs} &= C_{absr} = C_{bars} = C_{basr} = C_{rsab} && \text{(B.107)}\\
&= C_{rsba} = C_{srab} = C_{srba} \\
&= -\frac{1}{2}C_g c_a c_s C_0 - \frac{1}{2}C_g c_b c_r C_0 \\
C_{arbs} &= C_{arsb} = C_{rabs} = C_{rasb} && \text{(B.108)}
\end{aligned}
$$

$$
\begin{aligned}
&= C_{bsar}C_{bsra} = C_{sbar} = C_{sbra} \\
&= \frac{1}{4}C_g c_a c_b C_0 + \frac{1}{4}C_g c_a c_s C_0 + \frac{1}{4}C_g c_b c_r C_0 \\
&\quad + \frac{1}{4}C_g c_r c_s C_0 + \frac{\sqrt{3}}{4}C_g c_a c_b C_1 + \frac{\sqrt{3}}{4}C_g c_a c_s C_1 \\
&\quad + \frac{\sqrt{3}}{4}C_g c_b c_r C_1 + \frac{\sqrt{3}}{4}C_g c_r c_s C_1 \\
C_{asbr} &= C_{asrb} = C_{sabr} = C_{sarb} \qquad \text{(B.109)} \\
&= C_{bras}C_{brsa} = C_{rbas} = C_{rbsa} \\
&= \frac{1}{4}C_g c_a c_b C_0 + \frac{1}{4}C_g c_r c_s C_0 \\
&\quad + \frac{\sqrt{3}}{4}C_g c_a c_b C_1 + \frac{\sqrt{3}}{4}C_g c_r c_s C_1
\end{aligned}
$$

The f_i (one subscript), a_{ij}, and b_{ij} terms are included here because later they will make the orbital optimization equations considerably easier to interpret. Using these terms, we may rewrite the RCI energy as:

$$
\begin{aligned}
E_{RCI} &= 2f_k h_{kk} + 2f_a h_{aa} + 2f_b h_{bb} + 2f_r h_{rr} + 2f_s h_{ss} \qquad \text{(B.110)} \\
&\quad + a_{kk}J_{kk} + a_{aa}J_{aa} + a_{bb}J_{bb} + a_{rr}J_{rr} + a_{ss}J_{ss} \\
&\quad + 2a_{ka}J_{ka} + 4b_{ka}K_{ka} + 2a_{kb}J_{kb} + 4b_{kb}K_{kb} \\
&\quad + 2a_{kr}J_{kr} + 4b_{kr}K_{kr} + 2a_{ks}J_{ks} + 4b_{ks}K_{ks} \\
&\quad + 2a_{ab}J_{ab} + 4b_{ab}K_{ab} + 2a_{ar}J_{ar} + 4b_{ar}K_{ar} \\
&\quad + 2a_{as}J_{as} + 4b_{as}K_{as} + 2a_{br}J_{br} + 4b_{br}K_{br} \\
&\quad + 2a_{bs}J_{bs} + 4b_{bs}K_{bs} + 2a_{rs}J_{rs} + 4b_{rs}K_{rs} \\
&\quad + 8C_{abrs}(ab|rs) + 8C_{arbs}(ar|bs) + 8C_{asbr}(as|br)
\end{aligned}
$$

Note that the two electron operators do not have the usual $2J - K$ form here. This is because the coefficients have been adjusted to make the overall energy equation compatible with B.76, which is necessary for the orbital optimization equations, below.

B.8 GVB-RCI Orbital Optimization

Because we can write the energy expression in the form of equation B.76, we may use the Yaffe-Goddard equations [6] to update the RCI orbitals. The Yaffe-Goddard Equations are a general procedure for computing the orbital optimization equations given an energy expression. Given a set of trial orbitals $\{\phi^{Old}\}$, the optimal set of orbitals $\{\phi^{New}\}$ are obtained via the transformation

$$
[\phi^{New}] = \exp(\Delta)[\phi^{Old}] \qquad \text{(B.111)}
$$

where $[\phi^{Old}]$ and $[\phi^{New}]$ are the matrices whose columns are the orbitals $\{\phi^{Old}\}$ and $\{\phi^{New}\}$. Δ is the anti-symmetric matrix with zero diagonal defined by

$$\Delta = \begin{bmatrix} 0 & \frac{A_{ij}}{B_{ij}} \\ -\frac{A_{ij}}{B_{ij}} & 0 \end{bmatrix} \tag{B.112}$$

where A_{ij} contains terms of first-order in orbital mixing, and B_{ij} contains terms of second-order in orbital mixing.

The following modified Fock operators are useful in simplifying the orbital optimization equations

$$\begin{aligned} F^k &= f_{ch} + a_{kk}J^k + a_{ka}J^a + 2b_{ka}K^a + a_{cb}J^b + 2b_{kb}K^b && \text{(B.113)} \\ &\quad + a_{kr}J^r + 2b_{kr}K^r + a_{ks}J^s + 2b_{ks}K^s \\ F^a &= f_{ah} + a_{ka}J^k + 2b_{ka}K^k + a_{aa}J^a + a_{ab}J^b && \text{(B.114)} \\ &\quad + 2b_{ab}K^b + a_{ar}J^r + 2b_{ar}K^r + a_{as}J^s + 2b_{as}K^s \\ F^b &= f_{bh} + a_{kb}J^k + 2b_{kb}K^k + a_{ab}J^a + 2b_{ab}K^a && \text{(B.115)} \\ &\quad + a_{bb}J^b + a_{br}J^r + 2b_{br}K^r + a_{bs}J^s + 2b_{bs}K^s \\ F^r &= f_{rh} + a_{kr}J^k + 2b_{kr}K^k + a_{ar}J^a + 2b_{ar}K^a && \text{(B.116)} \\ &\quad + a_{br}J^b + 2b_{br}K^b + a_{rr}J^r + a_{rs}J^s + 2b_{rs}K^s \\ F^s &= f_{sh} + a_{ks}J^k + 2b_{ks}K^k + a_{as}J^a + 2b_{as}K^a && \text{(B.117)} \\ &\quad + a_{bs}J^b + 2b_{bs}K^b + a_{rs}J^r + 2b_{rs}K^r + a_{ss}J^s \end{aligned}$$

The following definitions are also useful:

$$\gamma_{ij} = 2(a_{ii} + a_{jj} - 2a_{ij})K_{ij} + (b_{ii} + b_{jj} - 2b_{ij})(J_{ij} + K_{ij}) \tag{B.118}$$

$$E_{abrs} = 2C_{abrs}(ab|rs) + 2C_{arbs}(ar|bs) + 2C_{asbr}(as|br) \tag{B.119}$$

With these definitions, we now define the orbital optimization equations.

B.8.1 Active-Core Mixing

$$\begin{aligned} A_{ak} &= F^k_{ak} - F^a_{ak} - 2C_{abrs}(rs|bk) && \text{(B.120)} \\ &\quad -2C_{arbs}(bs|rk) - 2C_{asbr}(br|sk) \\ B_{ak} &= F^k_{kk} - F^k_{aa} - F^a_{kk} + F^a_{aa} - \gamma_{ak} + E_{abrs} && \text{(B.121)} \\ A_{bk} &= F^k_{bk} - F^b_{bk} - 2C_{abrs}(rs|ak) && \text{(B.122)} \\ &\quad -2C_{arbs}(as|rk) - 2C_{asbr}(ar|sk) \\ B_{bk} &= F^k_{kk} - F^k_{bb} - F^b_{kk} + F^b_{bb} - \gamma_{bk} + E_{abrs} && \text{(B.123)} \\ A_{rk} &= F^k_{rk} - F^r_{rk} - 2C_{abrs}(as|bk) && \text{(B.124)} \\ &\quad -2C_{arbs}(bs|rk) - 2C_{asbr}(ab|sk) \\ B_{rk} &= F^k_{kk} - F^k_{rr} - F^r_{kk} + F^r_{rr} - \gamma_{rk} + E_{abrs} && \text{(B.125)} \\ A_{sk} &= F^k_{sk} - F^s_{sk} - 2C_{abrs}(br|ak) && \text{(B.126)} \\ &\quad -2C_{arbs}(ar|bk) - 2C_{asbr}(ab|rk) \\ B_{sk} &= F^k_{kk} - F^k_{ss} - F^s_{kk} + F^s_{ss} - \gamma_{sk} + E_{abrs} && \text{(B.127)} \end{aligned}$$

B.8.2 Active-Active Mixing

$$
\begin{aligned}
A_{ba} &= F^a_{ab} - F^b_{ab} - 2C_{abrs}(J^a_{rs} - J^b_{rs}) && \text{(B.128)}\\
&\quad -2C_{arbs}(K^a_{rs} - K^b_{rs}) - 2C_{asbr}(K^a_{rs} - K^b_{rs}) \\
B_{ba} &= F^a_{aa} - F^b_{aa} - F^a_{bb} + F^b_{bb} - \gamma_{ab} + 8C_{abrs}(ab|rs) && \text{(B.129)}\\
&\quad +4(C_{arbs} + C_{asbr})[(ar|bs) + (as|br)] \\
A_{ra} &= F^a_{ar} - F^r_{ar} - 2C_{abrs}(K^a_{bs} - J^r_{bs}) && \text{(B.130)}\\
&\quad -2C_{arbs}(J^a_{bs} - J^r_{bs}) - 2C_{asbr}(K^a_{bs} - K^r_{bs}) \\
B_{ra} &= F^a_{aa} - F^r_{aa} - F^a_{rr} + F^r_{rr} - \gamma_{ar} + 8C_{arbs}(ar|bs) && \text{(B.131)}\\
&\quad +4(C_{abrs} + C_{asbr})[(ab|rs) + (as|br)] \\
A_{sa} &= F^a_{as} - F^s_{as} - 2C_{abrs}(K^a_{br} - K^s_{br}) && \text{(B.132)}\\
&\quad -2C_{arbs}(K^a_{br} - K^s_{br}) - 2C_{asbr}(J^a_{br} - J^s_{br}) \\
B_{sa} &= F^a_{aa} - F^s_{aa} - F^a_{ss} + F^s_{ss} - \gamma_{as} + 8C_{asbr}(as|br) && \text{(B.133)}\\
&\quad +4(C_{abrs} + C_{arbs})[(ab|rs) + (ar|bs)] \\
A_{rb} &= F^b_{br} - F^r_{br} - 2C_{abrs}(K^b_{as} - K^r_{as}) && \text{(B.134)}\\
&\quad -2C_{arbs}(K^b_{as} - K^r_{as}) - 2C_{asbr}(J^b_{as} - J^r_{as}) \\
B_{rb} &= F^b_{bb} - F^r_{bb} - F^b_{rr} + F^r_{rr} - \gamma_{br} + 8C_{asbr}(as|br) && \text{(B.135)}\\
&\quad +4(C_{abrs} + C_{arbs})[(ab|rs) + (ar|bs)] \\
A_{sb} &= F^b_{bs} - F^s_{bs} - 2C_{abrs}(K^b_{ar} - K^s_{ar}) && \text{(B.136)}\\
&\quad -2C_{arbs}(K^b_{ar} - K^s_{ar}) - 2C_{asbr}(J^b_{ar} - J^s_{ar}) \\
B_{sb} &= F^b_{bb} - F^s_{bb} - F^b_{ss} + F^s_{ss} - \gamma_{bs} + 8C_{arbs}(ar|bs) && \text{(B.137)}\\
&\quad +4(C_{abrs} + C_{asbr})[(ab|rs) + (as|br)] \\
A_{rs} &= F^r_{rs} - F^s_{rs} - 2C_{abrs}(J^r_{ab} - J^s_{ab}) && \text{(B.138)}\\
&\quad -2C_{arbs}(K^r_{ab} - K^s_{ab}) - 2C_{asbr}(K^r_{ab} - K^s_{ab}) \\
B_{rs} &= F^r_{rr} - F^s_{rr} - F^r_{ss} + F^s_{ss} - \gamma_{rs} + 8C_{abrs}(ab|rs) && \text{(B.139)}\\
&\quad +4(C_{arbs} + C_{asbr})[(ar|bs) + (as|br)]
\end{aligned}
$$

B.8.3 Occupied-Virtual Mixing

$$
\begin{aligned}
A_{vk} &= F^k_{kv} && \text{(B.140)}\\
B_{vk} &= F^k_{kk} - F^k_{vv} - \gamma_{kv} && \text{(B.141)}\\
A_{va} &= F^a_{av} + 2C_{abrs}(rs|bv) + 2C_{arbs}(bs|rv) + 2C_{asbr}(br|sv) && \text{(B.142)}\\
B_{va} &= F^a_{aa} - F^a_{vv} - \gamma_{av} + E_{abrs} && \text{(B.143)}\\
A_{vb} &= F^b_{bv} + 2C_{abrs}(rs|av) + 2C_{arbs}(ar|sv) + 2C_{asbr}(as|rv) && \text{(B.144)}\\
B_{vb} &= F^b_{bb} - F^b_{vv} - \gamma_{bv} + E_{abrs} && \text{(B.145)}\\
A_{vr} &= F^r_{rv} + 2C_{abrs}(ab|sv) + 2C_{arbs}(bs|av) + 2C_{asbr}(as|rv) && \text{(B.146)}\\
B_{vr} &= F^r_{rr} - F^r_{vv} - \gamma_{rv} + E_{abrs} && \text{(B.147)}
\end{aligned}
$$

$$A_{vs} = F^s_{sv} + 2C_{abrs}(ab|rv) + 2C_{arbs}(ar|bv) + 2C_{asbr}(br|av) \quad \text{(B.148)}$$
$$B_{vs} = F^s_{ss} - F^s_{vv} - \gamma_{sv} + E_{abrs} \quad \text{(B.149)}$$

B.9 Operators Required For GVB-RCI

The Hartree-Fock wave function

$$\Psi_{HF} = |k\bar{k}a\bar{a}b\bar{b}\rangle \quad \text{(B.150)}$$

requires the computation of the one-electron operator h, and the two-electron operators J^a, K^a, J^b, and K^b—a total of $5n^2$ elements. When the two orbitals ϕ_a and ϕ_b are correlated using two GVB pairs, the resulting GVB wave function

$$\begin{aligned}\Psi_{GVB} &= c_{g1}c_{g2}|k\bar{k}a\bar{a}b\bar{b}\rangle + c_{g1}c_{u2}|k\bar{k}a\bar{a}s\bar{s}\rangle \\ &\quad + c_{u1}c_{g2}|k\bar{k}r\bar{r}b\bar{b}\rangle + c_{u1}c_{u2}|k\bar{k}r\bar{r}s\bar{s}\rangle\end{aligned} \quad \text{(B.151)}$$

requires computation of the above operators, plus the two-electron operators J^r, K^r, J^s, and K^s—for a total of $9n^2$ elements. From the preceding section, it is clear that when the GVB pairs are replaced by RCI pairs, the resulting wave function requires, in addition to the operators required by the GVB wave function, the two-electron elements $(ab|rx)$, $(ab|sx)$, $(ar|bx)$, $(ar|sx)$, $(as|bx)$, $(as|rx)$, $(br|ax)$, $(br|sx)$, $(bs|ax)$, $(bs|rx)$, $(rs|ax)$, and $(rs|bx)$, where x ranges over all occupied and virtual orbitals. This is a mere $12n$ elements, negligible in terms of memory and computation time compared to the $9n^2$ elements already required by the GVB wave function.

B.10 Conclusions

GVB-RCI wave functions are the next logical step beyond GVB-PP wave functions in terms of the amount of electron correlation included in the wave function. For the two-pair, closed-shell case, the GVB-RCI wave function the form in equation B.16. The GVB CI coefficients are chosen so that interaction between the $|gu\rangle$ terms in a pair is negligible with all other $|gg\rangle$ or $|uu\rangle$ terms. Hence, the only terms in the GVB-RCI energy expression that differ from the GVB-PP energy expression are the interaction between the two $|gu\rangle$ terms of different pairs. The resulting energy expression has the form of equation B.76. By proper assignment of coefficients, equation B.76 may be put in the form of equation B.76, where the Yaffe-Goddard equations may be used to obtain the orbital optimization equations in Sections B.8.1–B.8.3. Inspection of the energy expression B.76 and the orbital optimization equations in Sections B.8.1–B.8.3 show that GVB-RCI requires only an additional $12n$ two-electron integrals beyond the $9n^2$ integrals required by the two-pair GVB-PP wave function in equation B.2. Thus the additional expense required by the GVB-RCI wave function is negligible.

Bibliography

[1] Atilla Szabo and Neil S. Ostlund. *Modern Quantum Chemistry*. McGraw-Hill, New York, 1982.

[2] C.C.J. Roothan. Hartree Fock theory. *Reviews of Modern Physics*, 23:69, 1951.

[3] Frank W. Bobrowicz and William A. Goddard, III. The self-consistent field equations for generalized valence bond and open-shell Hartree-Fock wave functions. In Henry F. Schaefer, III, editor, *Methods of Electronic Structure Theory*, volume 3 of *Modern Theoretical Chemistry*, page 79. Plenum Press, New York, 1977.

[4] W. J. Hunt, William A. Goddard, III, and Thomas H. Dunning. The incorporation of quadratic convergence into open-shell self-consistent field equations. *Chemical Physics Letters*, 6:147, 1970.

[5] Ray A. Bair, Frank W. Bobrowicz, W. J. Hunt, P. J. Hay, and William A. Goddard, III. *GVB2P5 Program*. California Institute of Technology, 1977.

[6] Larry G. Yaffe and William A. Goddard, III. Orbital optimization in electronic wave functions: Equations for quadratic and cubic convergence in general multiconfiguration wave functions. *Physical Review A*, 13:1682, 1976.

[7] S. R. Cox and D. E. Williams. Atomic charges. *Journal of Computational Chemistry*, 2:304, 1981.

[8] J. B. Foresman, Martin Head-Gordon, John A. Pople, and Michael J. Frisch. Toward a systematic molecular orbital theory for excited states. *Journal of Physical Chemistry*, 96:135, 1992.

[9] Richard A. Friesner. Solution of self-consistent field electronic structure equations by a pseudospectral method. *Chemical Physics Letters*, 116:39, 1985.

[10] Richard A. Friesner. Solution of the Hartree-Fock equations by a pseudospectral method: Application to diatomic molecules. *Journal of Chemical Physics*, 85:1462, 1986.

[11] Richard A. Friesner. Solution of the Hartree-Fock equations for polyatomic molecules by a pseudospectral method. *Journal of Chemical Physics*, 86:3522, 1987.

[12] Richard A. Friesner. An automatic grid generation scheme for pseudospectral self-consistent field calculations on polyatomic molecules. *Journal of Physical Chemistry*, 92:3091, 1988.

[13] Murco N. Ringnalda, Youngdo Won, and Richard A. Friesner. Pseudospectral Hartree-Fock calculations on glycine. *Journal of Chemical Physics*, 92:1163, 1990.

[14] Murco N. Ringnalda, M. Belhadj, and Richard A. Friesner. Pseudospectral Hartree-Fock theory: Applications and algorithmic improvements. *Journal of Chemical Physics*, 93:3397, 1990.

[15] Jean-Marc Langlois, Richard P. Muller, Terry R. Coley, William A. Goddard, III, Murco N. Ringnalda, Yongdo Won, and Richard A. Friesner. Pseudospectral generalized valence bond calculations of methylene, ethylene, and silylene. *Journal of Chemical Physics*, 92:7488, 1990.

[16] Murco N. Ringnalda, Jean-Marc Langlois, B. H. Greeley, Thomas J. Russo, Richard P. Muller, Bryan Marten, Yongdo Won, Robert E. Donnelly, Jr., W. T. Pollard Gregory H. Miller, William A. Goddard, III, and Richard A. Friesner. *PS-GVB version 1.00*. Pasadena, 1993.

[17] V. I. Lebedev. Quadratures formulas for the sphere of 25th to 29th order accuracy. *Sibersk. Mat. Z.*, 18:132, 1977.

[18] A. H. Stroud. *Approximate Calculation of Multiple Integrals*. Prentice-Hall, Englewood Cliffs, N.J., 1987.

[19] Larry B. Harding and William A. Goddard, III. *Ab Initio* studies on singlet–triplet splitting of methylene (CH_2). *Journal of Chemical Physics*, 67:1777, 1976.

[20] Thomas H. Dunning and P. J. Hay. Basis sets for electronic structure theory. In Henry F. Schaefer, III, editor, *Modern Theoretical Chemistry: Methods of Electronic Structure Theory*, volume 3. Plenum, New York, 1977.

[21] Sigeru Huzinaga. Gaussian-type functions for polyatomic systems. i. *Journal of Chemical Physics*, 42:1293, 1965.

[22] A. K. Rappé, T. A. Smedley, and William A. Goddard, III. The shape and hamiltonian consistent (SHC) effective potentials. *Journal of Physical Chemistry*, 85:1662, 1981.

[23] P. J. Hay and W. R. Wadt. *Ab Initio* effective core potentials for molecular calculations—potentials for the transition-metal atoms Sc to Hg. *Journal of Chemical Physics*, page 270, 1985.

[24] M. H. MacAdon and William A. Goddard, III. Generalized valence bond studies of metallic bonding: Naked clusters and applications to bulk metals. *Journal of Physical Chemistry*, 91:2607, 1987.

[25] C. F. Melius, T. H. Upton, and William A. Goddard, III. Electronic properties of metal clusters (Ni_{13} to Ni_{87} and implications to chemisorption. *Solid State Communications*, 28:501, 1978.

[26] H.-J. Werner and P. J. Knowles. A second order multiconfiguration SCF procedure with optimum convergence. *Journal of Chemical Physics*, 82:5053, 1985.

[27] P.-A. Malmqvist, A. Rendell, and B. O. Roos. The restricted active space self-consistent field method, implemented with a split graph unitary group approach. *Journal of Physical Chemistry*, 94:5477, 1990.

[28] R. Shepard, I. Shavitt, and J. Simons. Comparison of the convergence characteristics of some iterative wave function optimization methods. *Journal of Chemical Physics*, 76:543, 1982.

[29] Peter Pulay. Convergence acceleration of iterative sequences. the case of SCF iteration. *Chemical Physics Letters*, 3:93, 1980.

[30] Peter Pulay. Improved convergence acceleration. *Journal of Computational Chemistry*, 3:556, 1982.

[31] Tracy P. Hamilton and Peter Pulay. Direct inversion in the iterative subspace (DIIS) optimization of open-shell, excited-state, and small multiconfiguration SCF wave functions. *Journal of Chemical Physics*, 84:5728, 1986.

[32] Richard P. Muller, Jean-Marc Langlois, Murco N. Ringnalda, Richard A. Friesner, and William A. Goddard, III. A generalized direct inversion in the iterative subspace approach for generalized valence bond wave functions. *Journal of Chemical Physics*, 100:1226, 1994.

[33] Jean-Marc Langlois, Terumasa Yamasaki, Richard P. Muller, and William A. Goddard, III. Rule-based trial wave functions for generalized valence bond theory. *Journal of Physical Chemistry*, 98:13498, 1994.

[34] Michael W. Schmidt, K. K. Baldridge, J. A. Boatz, J. H. Jensen, S. Doseki, Michael S. Gordon K. A. Nguyen, T. L. Windus, and S. T. Elbert. *GAMESS Program Suite*, 1995.

[35] Michael J. Frisch, Martin Head-Gordon, G. W. Trucks, J. B. Foresman, H. B. Schlegel, K. Raghavachari, Michael A. Robb, J. S. Binkley, C. Gonzales, D. J. Denfres, D. J. Fox, R. A. Whiteside, R. Seeger, Carl F. Melius, J. Baker, R. L. Martin, L. R. Kahn, J. J. P. Stewart, S. Topiol, and John A. Pople. *Gaussian 90*. Pittsburgh, PA., 1990.

[36] M. Page and J.W. McIver, Jr. Pseudoeigenvalue methods for orbital optimization—general theory and application to closed shell, open shell, and two-configuration SCF wave functions. *Journal of Chemical Physics*, 79:4985, 1983.

[37] R. Krishnan, J. S. Binkley, R. Seeger, and John A. Pople. *Journal of Chemical Physics*, 72:650, 1980.

[38] J. Deisenhofer, O. Epp, K. Miki, R. Huber, and H. Michel. X-ray structure-analysis of a membrane-protein complex—electron density map at 3 å resolution and a model of the chromophores of the photosynthetic reaction center from *Rhodopseudomonas Viridis*. *Journal of Molecular Biology*, 180:385, 1984.

[39] L. Stryer. *Biochemistry*. W. H. Freeman and Company, New York, N.Y., 1988.

[40] M. Klingenberg. *Archives of Biochemistry and Biophysics*, 75:396, 1958.

[41] P. E. Ellis and J. E. Lyons. Selective air oxidation of light alkanes catalyzed by activated metalloporphyrins—the search for a suprabiotic system. *Coordination Chemistry*, 105:181, 1990.

[42] J. F. Bartoli, O. Brigaud, P. Battioni, and D. Mansuy. Hydroxylation of linear alkanes catalyzed by iron porphyrins—particular efficacy and regioselectivity of perhalogenated porphyrins. *Journal of the Chemical Society: Chemical Communications*, 1991:440, 1991.

[43] Martin Gouterman. Optical spectra and electronic structure of porphyrins and related rings. In David Dolphin, editor, *The Porphyrins*, volume 3, page 1. Academic Press, New York, 1978.

[44] Martin Gouterman. Study of the effects of substitution on the adsorption spectra of porphin. *Journal of Chemical Physics*, 30:1139, 1959.

[45] Martin Gouterman. Spectra of porphyrins. *Journal of Molecular Spectroscopy*, 6:138, 1961.

[46] B. M. Chem and A. Tulinsky. *Journal of the American Chemical Society*, 94:4144, 1972.

[47] J. G. Radziszewski, J. Waluk, and J. Michl. FT visible absorption spectroscopy of porphine in noble-gas matrices. *Journal of Molecular Spectroscopy*, 140:373, 1990.

[48] L. Edwards, D. H. Dolphin, Martin Gouterman, and A. D. Adler. *Journal of Molecular Spectroscopy*, 36:16, 1971.

[49] W. J. Hunt and William A. Goddard, III. Excited states of H_20 using improved virtual orbitals. *Chemical Physics Letters*, 3:414, 1969.

[50] G. M. Maggiora and L. J. Weimann. *International Journal of Quantum Chemistry: Quantum Biology Symposia*, 1:179, 1974.

[51] C. Weiss, H. Kobayashi, and Martin Gouterman. Spectra of porphyrins. part III: Self-consistent molecular orbital calculations of porphyrin and related ring systems. *Journal of Molecular Spectroscopy*, 16:415, 1965.

[52] Frank W. Bobrowicz. PhD thesis, California Institute of Technology, Pasadena, California, 1974.